NASA
Technical
Paper
2293
C.2
May 1984

Decoupled-Control Analysis of a Large Flexible Space Antenna With Linear Quadratic Regulator Comparisons

John W. Young,
Harold A. Hamer, and
Katherine G. Johnson

NASA

NASA Technical Paper 2293

1984

Decoupled-Control Analysis of a Large Flexible Space Antenna With Linear Quadratic Regulator Comparisons

John W. Young,
Harold A. Hamer, and
Katherine G. Johnson

Langley Research Center
Hampton, Virginia

National Aeronautics
and Space Administration

**Scientific and Technical
Information Branch**

SUMMARY

A study has been conducted of the feasibility of employing decoupling procedures to control a large flexible space antenna. Control involves commanding changes in the rigid-body modes or nulling initial disturbances in the flexible modes. The study is intended to provide preliminary engineering-type data, in parametric form, which would be useful in the final design of a large space antenna control system. The data illustrate the effect on control requirements of the number of modes controlled; of the number, type, and location of control actuators; and of variations in the closed-loop dynamics of the control system. A brief analysis is included which compares decoupled-control results with those obtained by using a linear quadratic regulator approach. Time history responses are presented to illustrate the effects of the control procedures.

INTRODUCTION

The operational status of the NASA space transportation system (STS) has opened a wide area for application of large antenna systems which can be deployed in space. Examples of relatively near-term missions utilizing these antennae include personal communication systems, Earth observation systems, radio astronomy systems, and electronic mail systems. (See ref. 1.) In order to meet the stringent pointing and surface-contour requirements, extensive analysis is needed to develop efficient and reliable control-system designs for these systems. In the last several years, various methods of controlling the attitude and modal displacements of large space structures have been developed and analyzed. Examples of these studies are given in references 2 to 5. References 2 and 3 apply decoupled and modern control theory approaches, respectively, to control of a long flexible one-dimensional beam in orbit. Reference 4 uses similar approaches for control of a two-dimensional flexible space platform, and reference 5 applies modern control theory techniques to control of a three-dimensional space antenna.

This paper presents results of an antenna-control-system design procedure which utilizes linear decoupling theory. The 122-m-diameter hoop-column antenna (ref. 6), which can be deployed in a single STS flight, is used as the basis for the study. The hoop-column concept, shown in the sketch on page 2, consists of a deployable central column attached to a deployable hoop by cables in tension. The resulting structure has a large number of flexible modes in addition to the rigid-body rotation and translation modes. Decoupling theory is a convenient tool for devising control laws for such structures because the theory allows for independent control of each mode. For example, the rigid-body modes can be controlled without affecting the flexible modes. The theory also allows the feedback gains to be computed in closed form such that desired closed-loop dynamics are achieved while maintaining the independent control capability.

The objectives of this paper are (1) to apply the decoupled analyses of references 2 and 4 to control of a three-dimensional large space antenna, (2) to provide preliminary engineering-type data which could be used in the final design of a decoupled-control system for a large space antenna system, and (3) to compare the decoupled results with those obtained with a linear quadratic regulator approach.

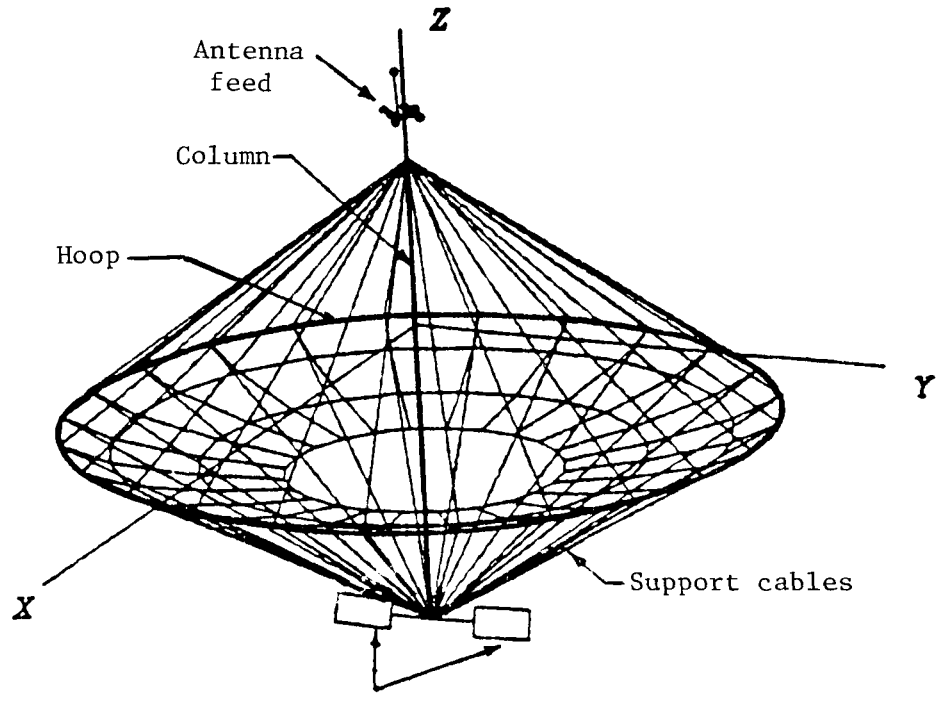

Hoop-column antenna

Results are presented for various arrangements of control-moment gyros on the antenna column and for arrangements of reaction-control jets on the column or hoop. Control requirements in terms of maximum torque/force and total momentum/impulse are presented in relation to closed-loop dynamics, which cover a wide range of frequencies and damping ratios. Although the results presented are primarily for the three rigid-body rotation modes and up to six of the lowest frequency flexible modes, limited results are included on the effect of controlling the three rigid-body translation modes. Comparisons are given between the decoupled-control results and those obtained with the linear quadratic regulator approach for a number of cases using control-moment gyros on the antenna column. Time histories of control requirements, along with the ensuing modal responses, are presented to illustrate the effects of the control procedures.

It should be noted that the results of this study represent the ideal performance of the decoupled-control approach, in that perfect estimates are assumed for the modal measurements required for feedback. In addition, the number of controllers equals the number of modes to be controlled in the system, and perfect controllers (no actuator dynamics included) are assumed. The important problem of stability in the presence of control and observation spillover due to the effects of uncontrolled modes (residual modes not included in the math model) is not included in this analysis. These effects are discussed in reference 7.

SYMBOLS AND ABBREVIATIONS

A	system matrix (eq. (B1))
A_{max}	maximum modal amplitude
A_n	modal amplitude (eq. (3)), where n is the mode number (1, 2, ..., 6)
A_s	steady-state modal amplitude
B	control influence matrix (eq. (B1))
B'	lower half of B matrix (eq. (B1))
C	matrix relating output (decoupled) vector to state vector (eq. (6))
CMG	control-moment gyro
c.g.	center of gravity
$\bar{d}$	displacement vector (eq. (4))
F	feedback gain matrix (eq. (7))
f	force
$\bar{f}$	force vector
$f_{i,j}$	component of force, where i is the control direction, and j is the actuator location
G	feedforward gain matrix (eq. (7))
g	acceleration of gravity
$\bar{I}$	moment of inertia matrix
$I_{i,j}$	impulse, where i is the control direction, and j is the actuator location
I_x, I_y, I_z, I_{xz}	center-of-gravity moments and product of inertia
J	objective function (eq. (11))
K	gain matrix (eq. (10))
L	lever arm matrix (eqs. (A2) and (A3))
LQR	linear quadratic regulator
ℓ	distance (fig. 1)
$M_{i,j}$	angular momentum, where i is the control direction, and j is the actuator location

m_n	modal mass
P	control-vector-weighting matrix (eq. (11))
Q	state-vector-weighting matrix (eq. (11))
RCS	reaction-control system
r	radius of hoop
s	Laplace operator
T	torque
$\bar{T}$	torque vector
$T_{i,j}$	components of torque, where i is the control direction, and j is the actuator location
T_n	natural period
t	time
t_1	time to damp to 1 percent of initial disturbance
$\bar{u}$	control vector (eq. (7))
$\bar{v}$	input command vector (eq. (7))
w	weight
X,Y,Z	coordinates of antenna center of gravity
x	state variable
$\bar{x}$	state vector
x,y,z	coordinates of modal data (fig. 1)
$\bar{y}$	output vector (eq. (6))
δ	angle between actuators on antenna hoop (fig. 1)
ζ	damping ratio
ζ_d	desired damping ratio
ζ_n	natural damping ratio
θ,ϕ,ψ	rotation angle about X-, Y-, and Z-axis, respectively
τ	time constant
Φ	mode shape matrix

ϕ' mode slope matrix

ω frequency

ω_d desired frequency

ω_n natural frequency

Subscripts:

d desired

flex flexible mode

i,j i is the control direction, and j is the actuator location

max maximum

n mode number

rb rigid-body mode

A bar over a symbol denotes a vector or a matrix.

MATHEMATICAL MODEL OF ANTENNA

A large space structure such as the hoop-column antenna has, in theory, an infinite number of flexible (vibration) modes. To facilitate analytical treatment of the control problem, a finite order, linearized model was formulated. For the analysis of this report, the structural model was selected to contain from three to six of the lowest flexible modes of the 122-m-diameter hoop-column antenna, as described in reference 6. The three rigid-body rotation modes are included in the analysis, and limited results which include the three rigid-body translation modes are presented.

The equations of motion used to represent the rigid-body and vibration modes of the antenna are given below. Details of their implementation for specific arrangements of control actuators are given in appendix A.

Rigid-body rotations (for small angles) about the antenna center of gravity are represented by

$$\begin{pmatrix} \ddot{\theta} \\ \ddot{\phi} \\ \ddot{\psi} \end{pmatrix} = \bar{I}^{-1} \begin{pmatrix} \Sigma T_x \\ \Sigma T_y \\ \Sigma T_z \end{pmatrix} \tag{1}$$

Translations of the antenna center of gravity can be expressed as

$$\begin{pmatrix} \ddot{X} \\ \ddot{Y} \\ \ddot{Z} \end{pmatrix} = \frac{g}{w} \begin{pmatrix} \Sigma f_x \\ \Sigma f_y \\ \Sigma f_z \end{pmatrix} \tag{2}$$

Variations in modal amplitudes of the flexible modes are represented by

$$\ddot{A}_n + 2\zeta_n \omega_n \dot{A}_n + \omega_n^2 A_n = \frac{1}{m_n}\left(\phi_n^T \bar{f} + \phi_n'^T \bar{T}\right) \qquad (n = 1, 2, \ldots, 6) \tag{3}$$

where $\bar{f}$ and $\bar{T}$ are vectors of control forces and torques, respectively, m_n is the modal mass, ϕ_n is the column of the mode shape matrix relating to the nth vibration mode, and ϕ_n' is the corresponding column of the mode slope matrix. (See appendix A for details.) It should be noted that A_n values in equation (3) are modal amplitude displacement variables and do not represent actual physical displacements. The physical displacement at some point on the antenna would include linear combinations of the modal amplitudes and mode shapes and is given by the transformation

$$\bar{d} = \phi \bar{A}_n \tag{4}$$

The mode shape and mode slope data used in the analysis were taken from unpublished results of a NASTRAN® model of the 122-m-diameter hoop-column antenna system and are provided in table I. The data of table I consist of orthogonal mode shapes and slopes at four positions on the mast as well as mode shapes at increments of 15° around the hoop of the antenna. Table II shows the weight and inertia properties of the antenna. The modal masses, frequencies, and natural damping ratios of the six flexible modes considered in the analysis are also given in table II.

DECOUPLED CONTROL

Since decoupling theory has been analyzed extensively in the literature (for example, see refs. 8 and 9), the discussion of this paper is limited to some general remarks concerning its application. Examples are given in appendix B to illustrate the manner in which the theory was applied to the system equations of the current analysis. Typical B, F, and G matrices for two six-control cases are shown in table III and are discussed subsequently.

The second-order equations in the analysis (eqs. (1) to (3)) can be reduced to first-order equations (state-vector form) and written as

$$\dot{\bar{x}} = A\bar{x} + B\bar{u} \tag{5}$$

The output vector $\bar{y}$ of states to be decoupled is defined as

$$\bar{y} = C\bar{x} \tag{6}$$

where C is a matrix which selects the states to be decoupled. For the present analysis, the output vector is taken to be the entire state amplitude vector, so that complete decoupling is obtained for all modes in the model. Complete decoupling requires as many actuators as there are state amplitudes to be decoupled.

The decoupling control law is taken as

$$\bar{u} = F\bar{x} + G\bar{v} \tag{7}$$

where $\bar{v}$ is the input command vector, and F and G are feedback and feedforward gain matrices, respectively. The output is related to the input through the transfer function $H(s)$ by

$$\hat{\bar{y}}(s) = H(s)\,\hat{\bar{v}}(s) \tag{8}$$

where $\bar{y}$ and $\bar{v}$ are of the same order. The circumflex in equation (8) indicates the Laplace transform and

$$H(s) = C(sI - A - BF)^{-1}BG \tag{9}$$

where I is the identity matrix. Decoupling theory provides a method for determining the F and G matrices such that the transfer function $H(s)$ is diagonal and nonsingular. Therefore, independent control is possible for each of the decoupled (output) variables. The dynamics of the transfer function can also be specified. This is important because the desired closed-loop dynamics of the decoupled variables having been specified, the transient and steady-state responses of the system are known. For the present application, these responses are simply solutions to the second-order equations $\left(\text{e.g., } \ddot{x} + 2\zeta_d\omega_d\dot{x} + \omega_d^2 x = \omega_d^2 v\right)$, where ω_d and ζ_d are the desired closed-loop frequency and damping ratio, and v is the command. Although closed-form solutions to these equations exist for specified initial conditions and step commands, in the present analysis the system equations (eq. (5)) were integrated numerically by using the feedback law of equation (7). This was done to facilitate control requirement computations. Various methods exist for determining the feedback and feedforward gains required to achieve decoupling. For example, the computer program of reference 8, based on algebraic theory of linear systems, provides a

general purpose approach to the problem. In the examples of appendix B, the method of reference 9 was used because it gives insight into the nature of the decoupling process.

Linear Quadratic Regulator Control

In order to establish a standard for comparison of the decoupled-control results, a limited analysis was made in which state feedback control gains were calculated by using the asymptotic linear quadratic regulator (LQR) approach of reference 10. (Ref. 11 provides a computer program for performing these computations.) The control law for the LQR results was given by

$$\bar{u} = K\bar{x} \tag{10}$$

The control gain matrix was computed subject to the constraint of equation (5) such that the following function was minimized:

$$J = \lim_{t\to\infty} \int_0^t \left(\bar{x}^T Q \bar{x} + \bar{u}^T P \bar{u}\right) dt \tag{11}$$

Q and P are weightings on the states and controls; these weightings are varied in order to achieve the desired closed-loop dynamics. Decoupled and LQR comparisons in the present analysis are limited to control of the rigid-body rotation and first three flexible modes with six torquers on the antenna mast.

Antenna Open-Loop Response

Vibratory response characteristics of the antenna caused by initial disturbances in the modal variables and by step control inputs will now be summarized. The unforced transient behavior of the six vibration modes considered in the analysis (eq. (3)) is presented in figure 2. Shown are the modal amplitude variations with time resulting from an initial displacement of 1 in. in each modal variable. These response characteristics and those for other assumed damping ratios are summarized in figure 3. Shown is the percent of initial displacement as a function of the number of cycles for various damping ratios. The time to damp to a certain percent can be determined from figure 3 by using the modal periods of table II. For example, mode 1 ($\zeta = 0.01$) requires 74 cycles or about 623 sec to damp to 1 percent of an initial displacement, whereas mode 6 requires 37 cycles, or about 41 sec, to achieve the same reduction in amplitude. Note that for $\zeta > 0.59$, vibrations will damp to 1 percent in less than 1 cycle.

Vibratory response characteristics of the system to step inputs in torque or force are given in table IV. Columns two, three, and four of the table show the steady-state and peak values attained in the modal variables for a unity control input, mode shape (ϕ), and mode slope (ϕ'). Since the system is linear, the results given in columns two, three, and four of table IV can be scaled to represent other values for torque, force, mode shape, or mode slope. For example, the last two columns of table IV show the maximum steady-state amplitudes attained for a unity force input on the hoop or a unity torque input on the column. These values are

obtained by multiplying the second column of table IV by the largest values of ϕ or ϕ' (table I) on the hoop or column, respectively.

As previously mentioned, the results of table IV are for modal amplitudes and should not be confused with physical displacements of the system. The actual displacement at some position on the antenna is given by equation (4) (where the values of ϕ are given in table I). For example, if we assume that all six modes have an amplitude of 1 in., then the deflection in the y-direction at position 1 (fig. 1) would be given in inches by

$$d_{y,1} = (0.2137)(1) + (0)(1) + (0.6703)(1) + (0)(1) + (-0.1131)(1) + (0.0045)(1) = 0.7754$$

RESULTS AND DISCUSSION

Results of the study are presented to illustrate the effect on control requirements of (1) the number of modes controlled, (2) the number, type, and location of control actuators, and (3) variations in the closed-loop dynamics (ω_d, ζ_d) of the control system. Although most of the results are limited to control of the three rigid-body rotation modes plus the first three vibration modes, the effect of adding up to three additional vibration modes and of including the three rigid-body translation modes is also considered. As described in appendix A, the controls utilized are either control-moment gyros (CMG's) or reaction-control-system (RCS) jets. The controllers are three-axis devices aligned along the x-, y-, and z-directions (fig. 1). Although most of the results involve the use of decoupled controls, comparisons are also presented between decoupled results and those obtained with a linear quadratic regulator (LQR) approach.

Typical Decoupled Responses

Typical position and rate responses are shown in figure 4 for a six-control case with initial displacements of 0.01 rad in the rigid-body modes and 1 in. in each of the first three flexible modes. The closed-loop characteristics of these responses are given in table III, along with the B, F, and G matrices. As explained in the previous section on decoupled control, the data of figure 4 are simply linear, second-order responses at the specified damping ratio and frequency and would be the same for any six-actuator arrangement for which the control influence matrix is invertible (eq. (B4)). Also, if initial modal amplitudes were set at zero for any of the variables of figure 4, those variables and their rates would remain at zero, and the other responses would be as shown.

Time histories of the control required to produce the responses of figure 4 are given in figure 5 for cases where either CMG (fig. 5(a)) or RCS (fig. 5(b)) actuators were used. Shown also are time histories for cases where initial disturbances were either in the rigid-body modes alone or in the flexible modes alone. The control time histories of figure 5 are for the actuator arrangement of table III.

The momentum and impulse time histories of figure 5 represent the total areas under the torque and force responses. Momentum and impulse, along with the maximum value for control inputs, are used in the report as a measure of control requirements when making various comparisons.

Consider the torque and force time histories of figure 5. The inputs at zero time are the result of rigid-body position gains, inasmuch as the flexible gains are zero because of the closed-loop requirement that the antenna vibrate at its natural frequency. The initial control peaks are caused by the flexible-mode rate feedback terms. The momentum and impulse histories of figure 5 indicate the predominant controllers for the various modes. For example, figure 5(a) shows that the CMG unit at position 2 is mainly used for rigid-body control.

Initial-Condition Effects

The control requirement results of figure 5 are summarized in the first three cases of table V. Shown are the maximum control inputs and the total impulse and momentum for the initial conditions of figure 5. The impulse and momentum values are the sums of those attained for each of the six controllers. Cases 4 through 9 of table V give results for initial displacements in the individual modes.

Since the system equations are linear, the results of table V can be scaled to any constant positive multiple of the initial conditions shown. For example, a disturbance of 0.1 rad in the rigid-body modes would result in a peak force of 53 lb and an impulse of 1250 lb-sec. Note that adding the contributions due to rigid-body disturbances alone (case 1) to those due to flexible-mode disturbances (case 2) does not give the result of simultaneous disturbances in all modes (case 3). Although control requirements vary linearly with initial-condition variations, they may be dependent on the direction of the initial-condition disturbance, as is shown in cases 10 through 13 of table V.

Consider the cases of table V which have initial conditions on only the rigid-body modes. The maximum control inputs for these cases occur at zero time (see fig. 5) and can be calculated from the initial conditions and the rigid-body position gains (first three columns) of the feedback matrices of table III. For example, consider case 1 of table V. Examination of the F matrix of table III(b) shows that the peak force occurs in the first controller and can be calculated by using the first three gains in the first row as follows:

$$f_{x,1} = (213 + 301 + 15)(0.01) = 5.3 \text{ lb}$$

Peak forces or torques for other combinations of initial rigid-body disturbances can be calculated in a similar manner.

The rigid-body results given in table V are for initial disturbances in the rigid-body modes, and control is effected through use of the feedback matrix. Similar results could be obtained if the initial rigid-body positions were set at zero and commanded to go to a nonzero condition. In this case, peak control inputs would result from the feedforward gains (G) of table III, and the control law would use both the F and G gain matrices. (For example, see ref. 2.)

The results of table V should be considered only as examples of the individual and collective effects of initial-condition variations. The control requirements for a particular set of initial disturbances can only be determined by solving the system equations. In the remaining discussions of the report, initial conditions will either be 0.01 rad in the rigid-body modes or 1 in. in the flexible modes.

Actuator Location Effects

The effect on control requirements of actuator placement on the antenna will now be considered for six-control cases. The use of CMG-type controllers was limited to the four positions on the column shown in figure 1, inasmuch as these were the only locations for which mode slope data were available (table I). RCS controllers could be located on either the column or the hoop. Comparisons are limited to systems using two three-axis controllers of either the CMG or the RCS type with their axes aligned along the x-, y-, and z-directions of figure 1. That is, one- or two-axis controllers, combinations of CMG or RCS units, and gimbaled controllers were not considered.

Positions 1 and 2 (top and bottom, respectively) on the column (fig. 1) were found to yield the lowest CMG control requirements. The results for this arrangement, as well as those for the two next best locations, are given in table VI. All other CMG locations on the mast required much higher values of torque and momentum.

Consider the results shown in table VI for which the flexible disturbances are zero. For these cases, the flexible modes add nothing to the feedback law because the modal displacements and rates remain at zero. Why then are the control requirements different for each CMG arrangement? This occurs because each arrangement requires different rigid-body feedback gains so as not to disturb the flexible modes. Had only the rigid-body modes been controlled with one three-axis CMG, all positions on the column would have given identical results.

The use of RCS-type controllers will now be considered. RCS controllers confined to the mast are excluded, since rigid-body rotations about the z-axis (fig. 1) of the antenna cannot be achieved with this arrangement. No combinations of RCS units on the column and hoop were found to be superior to the case where the RCS controls were placed only on the hoop. Figure 6 shows control requirements for cases where one three-axis RCS was located at position 5 (fig. 1) on the hoop and another three-axis RCS at various locations around the hoop. (The symbol δ represents the separation angle between the actuators as measured from position 5.) As the angle between the RCS's is reduced, a singular condition is approached, and the control requirements increase rapidly. The same is true as the separation angle approaches 180°. For the rigid-body and flexible-mode disturbances chosen, figure 6 shows that the optimum separation angle between the RCS's is about 120° to 150°. The results of figure 6 are, of course, dependent on the magnitude and direction of the initial disturbance, as was shown in case 10 of table V for the RCS controllers at positions 5 and 6. In the remainder of the report, RCS controls will be located at positions 5 and 6 when the effects on control requirements of changes in the closed-loop system dynamics are compared.

Closed-Loop Damping-Ratio Effects

Previous results of the report have used a closed-loop damping ratio (ζ_d) of 0.9 for all modes. The effect on control requirements of variations in ζ_d will now be considered for the CMG and RCS locations and closed-loop frequencies of table III. The effect of variations in the closed-loop frequency values of table III is presented in a later section of the report.

Figure 7 shows that for rigid-body disturbances, total momentum and impulse decrease as damping ratio is increased. Values of total momentum and impulse are approximately inversely proportional to the damping ratio. The magnitudes of peak

torques and forces are constant, since they are caused by position feedback operating on the initial conditions, as previously described.

Figure 8 shows that for flexible-mode disturbances, the control requirements are reduced as the damping ratio is reduced. The reduced damping ratio, of course, leads to an increase in time to damp the disturbances, as shown in figure 8(a). The time shown is that required to damp the first flexible mode to 1 percent and is independent of the controller type. The higher frequency modes would damp more rapidly for fixed damping ratios.

The maximum torques and forces shown in figure 8 are basically caused by the damping terms in feedback and cannot be determined from initial conditions and the F matrix, as is the case for rigid-body disturbances. It should be noted that the F matrices of table III can be converted to approximate (by neglecting the natural damping term in eq. (B6)) the feedback matrix obtained for other values of ζ_d by proper scaling of columns 7 through 12. For example, for 0.7 damping in the pitch mode, column 7 would be multiplied by 0.7/0.9.

Closed-loop damping-ratio effects can be summarized as follows: To minimize control requirements with respect to ζ_d, large values (0.9 or greater) should be used for the rigid-body rotation modes, but the flexible modes should be damped as lightly as is practical. The lower limit on flexible-mode damping would be determined by mission requirements, since a reduction in damping leads to an increase in time to damp an initial disturbance. An additional method for reducing control requirements, which involves the introduction of lag into the feedback gains, is discussed in a later section of the report.

Closed-Loop Frequency Effects

The effect on control requirements of variations in closed-loop frequency will now be considered for six-control cases. As in the previous section, the results are for the CMG and RCS locations of table III.

Figure 9 shows the effect on control requirements of changes in the rigid-body frequency for various combinations of initial disturbances in the rigid-body modes. The results of figure 9 are for a rigid-body damping ratio of 0.9, since this value results in nearly minimum total momentum and impulse (fig. 7).

Figure 9 shows that the total momentum and impulse are linear functions of the rigid-body frequency for the combinations of initial disturbances shown. The peak values of torque and force are functions of the initial disturbances and the term ω_d^2, which is included in the position feedback gain (eq. (B6)). As was the case with closed-loop damping ratio, the maximum control inputs of figure 9 can be determined from the feedback gain matrices of table III. For example, the peak force due to a rigid-body command in pitch ($\theta = 0.01$ rad) for $\omega_d = 0.1$ rad/sec comes from element $F_{4,1}$ of the feedback matrix of table III and is given by

$$f_{max} = (-223)(0.01) = -2.23 \text{ lb}$$

The corresponding peak force for $\omega_d = 0.2$ rad/sec would be

$$(-2.23)(0.2)^2/(0.1)^2 = -8.92 \text{ lb}$$

as is shown in figure 9(b). Peak control inputs for other combinations of rigid-body disturbances and frequencies can be calculated in a similar manner.

The rigid-body control requirements can be reduced by lowering the closed-loop frequency, but the time to damp an initial disturbance increases substantially, as shown in figure 10. Given is the time to damp an initial disturbance to 1 percent for $\zeta_d = 0.9$. The results shown are from time history computations but can be approximated for any closed-loop dynamics by the equation given in figure 10.

All previously presented results have been for the case where the flexible modes have been allowed to vibrate at their natural frequencies ($\omega_d = \omega_n$). The effect on control requirements of changes in the flexible-mode closed-loop frequency will now be presented. Figure 11 gives results obtained when the three flexible-mode frequencies were either increased or decreased by a certain percentage of their natural frequency. (The $\omega_d = \omega_n$ data correspond to previously given results for the controller arrangement of table III.)

Figure 11(a) shows total momentum and peak torque as a function of ω_d for various damping ratios for the six-torque case. As shown, the sensitivity to changes in vibration frequency (from ω_n) increases as the damping ratio is reduced. In general, the lowest control requirements occur at $\omega_d = \omega_n$. However, for damping ratios of 0.6 or greater, increases in the closed-loop frequency above ω_n lead to some reduction in total momentum with little increase in peak torque.

Figure 11(b) shows results of changes in the closed-loop vibration frequencies for the six-force case. The total impulse and peak force data of figure 11(b) follow similar trends to the previously discussed case using CMG controllers.

Figure 12 shows the effect on control requirements of setting all three flexible-mode frequencies at the same value. It is interesting to note that the minimum RCS control requirements occur approximately at the value for the lowest flexible-mode natural frequency. This is also true for the peak torque requirement of the CMG actuators. The trend of decreasing total momentum and impulse with decreasing damping ratio (figs. 8 and 11) is reversed in figure 12. That is, greater damping in the flexible modes generally gives lower momentum and impulse requirements. Also, for certain cases, the momentum and impulse requirements are competitive with those for which the vibration modes were left at their natural frequencies. For example, table VII compares CMG and RCS cases for which the vibration frequencies were all set at 1 rad/sec with a similar case for which the natural vibration mode frequencies were unchanged. For the RCS case of table VII with $\zeta_d = 0.6$, the total impulse is actually lower for $\omega_d = 1$ rad/sec than for $\omega_d = \omega_n$.

The previous discussions have considered rigid-body and flexible modes individually by varying their closed-loop dynamics (ζ_d, ω_d) and perturbing only the modes under consideration. What effect do the closed-loop dynamics of the unperturbed modes have on control requirements? For the idealized (perfect knowledge of antenna dynamics, no residual modes, perfect feedback measurements, etc.) results shown in the analysis, the unperturbed mode dynamics have no effect on control requirements, since the decoupling procedure does not disturb these modes.

Effect of Additional Modes on Control Requirements

Previously presented results have related to control of the rigid-body rotation modes and the first three flexible modes. The effect on control requirements of

including up to three additional flexible modes in the control law will now be considered. Results are limited to the case of CMG-type actuators located on the antenna column.

Results are summarized in table VIII for control of from six to nine modes. The desired closed-loop dynamics are given in the table, and results are shown for various combinations of initial disturbances in the rigid-body and flexible modes. The results of table VIII can be scaled to other initial conditions, as previously described.

Case 1 of table VIII is the previously discussed six-control case and is given for comparison. All other cases contain the CMG actuators for this case, plus additional actuators. Cases 2, 3, and 4 of table VIII give the minimum control requirements with respect to peak torque and total momentum for seven, eight, and nine controlled modes, respectively. (The F matrices and the nonzero portion of the B matrices are given in table IX for these cases.) Cases 5 to 7 were the next best controller arrangements found. (Replacing $T_{x,3}$ with $T_{x,4}$ gave virtually the same control requirements for the nine-control case as those of case 4 in table VIII.) Other actuator arrangements either gave an uncontrollable condition, or else the torque and momentum were orders of magnitude greater than those shown.

Consider case 2, the seven-control case, of table VIII as compared with the six-control case. Although the rigid-body control requirements increase only slightly, there is a large increase for initial disturbances in all flexible modes. (Note that for cases 2 and 3, including initial disturbances in the first three flexible modes only does not increase the control requirements substantially.) Case 3 of table VIII shows that inclusion of the eighth mode results in only slight increase in control requirements. However, the nine-mode case shows large increases in both rigid-body and flexible-mode control requirements.

Various approaches can be used to reduce the control requirements given in table VIII. The most obvious way is to reduce the damping in the flexible modes. Another method, which introduces time delays (lag) into the feedback gain matrix, will now be discussed.

Effects of Feedback Lag

An important characteristic of decoupled control is that columns of the feedback (or feedforward) gain matrix can be altered without affecting the decoupling process. The desired dynamics will be changed, but the system will still be decoupled. For example, multiplying a column corresponding to a particular rate feedback by a constant changes the desired damping ratio by that constant. (See eq. (B6).) Columns of the gain matrix can also be multiplied by time-varying quantities without affecting the decoupling. This approach was used to investigate the effect on control requirements of introducing time lag into the feedback matrix.

Time histories of the standard six-torque case of table III with and without lag are shown in figure 13. Figure 13(a) is for rigid-body disturbances with $\tau = 20$ sec, and figure 13(b) is for flexible-mode disturbances with $\tau = 10$ sec. Lag was introduced by multiplying the F matrix of table III by the quantity $(1 - e^{-t/\tau})$. The overall effect is that the closed-loop damping ratios increase from their natural values to 0.9, and the rigid-body frequencies rise from zero to 0.1 rad/sec as time increases. Note that, for both rigid-body and flexible disturbances, the peak torque and total momentum are reduced for the lagged cases of fig-

ure 13. The reduced control requirements do, however, result in an increased time to damp, as illustrated in the time histories in figure 13(b) and as shown in the following discussion.

Figure 14 shows the effect on control requirements of various lag times for the six-torque case of table III. Figure 14(a) gives results for rigid-body disturbances. Note that reductions in momentum and peak torque can be achieved with little increase in the time required to damp the initial disturbance.

Figure 14(b) gives results for disturbances in the flexible modes with the time-to-damp curve corresponding to the first flexible mode. As previously shown in figure 8(b), momentum and peak torque can also be lowered by reducing the closed-loop damping ratio in the flexible modes. For comparison purposes between reduced damping ratio and lag, suppose that it is desired to damp the first flexible mode to 1 percent in 20 sec. From figure 8(a), this would require $\zeta_d = 0.3$ and would result in a momentum and peak torque of 2640 ft-lb-sec and 154 ft-lb, respectively. Figure 14(b) shows that $\tau = 22.5$ sec would damp the mode in 20 sec and would result in momentum of 2480 ft-lb-sec and peak torque of 96 ft-lb. Thus, for this example, lag is more effective than reduced damping ratio.

Table X gives results for the eight-control case (case 3, table VIII) using lag, reduced flexible-mode damping, and combined lag and reduced damping. As shown in table X, significant reductions in control requirements are achieved, with the best result occurring in the case of reduced damping combined with lag. For this case, the 10-sec time constant increased the time to damp A_1 (to 1 percent) from 10 to about 18 sec.

Comparisons of Decoupled and Linear Quadratic Regulator Results

Control requirement comparisons are given in table XI for cases using the linear quadratic regulator (LQR) and decoupled approaches. The results shown are for three-axis CMG controllers at positions 1 and 2 on the antenna column. The procedure used for the LQR cases was to adjust the state variable weightings in the minimization function (diagonal of Q in eq. (11)) such that several sets of desired closed-loop dynamics were obtained. (The identity matrix was used for P.) The resultant damping ratios and undamped frequencies (ζ_d and ω_d) were then used as inputs to the decoupling program to calculate the decoupled gains. Thus, the closed-loop dynamics shown in table XI were identical for the LQR and decoupled comparison cases.

For all cases shown in table XI, the rigid-body modes have frequencies of about 0.1 rad/sec and damping ratios of about 0.9. The flexible-mode frequencies are near their natural values with damping ratios of about 0.9, 0.5, and 0.1 for cases 1, 2, and 3, respectively. The weightings (Q) required to obtain the dynamics shown in table XI, the associated LQR gains (K), and the decoupled feedback gains (F) are given in table XII. The B matrix is the same as that for the CMG case of table III.

Consider the cases shown in table XI with rigid-body disturbances. The total momentum results are comparable for the LQR and decoupled approaches, but the peak torques are lower for the LQR cases. For flexible disturbances, the peak torques are about the same, with the momentum being somewhat smaller for the LQR cases. Comparisons are also given in table XI for combined rigid-body and flexible disturbances.

Although the results of table XI tend to favor the LQR approach with respect to control requirements, the decoupled approach has advantages in other areas. For example, the decoupled feedback gains are computed in closed form and yield the exact desired closed-loop dynamics, but the LQR approach requires an iterative solution to obtain approximate desired closed-loop dynamics. Also, the decoupled gains give a known transient and steady-state response, whereas only the steady-state response is known by use of the LQR method. This is illustrated in figure 15 for case 2 of table XI. Shown are position, torque, and momentum responses for both rigid-body (fig. 15(a)) and flexible-mode (fig. 15(b)) disturbances. Note the transient excursions in the flexible-mode amplitudes in figure 15(a) and in the rigid-body attitude angles in figure 15(b) for the LQR cases.

The preceding comparisons are not intended to favor the LQR or the decoupled approach, since either method could be made superior for a given set of closed-loop dynamics. For example, lag could be introduced into the decoupled feedback gain matrix to produce reduced control requirements. The LQR results could also be improved with time-varying gains or by a judicious choice of weightings (P) on the control variables of equation (11). The results are only intended to show that for the conditions of table XI, the decoupled results are competitive with the LQR results. Further study of the two methods is warranted for the effects of spillover when residual modes are included in the analysis. Also, the two methods should be compared for the more practical situation where observers are incorporated into the control law design to estimate the required state variables.

Control of Rigid-Body Translation

Previously presented results have neglected the translation of the antenna center of gravity. This is adequate for angular-momentum-type (CMG) controllers but not for thruster (RCS) controllers. Results which include center-of-gravity translation effects will now be presented. The results are not intended as representative of control requirements for orbit changes, since more efficient methods exist for these maneuvers.

Translation modes (eq. (2)) were included by assuming that a three-axis RCS controller was located on the antenna column at the center of gravity such that it introduced no rotations. Since no modal data were available at this location, the data of table I at position 4 (near the c.g.) were used to approximate the effect of the flexible modes on the control requirements. Two controller arrangements were considered. In one case, three-axis RCS actuators were located at the c.g. and at positions 5 and 6. This was done for comparison with the standard six-mode RCS results previously presented. The second case used the c.g. thrusters along with three-axis CMG's at positions 1 and 2 for comparison with the previously given six-mode CMG results. In both cases, the modes controlled are the three translation, three rotation, and first three vibration modes. The nonzero rows (last 9) of the B matrix, the F matrix, and the associated state vector are given in table XIII for each of the cases considered.

Results for the previously described controller arrangements are given in table XIV for various combinations of rotation, translation, and flexible-mode initial conditions. Cases 1 and 2 of table XIV should be compared with cases 1 and 2 of table V to see the effects of adding c.g. control. Note that CMG control requirements are the same for cases 1 and 2 of tables XIV and V, since momentum devices do not cause translations of the antenna c.g. Cases 3 through 6 of table XIV show the effects of rigid-body translation commands. The arrangement which includes the six

CMG controllers provides the lowest RCS control requirements; however, some CMG control is required to maintain undisturbed vibrations.

The results of table XIV can be scaled to other initial conditions, as previously described. Also, the results (cases 3 to 6) can be scaled to other translation-mode closed-loop frequencies, as was the case with rotation modes. That is, the impulse and momentum are nearly linear functions of ω_{rb} and the peak forces and torques are functions of ω_{rb}^2.

CONCLUDING REMARKS

A study has been conducted of the feasibility of employing decoupling procedures to control a large flexible space antenna. Control involved commanding changes in the rigid-body modes or nulling initial disturbances in the flexible modes. The study was intended to provide preliminary engineering-type data, in parametric form, which would be useful in the final design of large space antenna control systems. The data illustrate the effect on control requirements of the number of modes controlled; of the number, type, and location of control actuators; and of variations in the closed-loop dynamics (frequency and damping ratio) of the control system. A brief analysis was also included which compared decoupled-control results with those obtained by using a linear quadratic regulator (LQR) approach. Observation based on the study indicates the following:

1. The location of controllers has a large effect on control requirements. For the limited amount of modal slope data, the best locations for two three-axis control-moment gyros (CMG's) were at the top and bottom of the column. When reaction-control-system (RCS) controllers were used, the lowest control requirements were obtained with the RCS units on the hoop. The optimum separation angle for two three-axis RCS units on the hoop was about 120° to 150°.

2. To minimize control requirements with respect to the selection of closed-loop damping ratio, large values (0.9 or greater) should be used for the rigid-body rotation modes, whereas the flexible modes should be damped as lightly as is practical. The lower limit on flexible-mode damping would be determined by mission requirements regarding the time to damp initial disturbances.

3. With regard to selecting the closed-loop frequency, rigid-body control requirements can be reduced by lowering the frequency; however, the time to damp an initial disturbance increases substantially. For vibration control, maintaining the closed-loop flexible-mode frequencies at their natural frequencies generally results in the lowest control requirements.

4. Increasing the number of flexible modes to be controlled (and the number of actuators) led to an increase in the control requirements. The increase was dramatic when the sixth flexible mode (nine controllers required) was added to the control law.

5. When a three-axis RCS controller was added at the center of gravity to control rigid-body translations, the arrangement which included six CMG controllers provided the lowest RCS control requirements. However, some CMG control was required to maintain undisturbed vibrations.

6. Incorporating lag into the feedback gains was an effective method of reducing control requirements without adversely affecting the decoupled performance. The

addition of lag gives an effect similar to that of lowering the closed-loop damping ratios.

7. For the present idealized cases, the decoupled-control results were comparable with LQR results with respect to control requirements. Further study of the two methods is warranted for the effects of spillover when residual modes are included in the analysis. Also, the two methods should be compared for the more practical situation where observers are incorporated into the control law design to estimate the required state variables.

Langley Research Center
National Aeronautics and Space Administration
Hampton, VA 23665
March 14, 1984

APPENDIX A

CONTROLLER ARRANGEMENT EXAMPLES

Controllers used in the analysis were either control-moment gyros (CMG's) or reaction-control-system (RCS) thrusters. The controllers were assumed to be perfect, in that no actuator dynamics were included in the analysis. They were used in a three-axis arrangement at points on the antenna such that control torques or forces were about the x-, y-, and z-directions as defined in figure 1. The manner in which the controllers were incorporated into the equations of motion is described below.

Consider the case of a three-axis RCS device located on the antenna column or hoop. The rigid-body rotation equations are given by

$$\ddot{\alpha} = \bar{I}^{-1} L \begin{Bmatrix} f_x \\ f_y \\ f_z \end{Bmatrix} \tag{A1}$$

where $\alpha = [\theta, \phi, \psi]^T$ and

$$\bar{I} = \begin{bmatrix} I_x & 0 & -I_{xz} \\ 0 & I_y & 0 \\ -I_{xz} & 0 & I_z \end{bmatrix}$$

For forces on the column at a distance ℓ above the center of gravity (fig. 1),

$$L = \begin{bmatrix} 0 & -\ell & 0 \\ \ell & 0 & 0 \\ 0 & 0 & 0 \end{bmatrix} \tag{A2}$$

For forces at an angle δ on the hoop (fig. 1),

$$L = \begin{bmatrix} 0 & \ell_z & r \sin \delta \\ -\ell_z & 0 & -r \cos \delta \\ -r \sin \delta & r \cos \delta & 0 \end{bmatrix} \tag{A3}$$

For the case of a three-axis CMG controller on the column, the rotation equations are given by

$$\ddot{\alpha} = \bar{I}^{-1} \begin{Bmatrix} T_x \\ T_y \\ T_z \end{Bmatrix} \tag{A4}$$

If more than three controllers are used, the control vector dimension increases, and the L and $\bar{I}$ matrices must be adjusted to be compatible with the controller arrangements, as shown in the following examples:

Consider the case of two three-axis RCS controllers located at positions 5 ($\delta = 0°$) and 6 ($\delta = 90°$) on the antenna hoop. The rigid-body rotation equations are given by

$$\ddot{\alpha} = \bar{I}^{-1} \begin{bmatrix} 0 & \ell_z & 0 & 0 & \ell_z & r \\ -\ell_z & 0 & -r & -\ell_z & 0 & 0 \\ 0 & r & 0 & -r & 0 & 0 \end{bmatrix} \bar{f} \tag{A5}$$

where $\bar{f} = [f_{x,5}, f_{y,5}, f_{z,5}, f_{x,6}, f_{y,6}, f_{z,6}]^T$. The first three vibration modes are given by

$$\begin{Bmatrix} \ddot{A}_1 \\ \ddot{A}_2 \\ \ddot{A}_3 \end{Bmatrix} = -\begin{Bmatrix} 2\zeta_{n,1}\omega_{n,1}\dot{A}_1 + \omega_{n,1}^2 A_1 \\ 2\zeta_{n,2}\omega_{n,2}\dot{A}_2 + \omega_{n,2}^2 A_2 \\ 2\zeta_{n,3}\omega_{n,3}\dot{A}_3 + \omega_{n,3}^2 A_3 \end{Bmatrix} \begin{bmatrix} \left(\phi_{x,5}^{(1)} & \phi_{y,5}^{(1)} & \phi_{z,5}^{(1)} & \phi_{x,6}^{(1)} & \phi_{y,6}^{(1)} & \phi_{z,6}^{(1)}\right)/m_1 \\ \left(\phi_{x,5}^{(2)} & \cdot & \cdot & \cdot & \cdot & \phi_{z,6}^{(2)}\right)/m_2 \\ \left(\phi_{x,5}^{(3)} & \cdot & \cdot & \cdot & \cdot & \phi_{z,6}^{(3)}\right)/m_3 \end{bmatrix} \bar{f} \tag{A6}$$

APPENDIX A

The superscripts on the mode shapes refer to the mode number, and the values are given in table I. For example $\phi^{(2)}_{x,5} = 0.2294$ and $\phi^{(3)}_{z,6} = -0.4889$. (Note that each element of the mode shape matrix is divided by the appropriate modal mass.)

Now consider three-axis CMG controllers at positions 1 and 2 on the column. The rotation equations are given by

$$\ddot{\bar{\alpha}} = \begin{bmatrix} \bar{I}^{-1} & \bar{I}^{-1} \end{bmatrix} \bar{T} \tag{A7}$$

where $\bar{T} = \left[T_{x,1}, T_{y,1}, T_{z,1}, T_{x,2}, T_{y,2}, T_{z,2}\right]^T$. The vibration equations would be the same as equations (A6) with $\bar{f}$ replaced by $\bar{T}$ and the mode shape matrix ϕ replaced by the mode slope matrix ϕ'. The elements of ϕ' come from table I at locations 1 and 2. For example, $\phi'^{(1)}_{x,1} = 0.2253 \times 10^{-3}$.

APPENDIX B

EXAMPLES OF DECOUPLING PROCEDURE

Decoupled gain matrix calculations are given below for the two most extensively studied actuator arrangements of the analysis. The first example uses two three-axis RCS controllers (six controls) located at positions 5 and 6 on the antenna hoop (fig. 1), and the second uses three-axis CMG controllers at positions 1 and 2 on the column. In each case, the controlled modes are the three rigid-body rotations and the first three flexible modes. Extensions to other actuator arrangements and to other controlled modes are straightforward.

Consider the RCS controller case of appendix A. Equations (A5) and (A6) can be written in state-vector notation as

$$\dot{\bar{x}}_{12\times1} = \begin{bmatrix} 0_{6\times6} & I_{6\times6} \\ - - - & - - - \\ -\Lambda_{6\times6} & -D_{6\times6} \end{bmatrix}_{12\times12} \bar{x}_{12\times1} + \begin{bmatrix} 0_{6\times6} \\ - - - - \\ R_{3\times6} \\ - - - - \\ \Phi_{3\times6} \end{bmatrix}_{12\times6} \bar{f}_{6\times1} = A\bar{x} + B\bar{f} \qquad \text{(B1)}$$

where the subscripts indicate the dimensions of the various elements, and

$$\bar{x} = \left[\theta,\ \phi,\ \psi,\ A_1,\ A_2,\ A_3,\ \dot{\theta},\ \dot{\phi},\ \dot{\psi},\ \dot{A}_1,\ \dot{A}_2,\ \dot{A}_3\right]^T$$

0 null matrix

I identity matrix

Λ $= \text{diag}\left(0,\ 0,\ 0,\ \omega_{n,1}^2,\ \omega_{n,2}^2,\ \omega_{n,3}^2\right)$

D $= \text{diag}\left(0,\ 0,\ 0,\ 2\zeta_{n,1}\omega_{n,1},\ 2\zeta_{n,2}\omega_{n,2},\ 2\zeta_{n,3}\omega_{n,3}\right)$

R matrix obtained from equation (A5) by multiplying $\bar{I}^{-1}$ by the 3 × 6 lever arm matrix

Φ mode shape matrix of equations (A6)

$\bar{f}$ defined in equation (A5)

The output quantities to be decoupled are the first six elements of $\bar{x}$. The decoupling procedure of reference 9 involves the time differentiation of the output variables until control quantities appear explicitly in the expression for y. The associated command $\bar{v}$ is then defined to give the desired transfer function between $\bar{v}$ and $\bar{y}$ and to permit solving for the control law in the form of equation (7) of the section on decoupled control.

APPENDIX B

Consider θ, the first variable to be decoupled:

$$y_1 = \theta$$

$$\ddot{y}_1 = \ddot{\theta} = (\text{Row 7 of B})\bar{f} \tag{B2}$$

We now add the desired second-order dynamics ($\omega_{d,\theta}$, $\zeta_{d,\theta}$) to both sides of equation (B2) and define this to be the command in pitch angle as follows:

$$\ddot{y}_\theta + 2\zeta_{d,\theta}\omega_{d,\theta}\dot{y}_\theta + \omega_{d,\theta}^2 y_\theta = 2\zeta_{d,\theta}\omega_{d,\theta}\dot{\theta} + \omega_{d,\theta}^2\theta + (\text{Row 7 of B})\bar{f} = \omega_{d,\theta}^2\theta_d \tag{B3}$$

Note that we are commanding a second-order response in pitch angle and that the command must be scaled to the desired frequency. Performing the above operations on the entire output vector gives

$$\left[\begin{array}{c} R \\ - - - \\ \Phi \end{array}\right]_{6\times6} \bar{f}_{6\times1} + \left[\begin{array}{c|c} & \\ \tilde{\Lambda}_{6\times6} & \tilde{D}_{6\times6} \\ & \end{array}\right]_{6\times12} \bar{x}_{12\times1} = \Lambda_{d_{6\times6}} \bar{v}_{6\times1} \tag{B4}$$

where $\Lambda_d = \text{diag}\left(\omega_{d,\theta}^2,\ \omega_{d,\phi}^2,\ \omega_{d,\psi}^2,\ \omega_{d,A_1}^2,\ \omega_{d,A_2}^2,\ \omega_{d,A_3}^2\right)$

$$\tilde{\Lambda} = \Lambda_d - \Lambda$$

$$\tilde{D} = \text{diag}\left(2\zeta_{d,\theta}\omega_{d,\theta},\ \ldots,\ 2\zeta_{d,A_3}\omega_{d,A_3}\right) - D$$

If the inverse of the control influence matrix $\left[\begin{array}{c} R \\ - - - \\ \Phi \end{array}\right]$ of equation (B4) exists, then the equation can be solved for the controls in the following form:

$$\underset{6\times1}{\bar{f}} = \underset{6\times12}{F}\ \underset{12\times1}{\bar{x}} + \underset{6\times6}{G}\ \underset{6\times1}{\bar{v}} \tag{B5}$$

where

$$F_{6\times12} = -\left[\begin{array}{c} R \\ - - - \\ \Phi \end{array}\right]^{-1}_{6\times6} \left[\begin{array}{c|c} \tilde{\Lambda} & \tilde{D} \end{array}\right]_{6\times12} \tag{B6}$$

and

$$G_{6\times6} = \left[\begin{array}{c} R \\ - - - \\ \Phi \end{array}\right]^{-1}_{6\times6} \Lambda_{d_{6\times6}} \tag{B7}$$

The elements of R and Φ are as defined in equations (A5) and (A6), respectively, of appendix A. For example, from tables I and II and figure 1, $R(1,2) = \ell_z = 677$ in., and $\Phi(2,1) = \phi^{(2)}_{x,5} / m_1 = 0.2294/153.157$. Note that the $\left[\begin{array}{c} R \\ - - - \\ \Phi \end{array}\right]$ matrix of equation (B6) is composed of only the nonzero rows of the B matrix of equation (B1). For the CMG controller case, the R matrix is replaced by the inertia matrix of equation (A7), and the mode shape matrix is replaced by the mode slope matrix, as explained in appendix A.

The B, F, and G matrices are given in table III for the previously discussed RCS and CMG cases. For these cases, the desired rigid-body frequencies (e.g., $\omega_{d,\theta}$) were set at 0.1 rad/sec, and the desired flexible-mode frequencies were taken to be the natural vibration frequencies of table II (e.g., $\omega_{d,A_1} = \omega_{n,1}$). The desired damping ratio for all modes was 0.9. The gain matrices of table III and of similar tables in the report are for the inch, pound, second system of units.

REFERENCES

1. Russell, R. A.; Campbell, T. G.; and Freeland, R. E.: A Technology Development Program for Large Space Antennas. NASA TM-81902, 1980.

2. Hamer, Harold A.; and Johnson, Katherine G.: Decoupled Control of a Long Flexible Beam in Orbit. NASA TP-1740, 1980.

3. Joshi, S. M.; and Groom, N. J.: Controller Design Approaches for Large Space Structures Using LQG Control Theory. Dynamics and Control of Large Flexible Spacecraft, L. Meirovitch, ed., American Inst. Aeronaut. & Astronaut., 1979, pp. 35-50.

4. Reddy, A. S. S. R.; Bainum, P. M.; Krishna, R.; and Hamer, H. A.: Control of a Large Flexible Platform in Orbit. J. Guid. & Control, vol. 4, no. 6, Nov.-Dec. 1981, pp. 642-649.

5. Joshi, S. M.: Attitude and Vibration Control of a Large Flexible Space-Based Antenna. NASA CR-165979, 1982.

6. Sullivan, Marvin R.: LSST (Hoop/Column) Maypole Antenna Development Program. NASA CR-3558, Part 2, 1982.

7. Balas, Mark J.: Trends in Large Space Structure Control Theory: Fondest Hopes, Wildest Dreams. IEEE Trans. Autom. Control, vol. AC-27, no. 3, June 1982, pp. 522-535.

8. Gilbert, Elmer G.; and Pivnichny, John R.: A Computer Program for the Synthesis of Decoupled Multivariable Feedback Systems. IEEE Trans. Autom. Control, vol. AC-14, no. 6, Dec. 1969, pp. 652-659.

9. Rekasius, Z. V.: Decoupling of Multivariable Systems by Means of State Variable Feedback. Proceedings Third Annual Allerton Conference on Circuit and System Theory, M. E. Van Valkenburg, ed., Univ. Illinois and Inst. Elec. Electron. Eng., Oct. 1965, pp. 439-448.

10. Kwakernaak, Huibert; and Sivan, Raphael: Linear Optimal Control Systems, John Wiley & Sons, Inc., c.1972.

11. Armstrong, Ernest S.: ORACLS - A System for Linear-Quadratic-Gaussian Control Law Design. NASA TP-1106, 1978.

TABLE I.- MODAL DATA

(a) Mode shape and mode slope data for column

Mode	Location	ϕ_x	ϕ_y	ϕ_z	ϕ'_x, in^{-1}	ϕ'_y, in^{-1}	ϕ'_z, in^{-1}
1	1	0	0.2137	0	0.2253×10^{-3}	0	-0.1799×10^{-1}
	2	0	-.0355	0	$-.6482 \times 10^{-4}$	0	$-.5786 \times 10^{-4}$
	3	0	.03883	0	$-.1115 \times 10^{-3}$	0	$-.8011 \times 10^{-2}$
	4	0	.2087	0	$-.1182 \times 10^{-3}$	0	$-.1096 \times 10^{-1}$
2	1	0.7087	0	-0.0097	0	-0.192×10^{-2}	0
	2	-.0921	0	-.0097	0	$.1666 \times 10^{-3}$	0
	3	.1467	0	-.0097	0	$.5137 \times 10^{-3}$	0
	4	1	0	-.0097	0	$.5408 \times 10^{-3}$	0
3	1	0	0.6703	0	0.1879×10^{-2}	0	0.2758×10^{-3}
	2	0	-.0678	0	$-.1902 \times 10^{-3}$	0	$.6176 \times 10^{-6}$
	3	0	.1634	0	$-.5025 \times 10^{-3}$	0	$.1262 \times 10^{-3}$
	4	0	1	0	$-.5063 \times 10^{-3}$	0	$.1706 \times 10^{-3}$
4	1	0	0	0	-0.1194×10^{-6}	0	0.1346×10^{-5}
	2	0	0	0	$.0270 \times 10^{-6}$	0	$-.3131 \times 10^{-4}$
	3	0	0	0	$.0332 \times 10^{-6}$	0	$.4615 \times 10^{-4}$
	4	0	-.0001	0	$.0239 \times 10^{-6}$	0	$.3700 \times 10^{-4}$
5	1	0	-0.1131	0	-0.2531×10^{-3}	0	-0.2282×10^{-4}
	2	0	-.0920	0	$-.4381 \times 10^{-2}$	0	$-.1665 \times 10^{-5}$
	3	0	.5482	0	$.5786 \times 10^{-3}$	0	$-.1127 \times 10^{-4}$
	4	0	-.0391	0	$.3076 \times 10^{-3}$	0	$-.1481 \times 10^{-4}$
6	1	0	0.0045	0	0.4311×10^{-4}	0	-0.2480×10^{-2}
	2	0	-.0007	0	$.5187 \times 10^{-4}$	0	$-.9804 \times 10^{-1}$
	3	0	.0010	0	$-.3416 \times 10^{-4}$	0	$-.3438 \times 10^{-1}$
	4	0	.0446	0	$-.4303 \times 10^{-5}$	0	$-.2455 \times 10^{-1}$

TABLE I.- Concluded

(b) Mode shape data for hoop

Mode	Location, δ, deg	ϕ_x	ϕ_y	ϕ_z
1	0 (position 5)	0	1	0
	15	.0177	.9977	-.0455
	30	.03411	.9908	-.0878
	45	.04820	.9800	-.1241
	60	.0590	.9659	-.1520
	75	.0658	.9494	-.1695
	90 (position 6)	.0683	.9318	-.1758
	105	.06589	.9141	-.1695
	120	.0591	.8977	-.1520
	135	.0482	.8836	-.1241
	150	.0341	.8727	-.0877
	165	.0176	.8659	-.0454
	180	0	.8636	0
2	0 (position 5)	0.2294	0	-0.5441
	15	.2208	-.0593	-.5226
	30	.1980	-.1145	-.4696
	45	.1616	-.1618	-.3853
	60	.1143	-.1982	-.2753
	75	.0592	-.2210	-.1472
	90 (position 6)	0	-.2286	-.0098
	105	-.0592	-.2210	.1278
	120	-.1143	-.1982	.2558
	135	-.1616	-.1618	.3658
	150	-.1980	-.1145	.4502
	165	-.2208	-.0593	.5032
	180	-.2294	0	.5246
3	0 (position 5)	0	0.2260	0
	15	.0592	.2182	-.1253
	30	.1142	.1953	-.2421
	45	.1615	.1590	-.3423
	60	.1978	.1117	-.4193
	75	.2206	.0565	-.4675
	90 (position 6)	.2297	-.00281	-.4889
	105	.2206	-.0621	-.4675
	120	.1978	-.1173	-.4193
	135	.1615	-.1646	-.3423
	150	.1142	-.2010	-.2421
	165	.0592	-.2238	-.1253
	180	0	-.2316	0
4	0 (position 5)	0	-0.07285	0
	15	↓	-.07283	↓
	30		-.07281	
	45		-.07280	
	60		-.07281	
	75		-.07283	
	90 (position 6)		-.07284	
	105		-.07281	
	120		-.07280	
	135		-.07280	
	150		-.07280	
	165		-.07282	
	180		-.07284	
5	0 (position 5)	0	-0.00363	0
	15	-.00106	-.00351	.02974
	30	-.00204	-.00316	.05745
	45	-.00288	-.00260	.08124
	60	-.00352	-.00187	.0995
	75	-.00389	-.00102	.1108
	90 (position 6)	-.00529	.00005	.1231
	105	-.00389	.00111	.1108
	120	-.00352	.00196	.0995
	135	-.00287	.00269	.0812
	150	-.00204	.00325	.0575
	165	-.00106	.00360	.0297
	180	0	.00372	0
6	0 (position 5)	0	1	0
	15	.00325	.9991	-.00172
	30	.00202	.9982	-.00158
	45	.00078	.9977	-.00142
	60	-.00051	.9977	-.00115
	75	-.00189	.9983	-.00072
	90 (position 6)	.00117	.9989	-.00225
	105	.00402	.9977	-.00313
	120	.00242	.9966	-.00231
	135	.00078	.9961	-.00142
	150	-.00091	.9962	-.00042
	165	-.00267	.9969	.00069
	180	0	.9977	0

TABLE II.- ANTENNA CHARACTERISTICS

[$I_x = 1.9577 \times 10^{10}$ lb-in^2; $I_y = 1.9566 \times 10^{10}$ lb-in^2;
$I_z = 1.499 \times 10^{10}$ lb-in^2; $I_{xz} = 0.8357 \times 10^{8}$ lb-in^2;
w = 10 020.3 lb]

Mode	ω_n, rad/sec	T_n, sec	ζ_n	m_n, lb-sec^2/in
1	0.7466	8.42	0.01	153.157
2	1.346	4.67	.01	5.233
3	1.7025	3.69	.01	3.073
4	3.1813	1.98	.01	.3046
5	4.5294	1.39	.02	1.993
6	5.5905	1.12	.02	723.522

TABLE III.- B, F, AND G MATRICES FOR SIX-CONTROL CASE OF APPENDIX B

$[\zeta_d = 0.9;\ \omega_{rb} = 0.1$ rad/sec; $\omega_{flex} = \omega_n]$

(a) Three-axis CMG controllers at positions 1 and 2 (fig. 1)

$B_{12\times6}$

0.	0.	0.	0.	0.	0.
0.	0.	0.	0.	0.	0.
0.	0.	0.	0.	0.	0.
0.	0.	0.	0.	0.	0.
0.	0.	0.	0.	0.	0.
0.	0.	0.	0.	0.	0.
.19737917E-07	0.	.11003987E-09	.19737917E-07	0.	.11003987E-09
0.	.19658120E-07	0.	0.	.19658120E-07	0.
.11003987E-09	0.	.25777798E-07	.11003987E-09	0.	.25777798E-07
.14712325E-05	0.	-.11745441E-03	-.42320542E-06	0.	-.37776195E-06
0.	-.36681003E-03	0.	0.	.31838614E-04	0.
.61143590E-03	0.	.89756447E-04	-.61885513E-04	0.	.20098311E-05

$F_{6\times12}$

-.46712427E+05	0.	.11921449E+04	0.	0.	0.
-.84082369E+06	0.	.21458608E+05	-.14761511E+04	0.	-.44912772E+04
0.	-.40627667E+05	0.	0.	0.	0.
0.	-.73129801E+06	0.	0.	.60100042E+04	0.
.10685880E+04	0.	.12632075E+04	0.	0.	0.
.19234584E+05	0.	.22737735E+05	.11327208E+05	0.	-.72674151E+02
-.45993871E+06	0.	.97063982E+03	0.	0.	0.
-.82788968E+07	0.	.17471517E+05	.14761511E+04	0.	.44912772E+04
0.	-.46806799E+06	0.	0.	0.	0.
0.	-.84252238E+07	0.	0.	-.60100042E+04	0.
.10941967E+04	0.	-.38920317E+06	0.	0.	0.
.19695540E+05	0.	-.70056570E+07	-.11327208E+05	0.	.72674151E+02

$G_{6\times6}$

.46712427E+07	0.	-.11921449E+06	.11107667E+04	0.	.14820496E+04
0.	.40627667E+07	0.	0.	-.25084746E+04	0.
-.10685880E+06	0.	-.12632075E+06	-.85234396E+04	0.	.23981307E+02
.45993871E+08	0.	-.97063982E+05	-.11107667E+04	0.	-.14820496E+04
0.	.46806799E+08	0.	0.	.25084746E+04	0.
-.10941967E+06	0.	.38920317E+08	.85234396E+04	0.	-.23981307E+02

TABLE III.- Concluded

(b) Three-axis RCS controllers at positions 5 and 6 (fig. 1)

$B_{12\times6}$

0.	0.	0.	0.	0.	0.
0.	0.	0.	0.	0.	0.
0.	0.	0.	0.	0.	0.
0.	0.	0.	0.	0.	0.
0.	0.	0.	0.	0.	0.
0.	0.	0.	0.	0.	0.
-.13311771E-04	.13630508E-04	0.	-.26470169E-06	.13365807E-04	.47479697E-04
0.	0.	-.47287744E-04	-.13311771E-04	0.	-.84876450E-13
-.26798102E-12	.62083189E-04	0.	-.62008674E-04	.74515152E-07	.26470169E-06
.43844165E-01	.65292350E-02	-.30658859E-12	.44562061E-03	.60839784E-02	-.11480484E-02
-.67151151E-10	-.44325882E-12	-.10397493E+00	.33665918E-06	-.43733215E-01	-.18666172E-02
	.73546530E-01	-.82997722E-10	.74749357E-01	-.91483437E-03	-.15908479E+00

$F_{6\times12}$

.21274325E+03	.30073311E+03	.15213955E+02	0.	0.	0.
.38293786E+04	.54131959E+04	.27385118E+03	-.19128428E+03	-.32769234E+02	.22883472E+02
-.22211148E+03	.20894115E-06	-.79846595E+02	0.	0.	0.
-.39980066E+04	.37609407E-05	-.14372387E+04	.63580122E+02	-.97413790E-08	-.21175510E+02
.28903092E+01	.12681319E+03	-.27204420E+02	0.	0.	0.
.52025566E+02	.22826374E+04	-.48967956E+03	.35949452E+02	.92247270E+01	-.48080123E+00
-.22301057E+03	.20894115E-06	.81425003E+02	0.	0.	0.
-.40141903E+04	.37609407E-05	.14656501E+04	.63580122E+02	-.97413789E-08	-.21175510E+02
.21531770E+03	-.21934680E-06	.79893382E+02	0.	0.	0.
.38757186E+04	-.39482424E-05	.14380809E+04	-.27983662E+03	.10166690E-07	.24119837E+02
-.20870887E+03	.29292501E-08	.88592644E+00	0.	0.	0.
-.37567596E+04	.52726501E-07	.15946676E+02	.60877442E+02	-.11972748E-09	-.82884506E+00

$G_{6\times6}$

-.21274325E+05	-.30073311E+05	-.15213955E+04	.14393662E+03	.13677327E+02	-.75511796E+01
.22211148E+05	-.20894115E-04	.79846595E+04	-.47842446E+02	.40658877E-08	.69875793E+01
-.28903092E+03	-.12681319E+05	.27204420E+04	-.27051060E+02	-.38502458E+01	.15865671E+00
.22301057E+05	-.20894115E-04	-.81425003E+04	-.47842445E+02	.40658877E-08	.69875793E+01
-.21531770E+05	.21934680E-04	-.79893382E+04	.21057003E+03	-.42434053E-08	-.79591603E+01
.20870887E+05	-.29292501E-06	-.88592644E+02	-.45808746E+02	.49972236E-10	.27350561E+00

TABLE IV.- ANTENNA RESPONSE TO STEP INPUTS

[1-in-lb torque or 1-lb force]

Mode	For $\phi = \phi' = 1$			A_s, in.	
	A_s, in.	A_{max}, in.	$\dot{A}_{max}$, in/sec	For $\lvert\phi_{max}\rvert$ on hoop	For $\lvert\phi'_{max}\rvert$ on column
1	0.0117	0.023	0.0086	0.0117	0.21×10^{-3}
2	.1054	.208	.140	.0573	$.20 \times 10^{-3}$
3	.1123	.221	.188	.0549	$.21 \times 10^{-3}$
4	.3244	.639	1.016	.0236	$.15 \times 10^{-4}$
5	.0245	.048	.109	.0030	$.11 \times 10^{-3}$
6	$.0044 \times 10^{-2}$	$.087 \times 10^{-3}$	$.243 \times 10^{-3}$	$.0044 \times 10^{-2}$	$.43 \times 10^{-5}$

TABLE V.- INITIAL-CONDITION EFFECTS ON CONTROL REQUIREMENTS

[$\zeta_d = 0.9$; $\omega_{rb} = 0.1$ rad/sec; $\omega_{flex} = \omega_n$]

Case	Initial conditions						Control requirements			
	Rigid-body, rad			Flexible, in.			Three-axis RCS at positions 5 and 6 on hoop (fig. 1)		Three-axis CMG at positions 1 and 2 on column (fig. 1)	
	θ	ϕ	ψ	A_1	A_2	A_3	$\lvert f_{max}\rvert$, lb	Impulse, lb-sec	$\lvert T_{max}\rvert$, ft-lb	Momentum, ft-lb-sec
1	0.01	0.01	0.01	0	0	0	5.3	125	390	9 217
2	0	0	0	1	1	1	74	653	278	3 878
3	.01	.01	.01	1	1	1	76	766	621	10 339
4	.01	0	0	0	0	0	2.2	84	389	3 250
5	0	.01	0	0	0	0	3.0	34	390	3 340
6	0	0	.01	0	0	0	.8	22	324	2 578
7	0	0	0	1	0	0	82	697	278	2 140
8	0	0	0	0	1	0	17	42	265	1 003
9	0	0	0	0	0	1	16	91	251	761
10	-.01	.01	-.01	0	0	0	3.0	92	390	9 217
11	0	0	0	-1	1	1	93	745	280	3 555
12	-.01	-.01	-.01	0	0	0	5.3	125	390	9 217
13	0	0	0	-1	-1	-1	93	829	278	3 878

TABLE VI.- CONTROL REQUIREMENTS FOR CMG LOCATIONS ON COLUMN

[$\zeta_d = 0.9$; $\omega_{rb} = 0.1$ rad/sec; $\omega_{flex} = \omega_n$]

Actuator locations (fig. 1)	Initial conditions		Control requirements	
	Rigid-body, rad	Flexible, in.	$\lvert T_{max} \rvert$, ft-lb	M, ft-lb-sec
1, 2	0.01	0	390	9 217
1, 3	.01	0	581	13 281
1, 4	.01	0	825	17 128
1, 2	0	1	278	3 878
1, 3	0	1	495	5 102
1, 4	0	1	702	6 507

TABLE VII.- FLEXIBLE-MODE CONTROL REQUIREMENTS FOR $\omega_d = 1$ rad/sec AND $\omega_d = \omega_n$

[Table III controller arrangements; $\zeta_d = 0.6$; Initial disturbances = 1 in.]

Parameter	$\omega_d = 1$ rad/sec	$\omega_d = \omega_n$
$\lvert T_{max} \rvert$, ft-lb	318	233
Momentum, ft-lb-sec ...	3780	3000
$\lvert f_{max} \rvert$, lb	108	65
Impulse, lb-sec	521	535

TABLE VIII.- EFFECT OF ADDITIONAL MODES ON CONTROL REQUIREMENTS

[Controllers 1 through 6 are three-axis CMG's at positions 1 and 2 (fig. 1); $\omega_{rb} = 0.1$ rad/sec; $\omega_{flex} = \omega_n$; $\zeta_d = 0.9$]

Case	Modes controlled	Controller			Initial conditions					Control requirements	
		7	8	9	Rigid-body, rad	Flexible, in.				$\lvert T_{max} \rvert$, ft-lb	Momentum, ft-lb-sec
						A_1-A_3	A_4	A_5	A_6		
1	6				0.01	0				390	9 217
					0	1				278	3 878
2	7	$T_{z,3}$			0.01	0	0			390	10 341
					0	1	0			278	4 311
					0	1	1			2 917	8 379
3	8	$T_{x,3}$	$T_{z,3}$		0.01	0	0	0		390	10 342
					0	1	0	0		265	4 199
					0	1	1	0		2 917	8 267
					0	1	1	1		2 917	8 539
4	9	$T_{x,3}$	$T_{z,3}$	$T_{z,4}$	0.01	0	0	0	0	28 313	467 869
					0	1	0	0	0	23 268	165 298
					0	1	1	0	0	50 551	181 456
					0	1	1	1	0	50 513	181 689
					0	1	1	1	1	1.503×10^8	1.515×10^8
5	7	$T_{z,4}$			0.01	0	0			390	11 218
					0	1	1			3 791	10 068
6	8	$T_{x,3}$	$T_{z,4}$		0.01	0	0	0		390	11 218
					0	1	1	1		3 791	10 068
7	8	$T_{z,3}$	$T_{z,4}$		0.01	0	0	0		390	10 342
					0	1	1	1		2 918	8 546

TABLE IX.- B AND F MATRICES FOR SEVEN, EIGHT, AND NINE CONTROLLED MODES USING CMG'S (CASES 2, 3, AND 4 OF TABLE VIII)

(a) Seven controlled modes

$B'_{7\times7}$

.19737917E-07	0.	.11003987E-09	.19737917E-07	0.	.11003987E-09
.11003987E-09					
0.	.19658120E-07	0.	0.	.19658120E-07	0.
0.					
.11003987E-09	0.	.25777798E-07	.11003987E-09	0.	.25777798E-07
.25777798E-07					
.14712325E-05	0.	-.11745441E-03	-.42320542E-06	0.	-.37776195E-06
-.52310300E-04					
0.	-.36681003E-03	0.	0.	.31838614E-04	0.
0.					
.61143590E-03	0.	.89756447E-04	-.61885513E-04	0.	.20098311E-05
.41067000E-04					
-.39200000E-06	0.	.44190000E-05	.89000000E-07	0.	-.10280000E-03
.15150000E-03					

$F_{7\times14}$

-.46712554E+05	0.	.12308675E+04	0.	0.	0.
0.	-.84082596E+06	0.	.22155616E+05	-.14749752E+04	0.
-.44912826E+04	.54797917E+01				
0.	-.40627667E+05	0.	0.	0.	0.
0.	0.	-.73129801E+06	0.	0.	.60100042E+04
0.	0.				
.78883708E+03	0.	.87119300E+05	0.	0.	0.
0.	.14199067E+05	0.	.15681474E+07	.13934524E+05	0.
-.84757525E+02	.12149819E+05				
-.45993859E+06	0.	.93191712E+03	0.	0.	0.
0.	-.82788946E+07	0.	.16774509E+05	.14749752E+04	0.
.44912826E+04	-.54797946E+01				
0.	-.46806799E+06	0.	0.	0.	0.
0.	0.	-.84252238E+07	0.	0.	-.60100042E+04
0.	0.				
.74327849E+03	0.	-.28150569E+06	0.	0.	0.
0.	.13379013E+05	0.	-.50671025E+07	-.80566034E+04	0.
.57516924E+02	.15240675E+05				
.63066911E+03	0.	-.19355357E+06	0.	0.	0.
0.	.11352044E+05	0.	-.34839643E+07	-.58779205E+04	0.
.27240700E+02	-.27390495E+05				

TABLE IX.- Continued

(b) Eight controlled modes

$B'_{8\times8}$

.19737917E-07	0.	.11003987E-09	.19737917E-07	0.	.11003987E-09
.19737917E-07	.11003987E-09				
0.	.19658120E-07	0.	0.	.19658120E-07	0.
0.	0.				
.11003987E-09	0.	.25777798E-07	.11003987E-09	0.	.25777798E-07
.11003987E-09	.25777798E-07				
.14712325E-05	0.	-.11745441E-03	-.42320542E-06	0.	-.37776195E-06
-.72800000E-06	-.52310000E-04				
0.	-.36681003E-03	0.	0.	.31838614E-04	0.
0.	0.				
.61143590E-03	0.	.89756447E-04	-.61885513E-04	0.	.20098311E-05
-.16350000E-03	.41067000E-04				
-.39200000E-06	0.	.44190000E-05	.89000000E-07	0.	-.10280000E-03
.10900000E-06	.15150000E-03				
-.12700000E-03	0.	-.11450000E-04	-.21980000E-02	0.	-.83500030E-06
.29030000E-03	-.56300000E-05				

$F_{8\times16}$

-.10150999E+06	0.	.13320395E+04	0.	0.	0.
0.	0.	-.18271799E+07	0.	.23976711E+05	-.13039109E+04
0.	-.39900817E+04	.47406686E+01	-.42958647E+03		
0.	-.40627667E+05	0.	0.	0.	0.
0.	0.	0.	-.73129801E+06	0.	0.
.60100042E+04	0.	0.	0.		
.90173030E+03	0.	.87119092E+05	0.	0.	0.
0.	0.	.16231145E+05	0.	.15681437E+07	.13934171E+05
0.	-.85790094E+02	.12149821E+05	.88503040E+00		
-.42090792E+05	0.	.16044902E+03	0.	0.	0.
0.	0.	-.75763426E+06	0.	.28880823E+04	.17055563E+03
0.	.66946741E+03	.15625216E+00	.32757327E+04		
0.	-.46806799E+06	0.	0.	0.	0.
0.	0.	0.	-.84252238E+07	0.	0.
-.60100042E+04	0.	0.	0.		
.75307835E+03	0.	-.28150571E+06	0.	0.	0.
0.	0.	.13555410E+05	0.	-.50671028E+07	-.80566340E+04
0.	.57427191E+02	.15240676E+05	.76826340E-01		
-.36305035E+06	0.	.67029615E+03	0.	0.	0.
0.	0.	-.65349063E+07	0.	.12065331E+05	.11333552E+04
0.	.33206143E+04	-.48969237E+01	-.28461462E+04		
.50797597E+03	0.	-.19355334E+06	0.	0.	0.
0.	0.	.91435675E+04	0.	-.34839602E+07	-.58775375E+04
0.	.28362905E+02	-.27390497E+05	-.96185726E+00		

TABLE IX.- Concluded

(c) Nine controlled modes

$B_{9\times9}$

.19737917E-07	0.	.11003987E-09	.19737917E-07	0.	.11003987E-09
.19737917E-07	.11003987E-09	.11003987E-09			
0.	.19658120E-07	0.	0.	.19658120E-07	0.
0.	0.	0.			
.11003987E-09	0.	.25777798E-07	.11003987E-09	0.	.25777798E-07
.11003987E-09	.25777798E-07	.25777798E-07			
.14712325E-05	0.	-.11745441E-03	-.42320542E-06	0.	-.37776195E-06
-.72800000E-06	-.52310000E-04	-.71560000E-04			
0.	-.36681003E-03	0.	0.	.31838614E-04	0.
0.	0.	0.			
.61143590E-03	0.	.89756447E-04	-.61885513E-04	0.	.20098311E-05
-.16350000E-03	.41070000E-04	.55520000E-04			
-.39200000E-06	0.	.44190000E-05	.89000000E-07	0.	-.10280000E-03
.10900000E-06	.15150000E-03	.12150000E-03			
-.12700000E-03	0.	-.11450000E-04	-.21980000E-02	0.	-.83500000E-06
.29030000E-03	-.56300000E-05	-.74310000E-05			
.59600000E-07	0.	-.34350000E-05	.71700000E-07	0.	-.13600000E-03
-.47200000E-07	-.47500000E-04	-.33930000E-04			

$F_{9\times18}$

-.10150408E+06	0.	-.96377126E+03	0.	0.	0.
0.	0.	0.	-.18270734E+07	0.	-.17347883E+05
-.13684780E+04	0.	-.39896336E+04	.44444002E+02	-.42960476E+03	-.47895189E+03
0.	-.40627667E+05	0.	0.	0.	0.
0.	0.	0.	0.	-.73129801E+06	0.
0.	.60100042E+04	0.	0.	0.	0.
.24304934E+05	0.	-.89947740E+07	0.	0.	0.
0.	0.	0.	.43748881E+06	0.	-.16190593E+09

-.24149075E+06	0.	.16869523E+04	.16873030E+06	-.71456269E+02	-.18940332E+07
-.42089119E+05	0.	-.48894023E+03	0.	0.	0.
0.	0.	0.	-.75760414E+06	0.	-.88009241E+04
.15229150E+03	0.	.66959416E+03	.11331976E+02	.32757275E+04	-.13540369E+03
0.	-.46806799E+06	0.	0.	0.	0.
0.	0.	0.	0.	-.84252238E+07	0.
0.	-.60100042E+04	0.	0.	0.	0.
-.24274215E+04	0.	.95272529E+06	0.	0.	0.
0.	0.	0.	-.43693586E+05	0.	.17149055E+08
.26655662E+05	0.	-.18348884E+03	-.60386423E+04	.99080227E+01	.25739948E+06
-.36305794E+06	0.	.36154969E+04	0.	0.	0.
0.	0.	0.	-.65350429E+07	0.	.65078945E+05
.12161865E+04	0.	.33200393E+04	-.55775995E+02	-.28461227E+04	.61435575E+03
.68064221E+05	0.	-.26409563E+08	0.	0.	0.
0.	0.	0.	.12251560E+07	0.	-.47537213E+09
-.74319321E+06	0.	.51456033E+04	.42459843E+06	-.20978398E+03	-.54673615E+07
-.87778949E+05	0.	.34063672E+08	0.	0.	0.
0.	0.	0.	-.15800211E+07	0.	.61314609E+09
.95802830E+06	0.	-.66490668E+04	-.58729009E+06	.27133222E+03	.71039953E+07

TABLE X.- EFFECT OF LAG AND REDUCED DAMPING ON CONTROL REQUIREMENTS FOR EIGHT-CONTROL CASE

[ω_{rb} = 0.1 rad/sec; $\omega_{flex} = \omega_n$; ζ_{rb} = 0.9]

Initial conditions		$\zeta_{d_{flex}}$	τ, sec	Control requirements	
Rigid-body, rad	Flexible, in.			$\lvert T_{max} \rvert$, ft-lb	Momentum, ft-lb-sec
0.01	0	0.9	0 30	390 80	10 342 8 151
0	1	0.9	0 10	2917 722	8 539 5 221
0	1	(a) (a)	0 10	930 270	4 975 4 214

[a]

Mode	ζ_d
1	0.62
2	.34
3	.27
4	.14
5	.10

t_1 = 10 sec for all modes for τ = 0.

TABLE XI.- COMPARISON OF DECOUPLED AND LQR RESULTS

[Three-axis CMG controllers at positions 1 and 2 on antenna column (fig. 1)]

(a) Decoupled and LQR results

Case	Initial conditions		Control requirements			
			LQR		Decoupled	
	Rigid-body, rad	Flexible, in.	$\lvert T_{max} \rvert$, ft-lb	Momentum, ft-lb-sec	$\lvert T_{max} \rvert$, ft-lb	Momentum, ft-lb-sec
1	0.01	0	292	9 895	488	9 910
	0	1	276	3 543	278	3 850
	.01	1	342	10 542	614	10 652
2	0.01	0	281	9 945	486	9 876
	0	1	210	2 400	212	2 850
	.01	1	310	10 152	539	10 560
3	0.01	0	267	9 976	485	9 860
	0	1	63	1 355	65	2 378
	.01	1	270	9 996	484	10 716

(b) Closed-loop characteristics

Case	Mode											
	θ		ϕ		ψ		A_1		A_2		A_3	
	ω, rad/sec	ζ	ω, rad/sec	ζ	ω, rad/sec	ζ	ω, rad/sec	ζ	ω, rad/sec	ζ	ω, rad/sec	ζ
1	0.099	0.903	0.112	0.900	0.112	0.901	0.7482	0.885	1.342	0.898	1.681	0.897
2	.098	.904	.112	.900	.112	.901	.7453	.502	1.345	.511	1.700	.502
3	.098	.904	.112	.900	.113	.901	.7465	.099	1.346	.106	1.7025	.107

TABLE XII.- F, K, AND Q FOR DECOUPLED AND LQR COMPARISONS

(a) Case 1 of table XI

$F_{6\times12}$

-.45853170E+05	0.	.14932910E+04	-.26067349E+01	0.	.10681548E+03
-.83564059E+06	0.	.24043959E+05	-.14537522E+04	0.	-.44184043E+04
0.	-.50799667E+05	0.	0.	-.25961151E+02	0.
0.	-.81788281E+06	0.	0.	.59784666E+04	0.
.10489317E+04	0.	.15823046E+04	.20002713E+02	0.	.17284002E+01
.19120591E+05	0.	.25477197E+05	.11155330E+05	0.	-.71494983E+02
-.45147831E+06	0.	.12156318E+04	.26067349E+01	0.	-.10681548E+03
-.82298323E+07	0.	.19576500E+05	.14537522E+04	0.	.44184043E+04
0.	-.58525875E+06	0.	0.	.25961151E+02	0.
0.	-.94227601E+07	0.	0.	-.59784666E+04	0.
.10740694E+04	0.	-.48751925E+06	-.20002713E+02	0.	-.17284002E+01
.19578816E+05	0.	-.78497046E+07	-.11155330E+05	0.	.71494983E+02

$K_{6\times12}$

-.285971E+06	0.	.701406E+04	-.257889E+03	0.	-.365543E+03	-.486034E+07	0.
.140734E+06	-.914093E+03	0.	-.477448E+04				
0.	-.278133E+06	0.	0.	.488266E+03	0.	0.	-.480329E+07
0.	0.	.643333E+04	0.				
-.872581E+04	0.	-.152320E+06	.704276E+03	0.	-.229736E+03	-.155924E+06	0.
-.312996E+07	.109030E+05	0.	-.540861E+03				
-.343719E+06	0.	-.111154E+04	-.125926E+02	0.	-.410158E+03	-.553534E+07	0.
-.184118E+05	.160365E+03	0.	.505307E+03				
0.	-.350203E+06	0.	0.	.547471E+03	0.	0.	-.565439E+07
0.	0.	-.604017E+03	0.				
-.136273E+04	0.	-.216213E+06	.876265E+03	0.	-.298839E+02	-.141644E+05	0.
-.402198E+07	-.157822E+03	0.	-.850990E+01				

$Q = \mathrm{diag}(0.2 \times 10^{12}, 0.2 \times 10^{12}, 0.7 \times 10^{11}, 1, 1, 1, 0.2 \times 10^{14}, 0.2 \times 10^{14}, 0.92 \times 10^{13}, 0.125 \times 10^{9}, 0.43 \times 10^{8}, 0.24 \times 10^{8})$

TABLE XII.- Continued

(b) Case 2 of table XI

$F_{6\times12}$

-.45305922E+05	0.	.14898239E+04	.21874124E+01	0.	.13463266E+02
-.83136227E+06	0.	.24018963E+05	-.81472311E+03	0.	-.24805082E+04
0.	-.50605413E+05	0.	0.	-.83696319E+01	0.
0.	-.81650799E+06	0.	0.	.33828143E+04	0.
.10364129E+04	0.	.15786309E+04	-.16785053E+02	0.	-.21785149E+00
.19018145E+05	0.	.25450711E+05	.62517569E+04	0.	-.40137542E+02
-.44609002E+06	0.	.12130090E+04	-.21874124E+01	0.	-.13463266E+02
-.81857380E+07	0.	.19556148E+05	.81472311E+03	0.	.24805082E+04
0.	-.58302077E+06	0.	0.	.83696319E+01	0.
0.	-.94069209E+07	0.	0.	-.33828143E+04	0.
-.10612506E+04	0.	-.48636736E+06	.16785053E+02	0.	-.21785149E+00
.19473915E+05	0.	-.78415440E+07	-.62517569E+04	0.	.40137542E+02

$K_{6\times12}$

-.298954E+06	0.	.549278E+04	-.164308E+03	0.	-.217185E+03	-.496916E+07	0.	
.105906E+06	-.379852E+03	0.	-.265962E+04					
0.	-.293977E+06	0.	0.	.298704E+03	0.	0.	-.493832E+07	
0.	0.	.363859E+04	0.					
-.643776E+04	0.	-.166435E+06	.446188E+03	0.	-.160382E+03	-.111494E+06	0.	
-.327119E+07	.619151E+04	0.	-.324594E+03					
-.332541E+06	0.	-.921316E+03	.915410E+00	0.	-.234356E+03	-.535499E+07	0.	
-.134411E+05	.804148E+02	0.	.281736E+03					
0.	-.337012E+06	0.	0.	.319770E+03	0.	0.	-.543606E+07	
0.	0.	-.342500E+03	0.					
-.128526E+04	0.	-.205592E+06	.519965E+03	0.	-.221741E+02	-.124421E+05	0.	
-.380137E+07	-.935697E+02	0.	-.362612E+01					

$Q = \mathrm{diag}(0.2 \times 10^{12}, 0.2 \times 10^{12}, 0.7 \times 10^{11}, 1, 1, 1, 0.2 \times 10^{14}, 0.2 \times 10^{14}, 0.92 \times 10^{13}, 0.41 \times 10^{8}, 0.14 \times 10^{8}, 0.76 \times 10^{7})$

TABLE XII.- Concluded

(c) Case 3 of table XI

$F_{6\times12}$

-.45062430E+05	0.	.14882251E+04	.13268063E+00	0.	.25231524E+00
-.82931792E+06	0.	.24007403E+05	-.14836703E+03	0.	-.48801948E+03
0.	-.50515674E+05	0.	0.	-.33763441E+00	0.
0.	-.81585620E+06	0.	0.	.64979661E+03	0.
.10308428E+04	0.	.15769368E+04	-.10181215E+01	0.	.40827575E-02
.18971379E+05	0.	.25438462E+05	.11364906E+04	0.	-.78967296E+01
-.44369255E+06	0.	.12117072E+04	-.13268063E+00	0.	-.25231524E+00
-.81656090E+07	0.	.19546737E+05	.14836703E+03	0.	.48801948E+03
0.	-.58198689E+06	0.	0.	.33763441E+00	0.
0.	-.93994116E+07	0.	0.	-.64979661E+03	0.
.10555470E+04	0.	-.48586539E+06	.10181215E+01	0.	-.40827575E-02
.19426022E+05	0.	-.78377702E+07	-.11364906E+04	0.	.78967296E+01

$K_{6\times12}$

-.312787E+06	0.	.833640E+03	-.120151E+02	0.	-.461109E+02	-.507625E+07	0.	
.179102E+05	-.176532E+02	0.	-.520975E+03					
0.	-.311818E+06	0.	0.	.624999E+02	0.	0.	-.507598E+07	
0.	0.	.698589E+03	0.					
-.543540E+03	0.	-.183155E+06	.955343E+02	0.	-.176351E+02	-.463744E+04	0.	
-.341430E+07	.114810E+04	0.	-.751563E+02					
-.319630E+06	0.	-.562527E+02	.448101E+00	0.	-.468306E+02	-.515321E+07	0.	
.333990E+04	.654177E+01	0.	.552133E+02					
0.	-.320577E+06	0.	0.	.633714E+02	0.	0.	-.517479E+07	
0.	0.	-.659323E+02	0.					
-.699901E+03	0.	-.190929E+06	.969607E+02	0.	-.679017E+01	-.306160E+04	0.	
-.351542E+07	-.181059E+02	0.	-.198487E+01					

$Q = \mathrm{diag}(0.2 \times 10^{12},\ 0.2 \times 10^{12},\ 0.7 \times 10^{11},\ 1,\ 1,\ 1,\ 0.2 \times 10^{14},\ 0.2 \times 10^{14},\ 0.92 \times 10^{13},\ 0.16 \times 10^{7},\ 0.7 \times 10^{6},\ 0.34 \times 10^{6})$

TABLE XIII.- B AND F MATRICES FOR C.G. CONTROL CASES OF TABLE XIV

(a) RCS controllers at positions 4, 5, and 6 (fig. 1)

$B'_{9\times9}$

0.	.13630508E-04	0.	-.26470169E-06	.13365807E-04	.47479607E-04
0.	0.	0.			
-.13311771E-04	0.	-.47287744E-04	-.13311771E-04	0.	0.
0.	0.	0.			
0.	.62083109E-04	0.	-.62008674E-04	.74515041E-07	.26470169E-06
0.	0.	0.			
-.26798102E-12	.65292350E-02	-.30658859E-12	.44562061E-03	.60839784E-02	-.11480484E-02
0.	.13626513E-02	0.			
.43844165E-01	-.44325842E-12	-.10397493E+00	.33655918E-06	-.43733215E-01	-.18666172E-02
.19109665E+00	0.	-.18536375E-02			
-.67151151E-10	.73546530E-01	-.62997656E-10	.74749357E-01	-.91483437E-03	-.15908479E+00
0.	.32540495E+00	0.			
.38560000E-01	0.	0.	.38560000E-01	0.	0.
.38560000E-01	0.	0.			
0.	.38560000E-01	0.	0.	.38560000E-01	0.
0.	.38560000E-01	0.			
0.	0.	.38560000E-01	0.	0.	.38560000E-01
0.	0.	.38560000E-01			

$F_{9\times18}$

.23958737E+03	-.18223504E+03	-.14112735E+03	0.	0.	0.
-.41819637E+00	-.51558609E+00	.40565048E-02	.43125726E+04	-.32802307E+04	-.25402924E+04
.44610350E+03	.20217584E+02	.14255136E+02	-.75275346E+01	-.92806017E+01	.73017086E-01
-.23582174E+03	.57019242E-07	-.79752176E+02	0.	0.	0.
-.11336461E-09	.52335642E+00	.11001358E-11	-.42447913E+04	.10263463E-05	-.14355302E+04
-.37283896E+03	.54806053E-08	-.15233673E+02	-.20405630E-08	.94204155E+01	.19802445E-10
-.80694486E+00	.26277149E+03	.16779974E+02	0.	0.	0.
.11772467E+00	-.21865773E-02	-.11419293E-02	-.14525006E+02	.47298868E+04	.30203954E+03
-.20624335E+02	-.56913658E+01	.27546391E+00	.21190441E+01	-.39358392E-01	-.20554728E-01
-.23672043E+03	.57019116E-07	.81519422E+02	0.	0.	0.
-.11336450E-09	.52335642E+00	.10997855E-11	-.42609750E+04	.10263441E-05	.14673496E+04
-.37283896E+03	.54806063E-08	-.15233673E+02	-.20405609E-08	.94204155E+01	.19796138E-10
.22961407E+03	-.60799395E-07	.79794927E+02	0.	0.	0.
.11832425E-09	-.54572958E+00	-.11481616E-11	.41330532E+04	-.10943891E-05	.14363087E+04
.17523912E+03	-.57203649E-08	.17923991E+02	.21298372E-08	-.98231324E+01	-.20666909E-10
-.20887386E+03	.10644852E-08	.88706272E+00	0.	0.	0.
-.13959927E-11	.62981734E-02	.13742670E-13	-.37597295E+04	.19160734E-07	.15967129E+02
.55625489E+02	.67523650E-10	-.75733983E+00	-.25127869E-10	.11336712E+00	.24736805E-12
-.28665307E+01	.18223504E+03	.39607932E+02	0.	0.	0.
.15886027E+00	-.77674347E-02	-.40565048E-02	-.51597552E+02	.32802307E+04	.10729428E+04
-.73264531E+02	-.20217584E+02	.97453749E+00	.28594848E+01	-.13981382E+00	-.73017086E-01
.62076696E+01	.37800947E-08	-.42750583E-01	0.	0.	0.
-.49596850E-11	-.23696294E+00	.47950654E-13	.11173805E+03	.68041704E-07	-.76951050E+00
.19759985E+03	.23978403E-09	-.26903177E+01	-.89274330E-10	-.42653329E+01	.86311177E-12
.20968080E+03	-.26277149E+03	-.17667037E+02	0.	0.	0.
-.11772467E+00	-.41115950E-02	-.65819417E+00	.37742545E+04	-.47298868E+04	-.31800667E+03
-.35001104E+02	.56913658E+01	.48187593E+00	-.21190441E+01	-.74008728E-01	-.46474951E+01

$$\bar{\chi} = (\theta,\ \phi,\ \psi,\ A_1,\ A_2,\ A_3,\ X,\ Y,\ Z,\ \dot{\theta},\ \dot{\phi},\ \dot{\psi},\ \dot{A}_1,\ \dot{A}_2,\ \dot{A}_3,\ \dot{X},\ \dot{Y},\ \dot{Z})^T$$

TABLE XIII.- Concluded

(b) CMG controllers at positions 1 and 2 and RCS controllers at position 4 (fig. 1)

$B'_{9\times9}$

.19737917E-07	0.	.11003987E-09	.19737917E-07	0.	.11003987E-09
0.	0.	0.			
0.	.19658120E-07	0.	0.	.19658120E-07	0.
0.	0.	0.			
.11003987E-09	0.	.25777798E-07	.11003987E-09	0.	.25777798E-07
0.	0.	0.			
.14712325E-05	0.	-.11745441E-03	-.42320542E-06	0.	-.37776195E-06
0.	.13626513E-02	0.			
0.	-.36681003E-03	0.	0.	.31838614E-04	0.
.19109665E+00	0.	-.18536375E-02			
.61143590E-03	0.	.89756447E-04	-.61885513E-04	0.	.20098311E-05
0.	.32540495E+00	0.			
0.	0.	0.	0.	0.	0.
.38560000E-01	0.	0.			
0.	0.	0.	0.	0.	0.
0.	.38560000E-01	0.			
0.	0.	0.	0.	0.	0.
0.		.38560000E-01			

$F_{9\times18}$

-.46712427E+05	0.	.11921449E+04	0.	0.	0.
0.	.12546158E+03	0.	-.84082369E+06	0.	.21458608E+05
-.14761511E+04	0.	-.44912772E+04	0.	.22583085E+04	0.
0.	-.40627667E+05	0.	0.	0.	0.
-.12431564E+03	0.	.12058617E+01	0.	-.73129801E+06	0.
0.	.60100042E+04	0.	-.22376815E+04	0.	.21705511E+02
.10685880E+04	0.	.12632075E+04	0.	0.	0.
0.	-.98828850E+00	0.	.19234584E+05	0.	.22737735E+05
.11327208E+05	0.	-.72674151E+02	0.	-.17789193E+02	0.
-.45993871E+06	0.	.97063982E+03	0.	0.	0.
0.	-.12546158E+03	0.	-.82788968E+07	0.	.17471517E+05
.14761511E+04	0.	.44912772E+04	0.	-.22583085E+04	0.
0.	-.46806799E+06	0.	0.	0.	0.
.12431564E+03	0.	-.12058617E+01	0.	-.84252238E+07	0.
0.	-.60100042E+04	0.	.22376815E+04	0.	0.
.10941967E+04	0.	-.38920317E+06	0.	0.	-.21705511E+02
0.	.98828850E+00	0.	.19695540E+05	0.	0.
-.11327208E+05	0.	.72674151E+02	0.	.17789193E+02	-.70056570E+07
0.	.40598426E-12	0.	0.	0.	0.
-.25933610E+00	0.	-.16717650E-16	0.	.73077167E-11	0.
0.	-.62882158E-13	0.	-.46680498E+01	0.	0.
-.39896290E-12	0.	.11391269E-13	0.	0.	-.30091770E-15
0.	-.25933610E+00	0.	-.71813322E-11	0.	0.
-.17298105E-13	0.	-.39171693E-13	0.	-.46680498E+01	.20504284E-12
0.	0.	0.	0.	0.	0.
0.	0.	-.25933610E+00	0.	0.	0.
0.	0.	0.	0.	0.	-.46680498E+01

TABLE XIV.- EFFECT OF ADDING CENTER-OF-GRAVITY TRANSLATION CONTROL TO CMG AND RCS CASES OF TABLE III

$[\zeta_d = 0.9;\quad \omega_{rb} = 0.1 \text{ rad/sec};\quad \omega_{flex} = \omega_n]$

Case	Initial conditions					Control requirements					
			c.g., in.			Nine RCS controllers		Three RCS and six CMG controllers			
	Rotation, rad	Flexible, in.	X	Y	Z	$\lvert f_{max} \rvert$, lb	Impulse, lb-sec	$\lvert f_{max} \rvert$, lb	Impulse, lb-sec	$\lvert T_{max} \rvert$, ft-lb	Momentum, ft-lb-sec
1	0.01	0	0	0	0	3.2	131	0	0	390	9217
2	0	1	0	0	0	146	1851	0	0	278	3878
3	0	0	1	1	1	.93	27	.26	6	10.5	328
4	0	0	1	0	0	.42	6.4	.26	2	10.4	163
5	0	0	0	1	0	.55	19	.26	2	10.5	166
6	0	0	0	0	1	.26	2.1	.26	2	.1	1.6

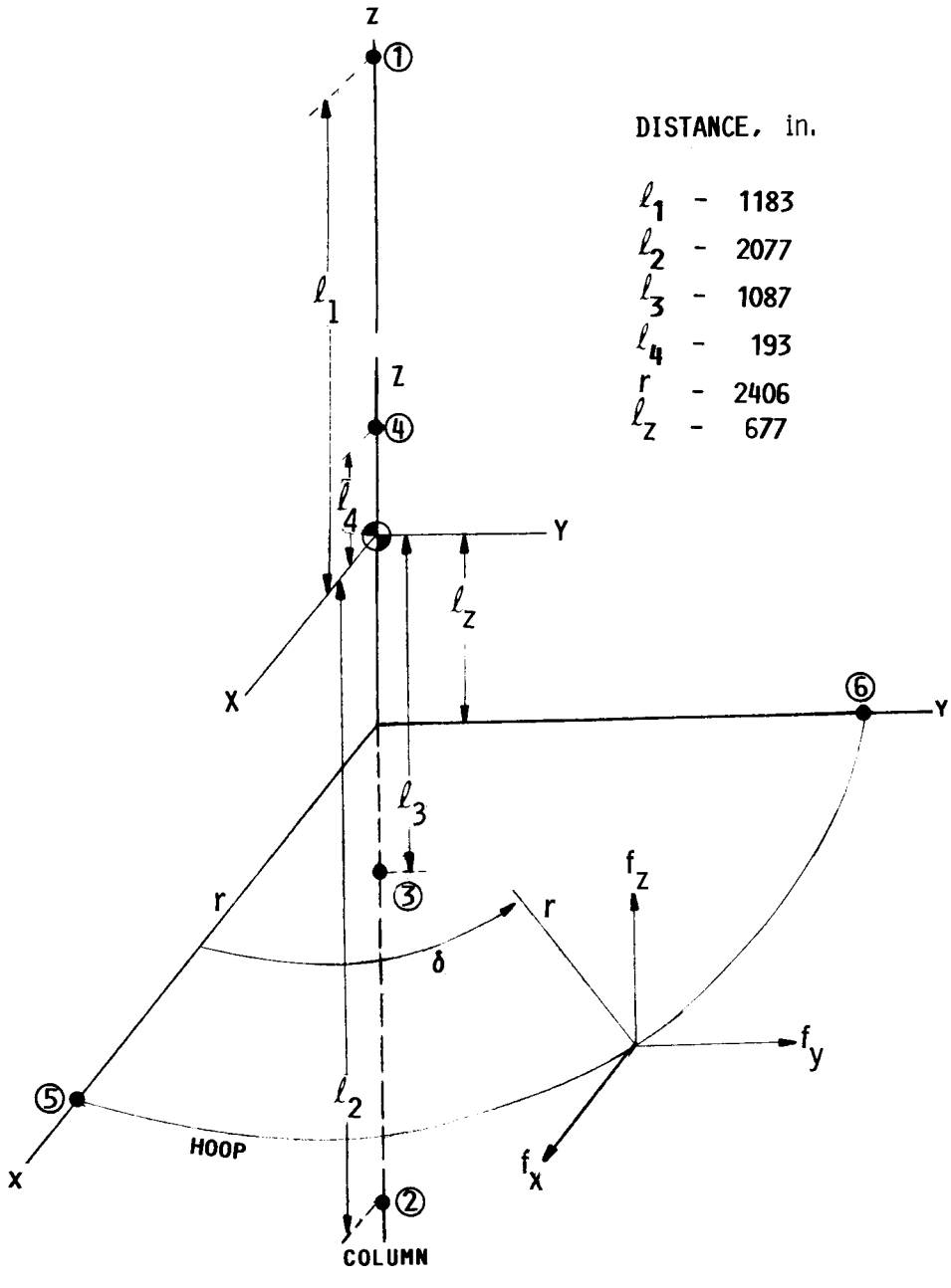

Figure 1.- Antenna coordinates and actuator locations.

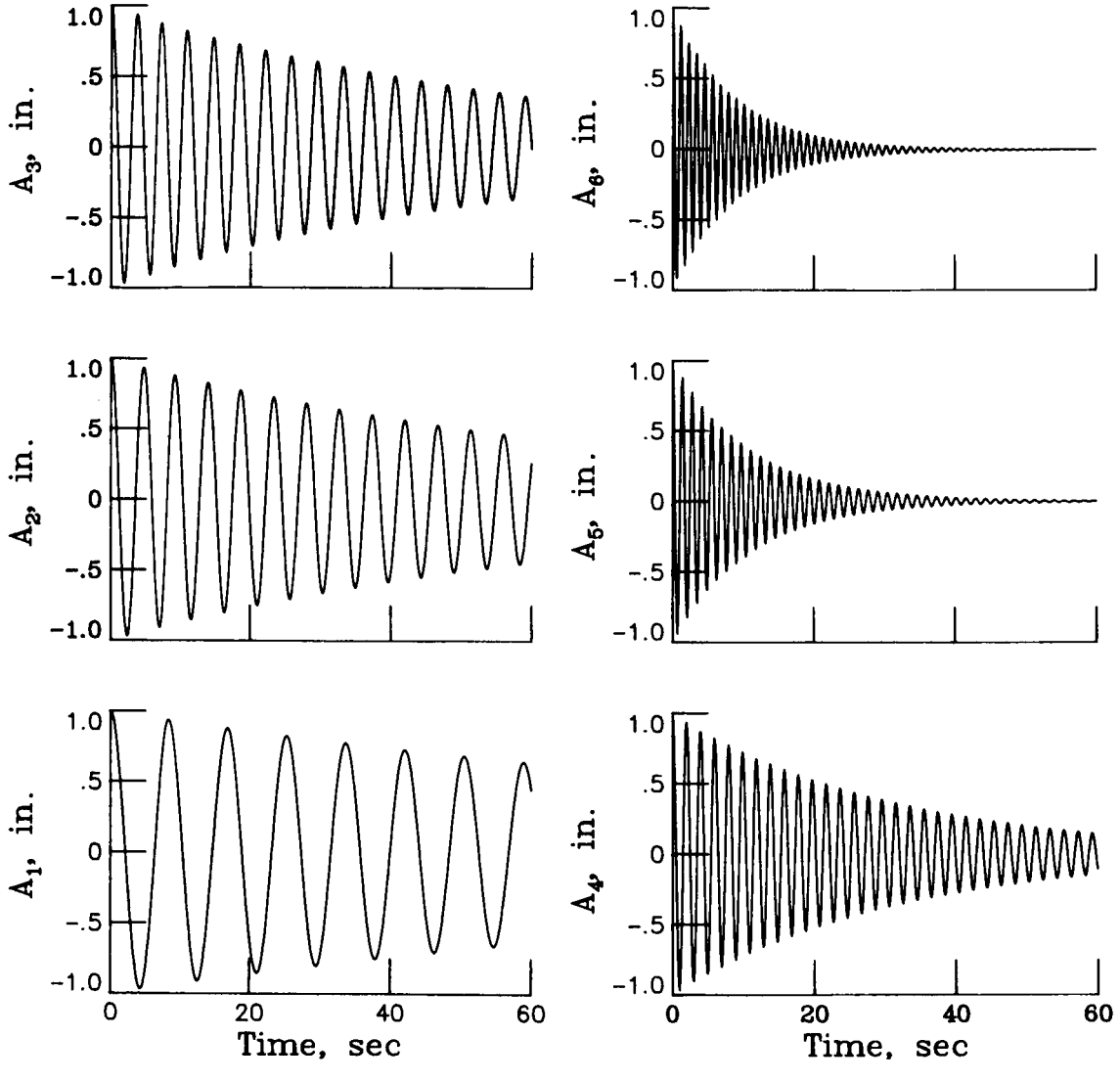

Figure 2.- Unforced responses of natural vibration modes.

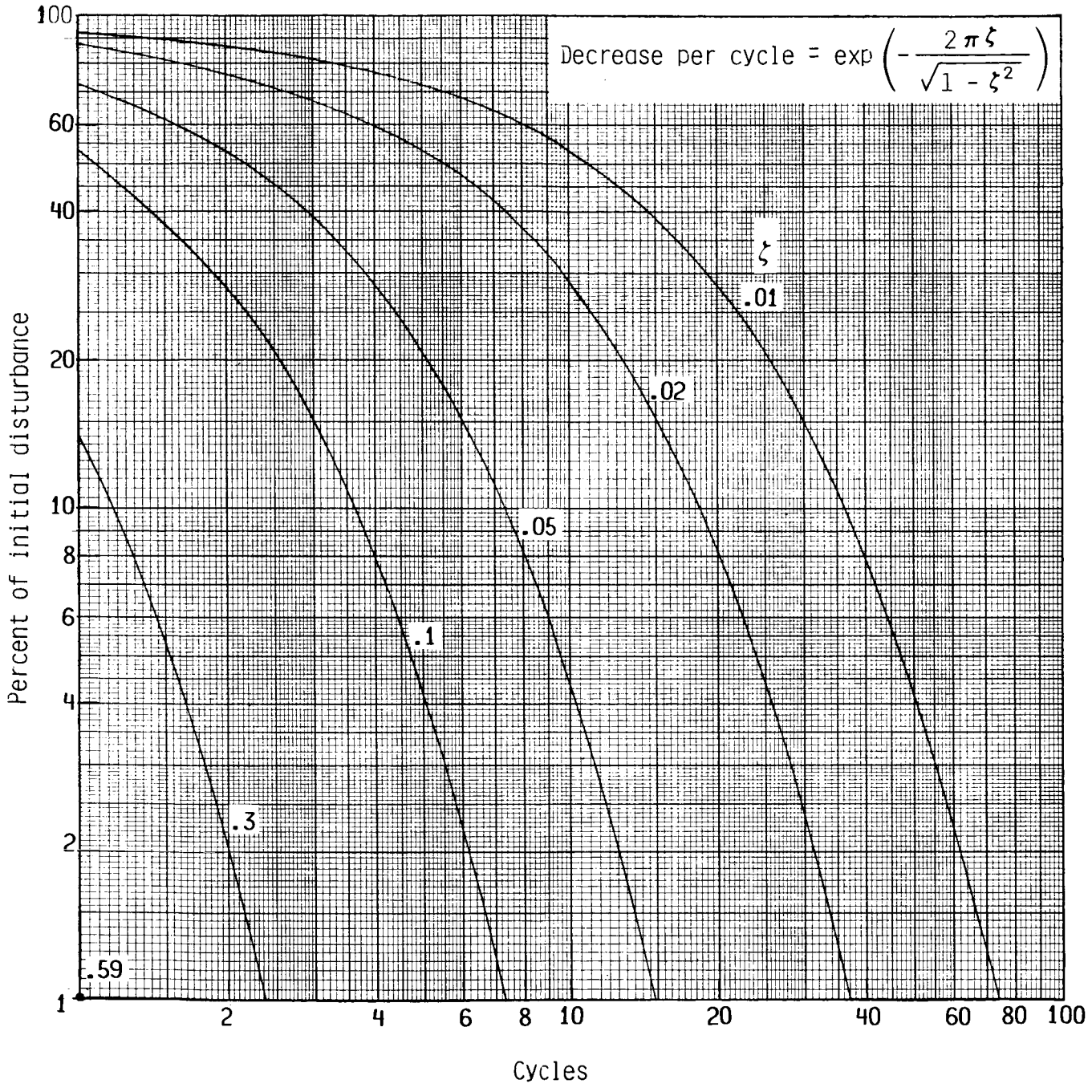

Figure 3.- Decrease in initial disturbance per cycle for second-order systems.

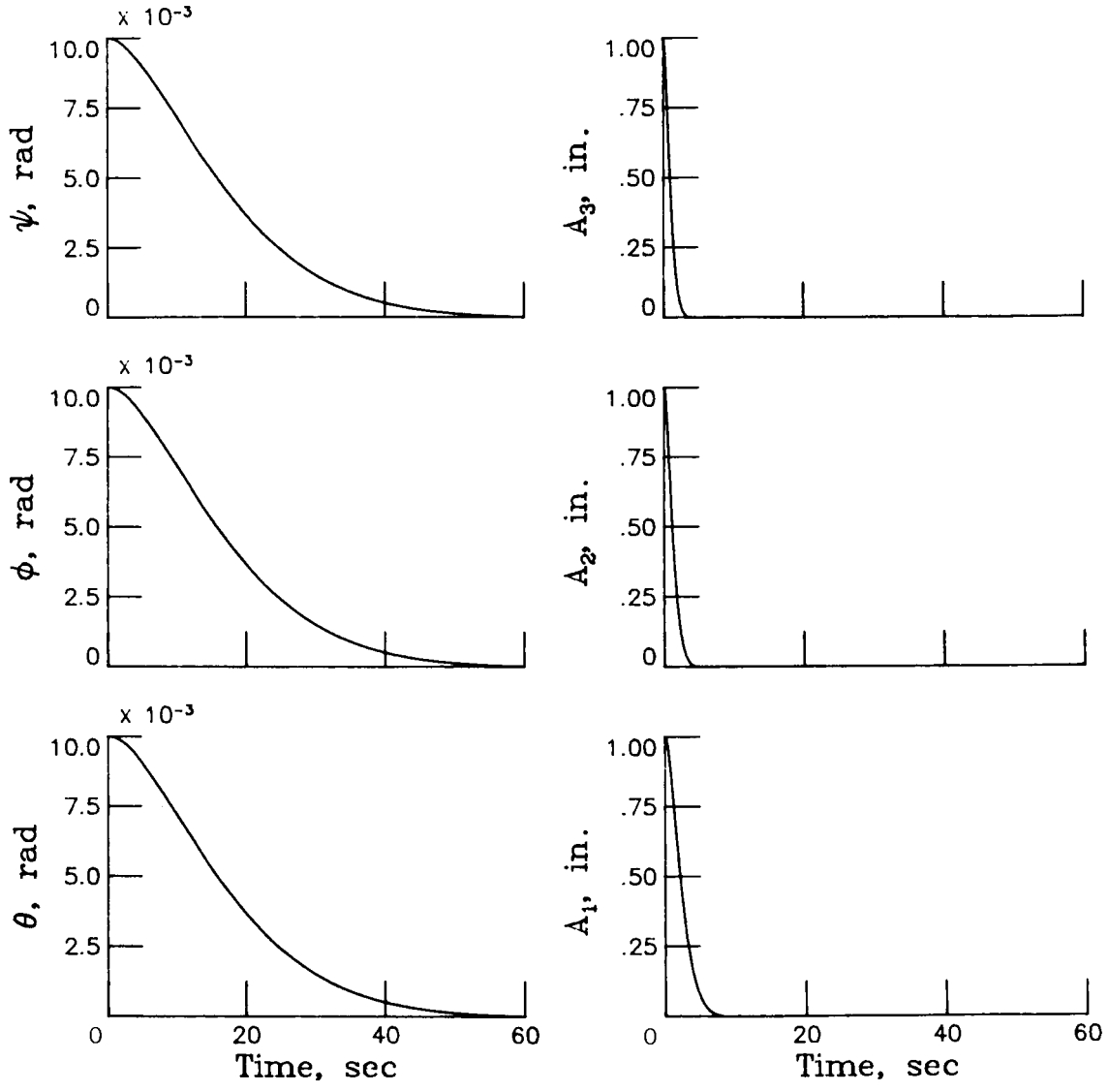

Figure 4.- Decoupled responses in position and rate for typical six-control case. $\zeta_d = 0.9$; $\omega_{rb} = 0.1$ rad/sec; $\omega_{flex} = \omega_n$.

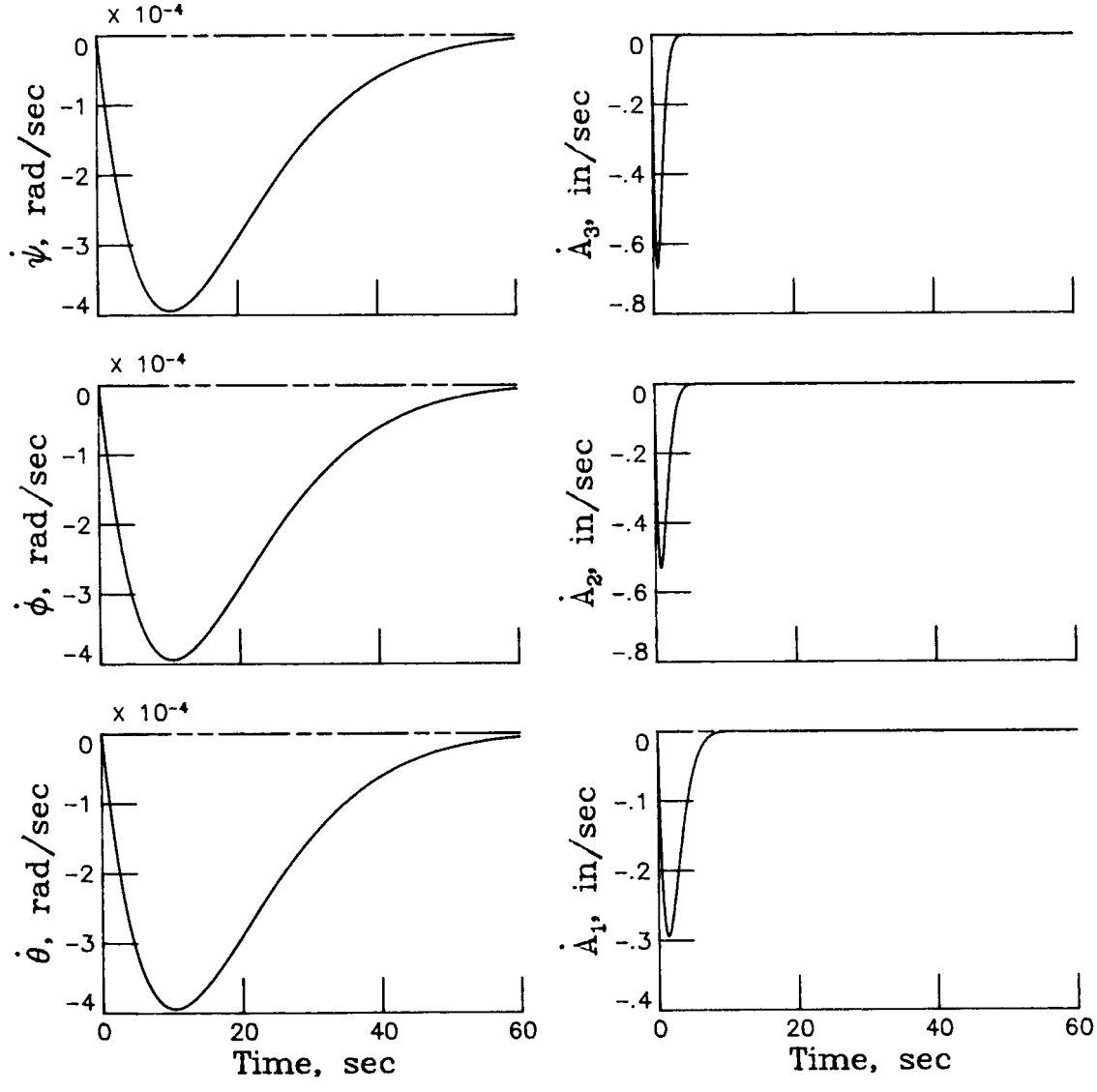

Figure 4.- Concluded.

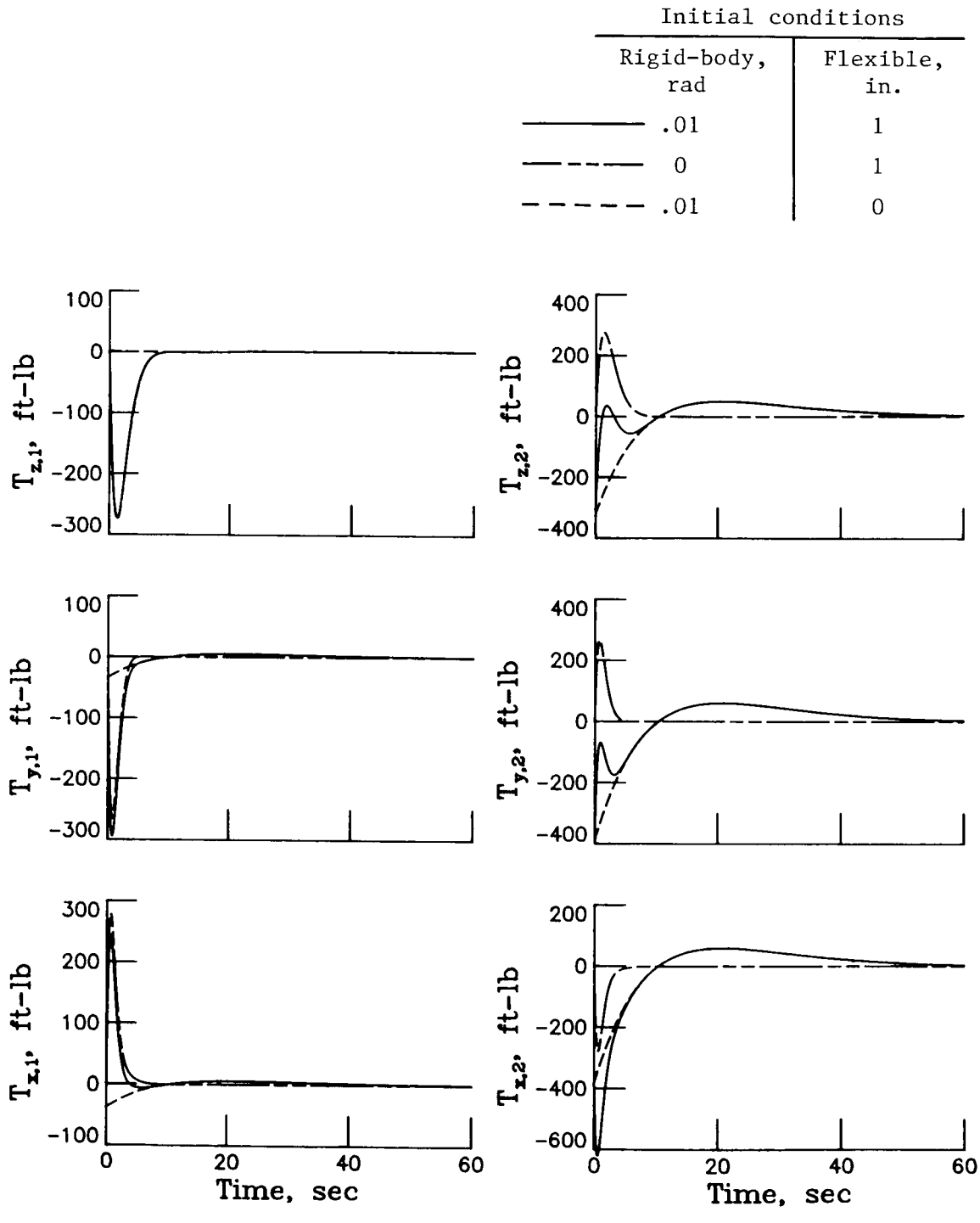

(a) Torque and momentum for CMG controllers.

Figure 5.- Control responses for typical six-mode cases of table III.

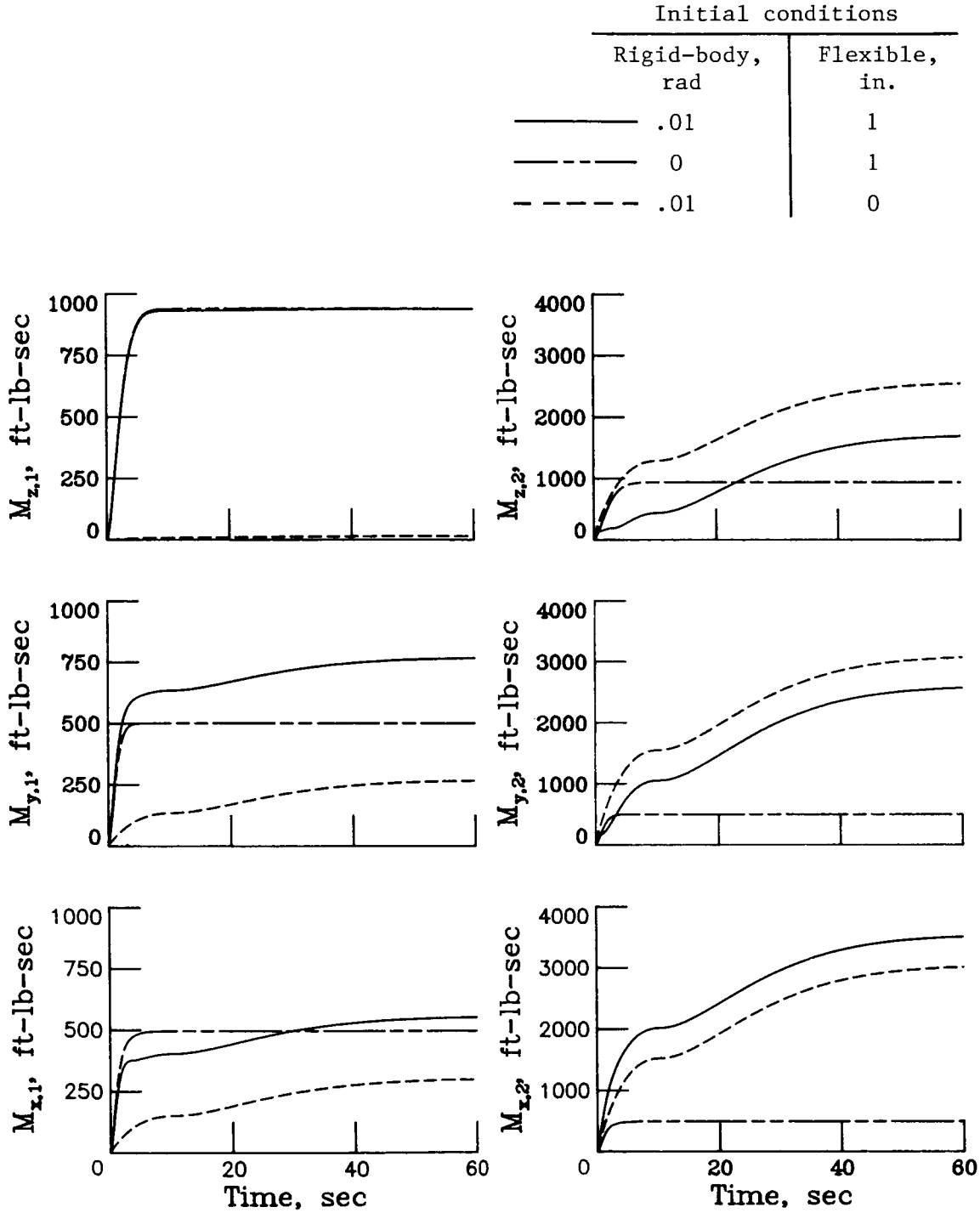

(a) Concluded.

Figure 5.- Continued.

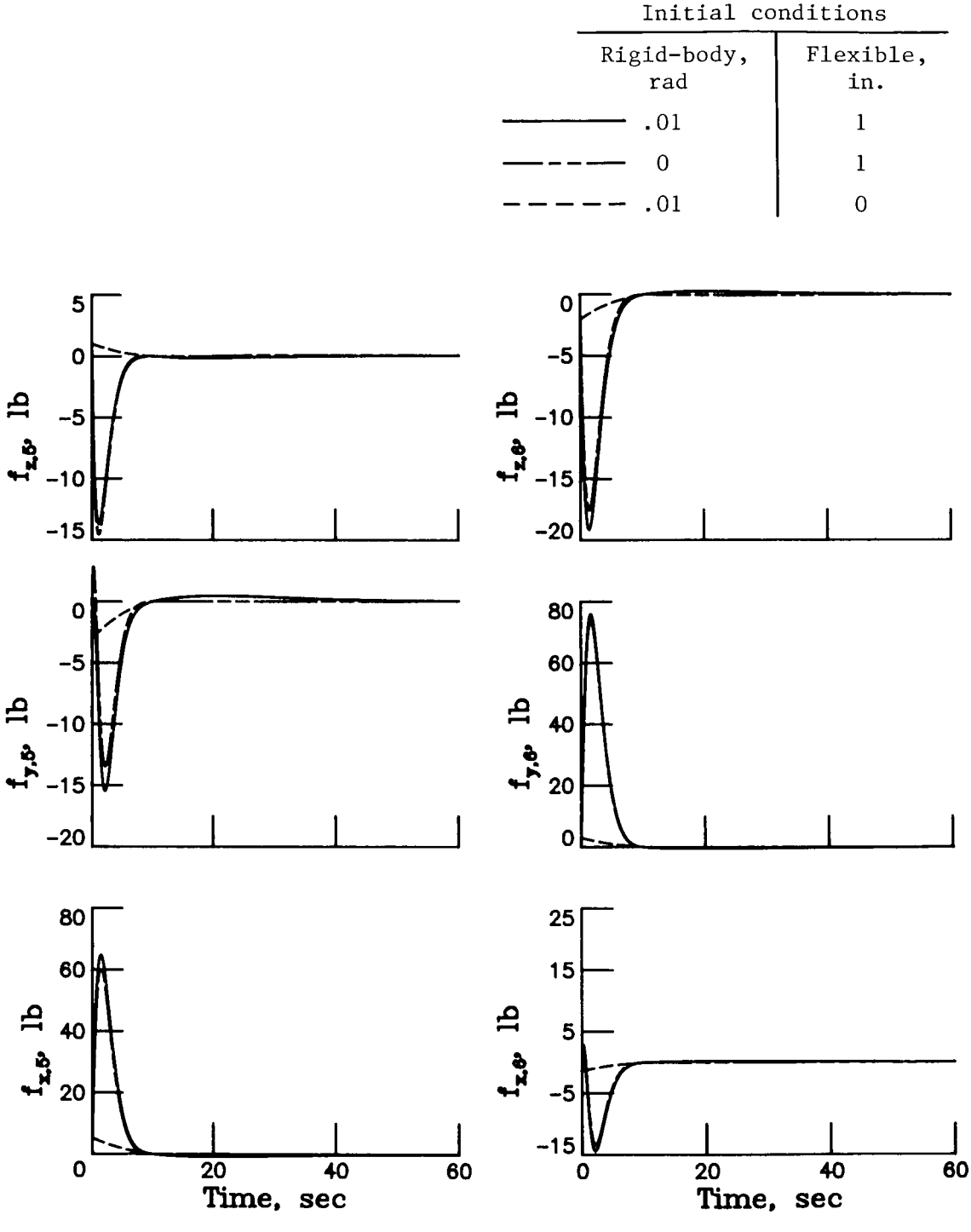

(b) Force and impulse for RCS controllers.

Figure 5.- Continued.

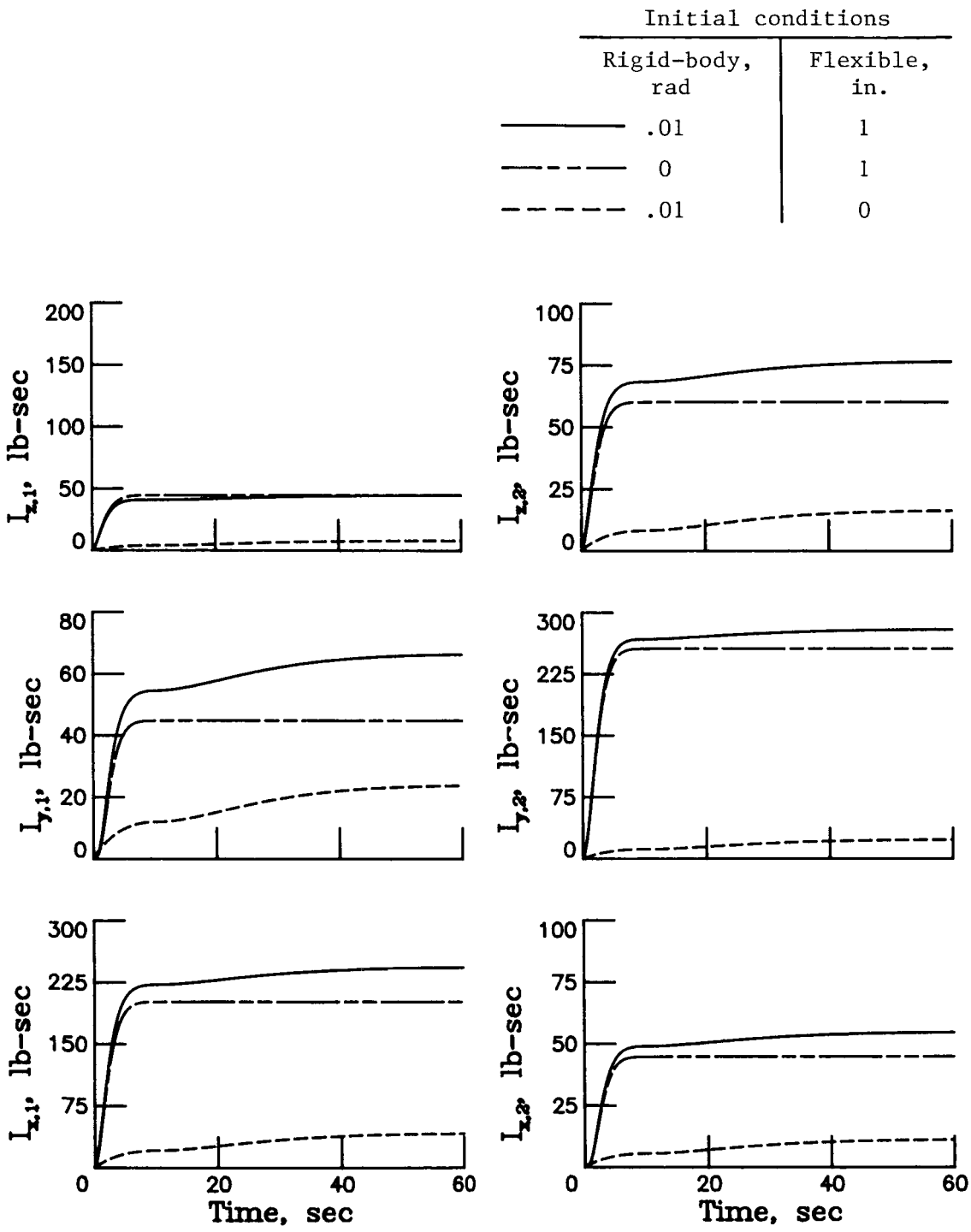

(b) Concluded.

Figure 5.- Concluded.

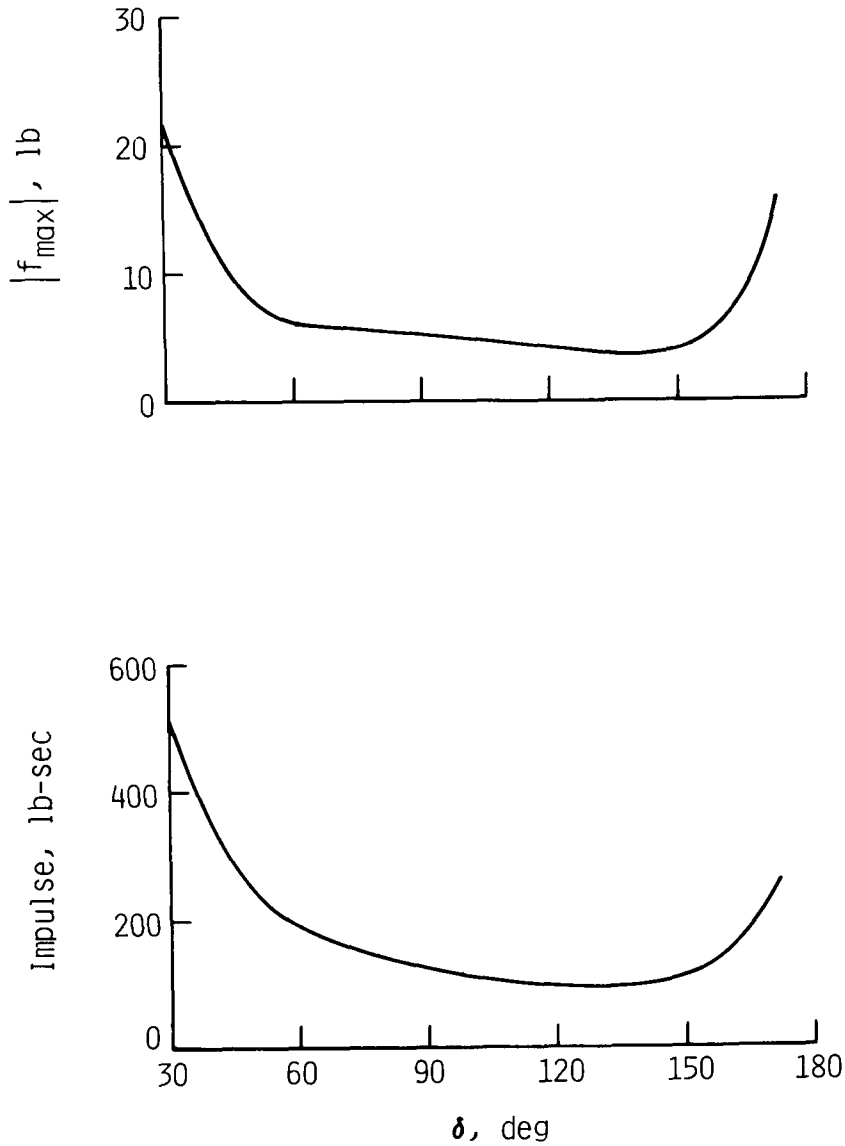

(a) Rigid-body effects. (Initial disturbances = 0.01 rad.)

Figure 6.- Effect on control requirements of placement of RCS actuators on antenna hoop. $\zeta_d = 0.9$; $\omega_{rb} = 0.1$ rad/sec; $\omega_{flex} = \omega_n$.

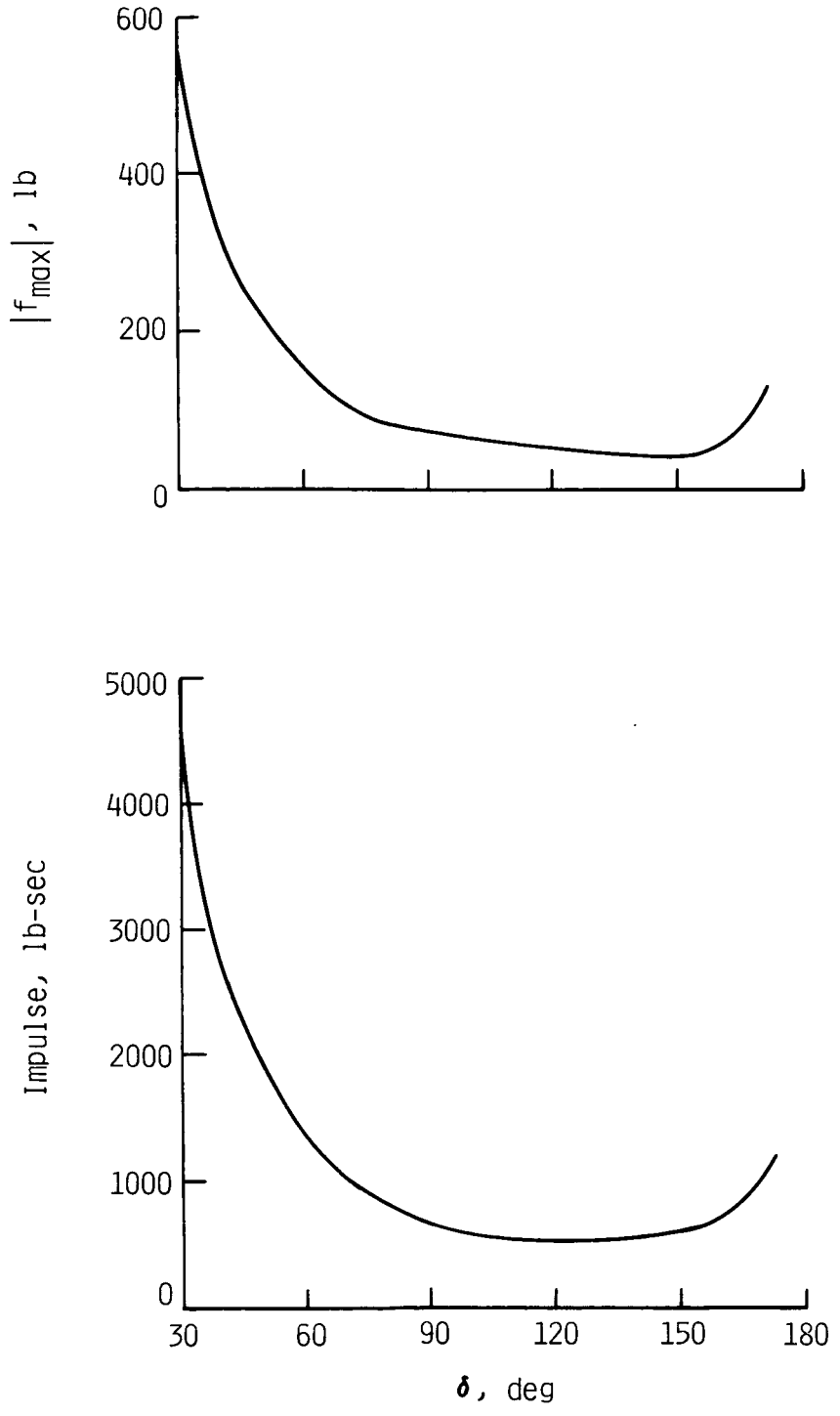

(b) Flexible-mode effects. (Initial disturbances = 1 in.)

Figure 6.- Concluded.

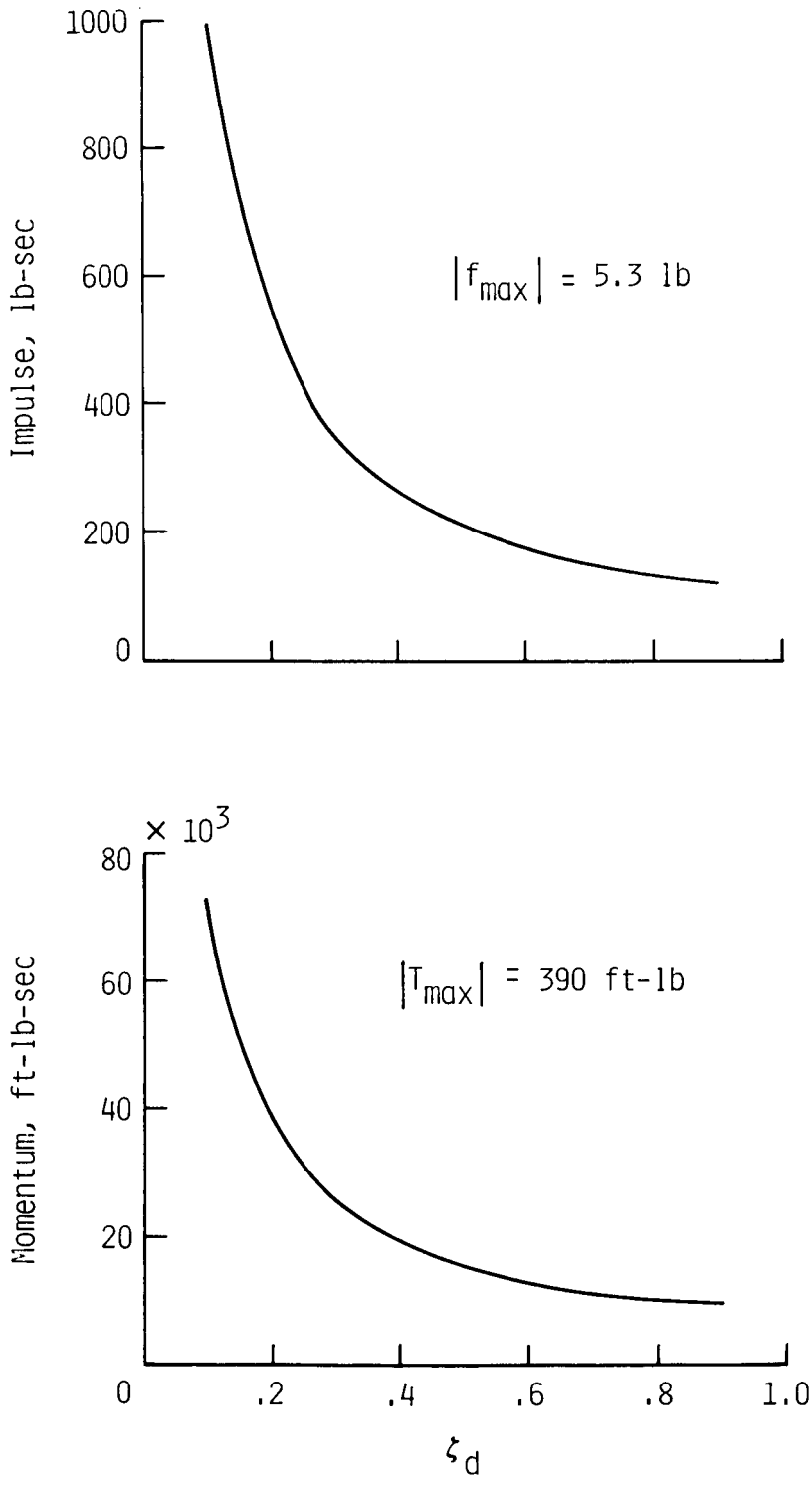

Figure 7.- Effect of closed-loop damping ratio on rigid-body control requirements. Table III controller arrangements; Initial disturbances = 0.01 rad.

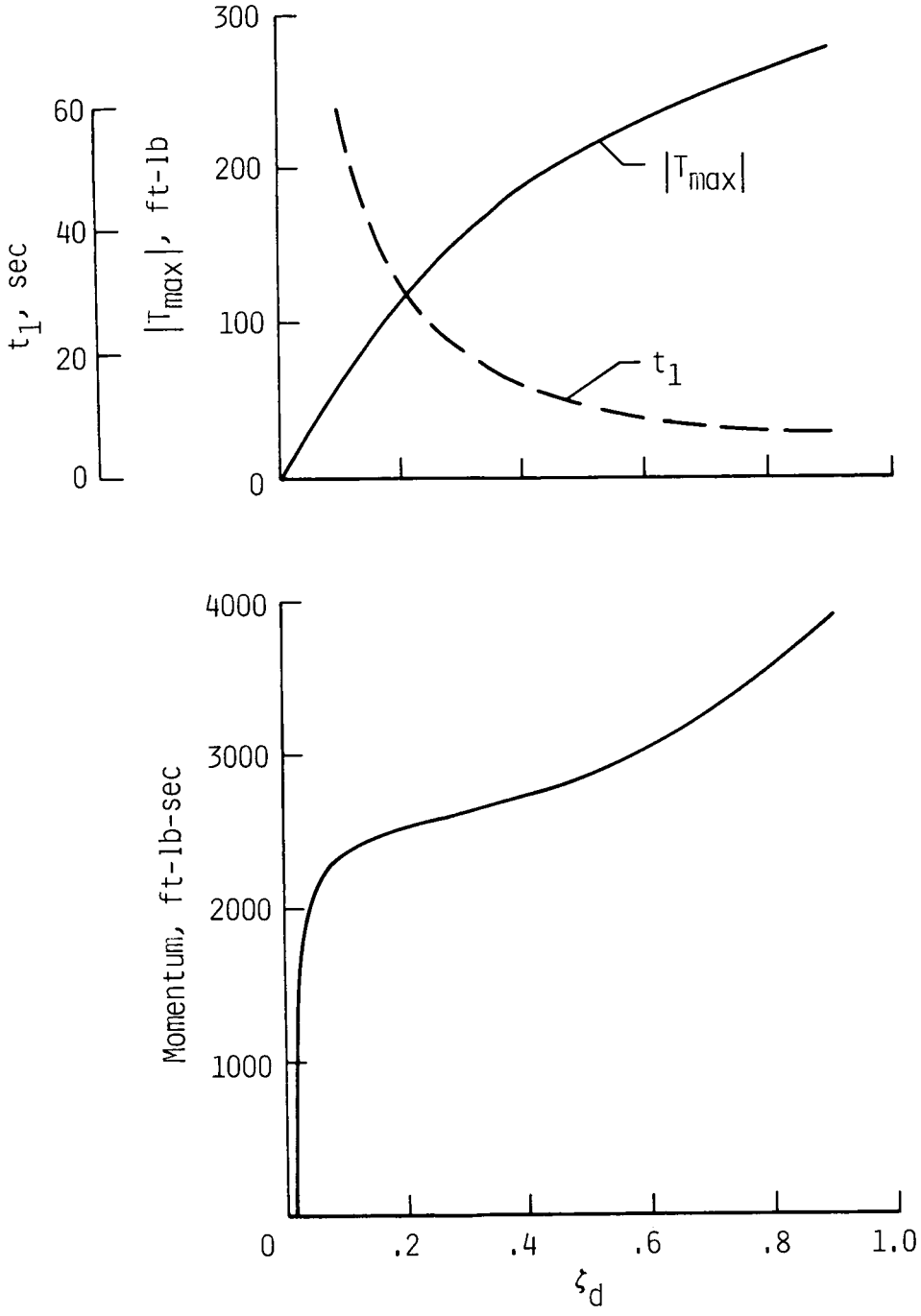

(a) CMG controllers.

Figure 8.- Effect of closed-loop damping ratio on flexible-mode control requirements. Table III controller arrangements; Initial disturbances = 1 in.

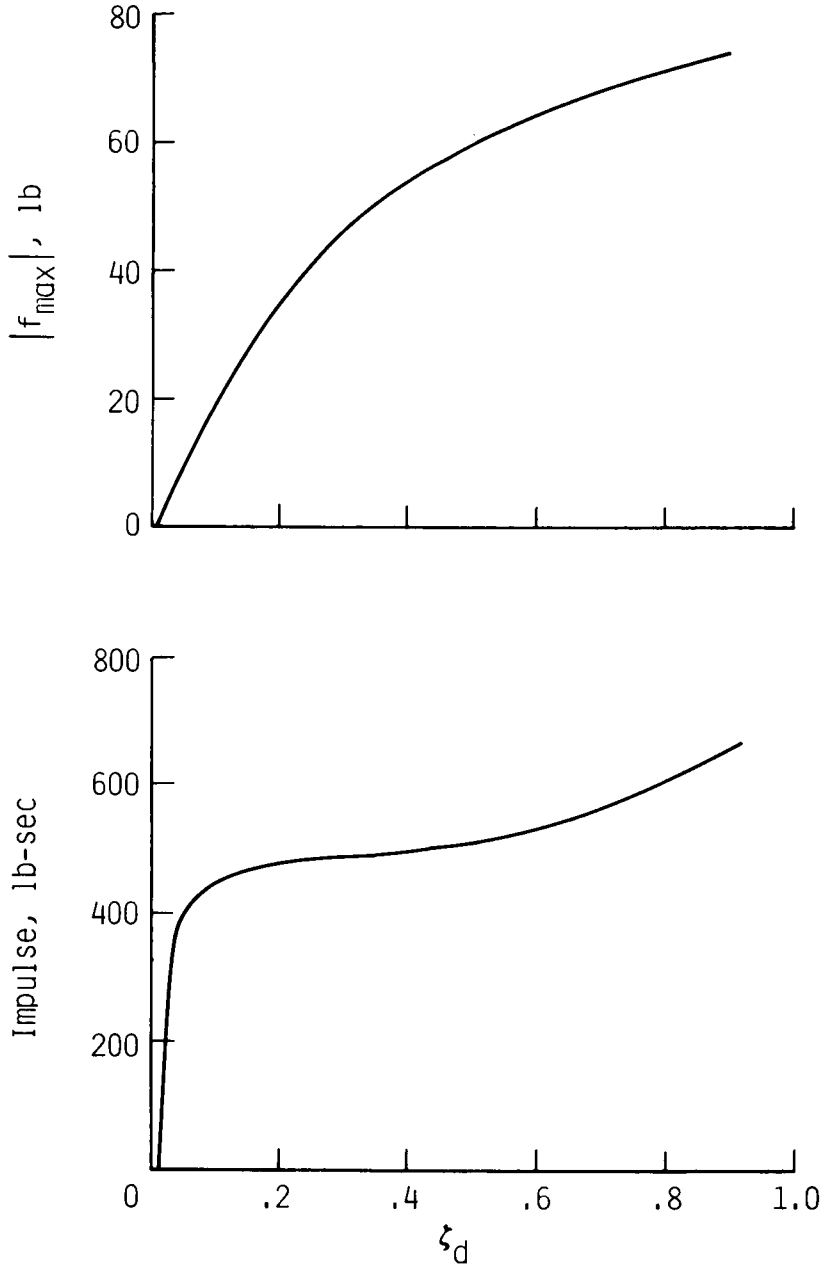

(b) RCS controllers.

Figure 8.- Concluded.

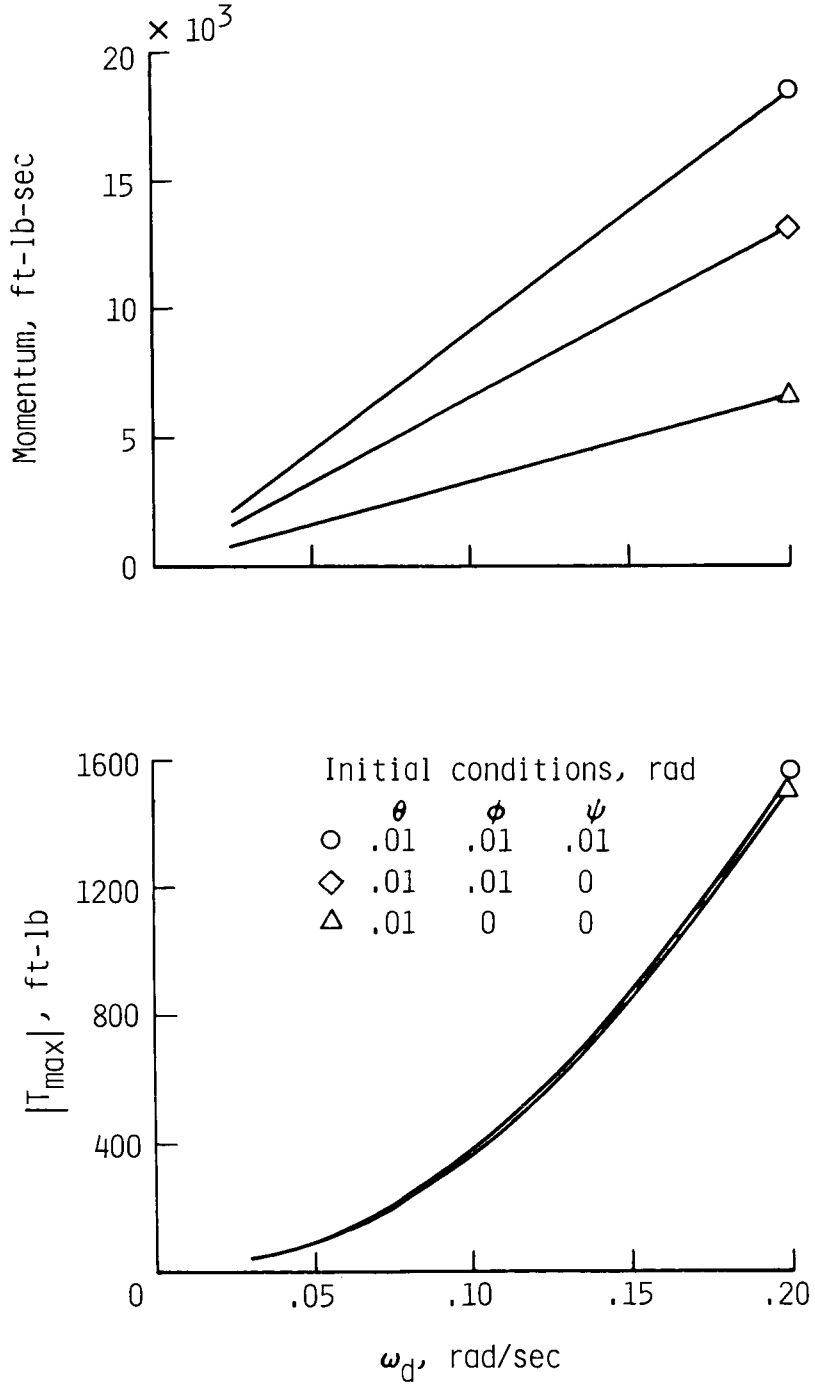

(a) CMG controllers.

Figure 9.- Effect of closed-loop frequency on rigid-body control requirements. Table III control arrangements.

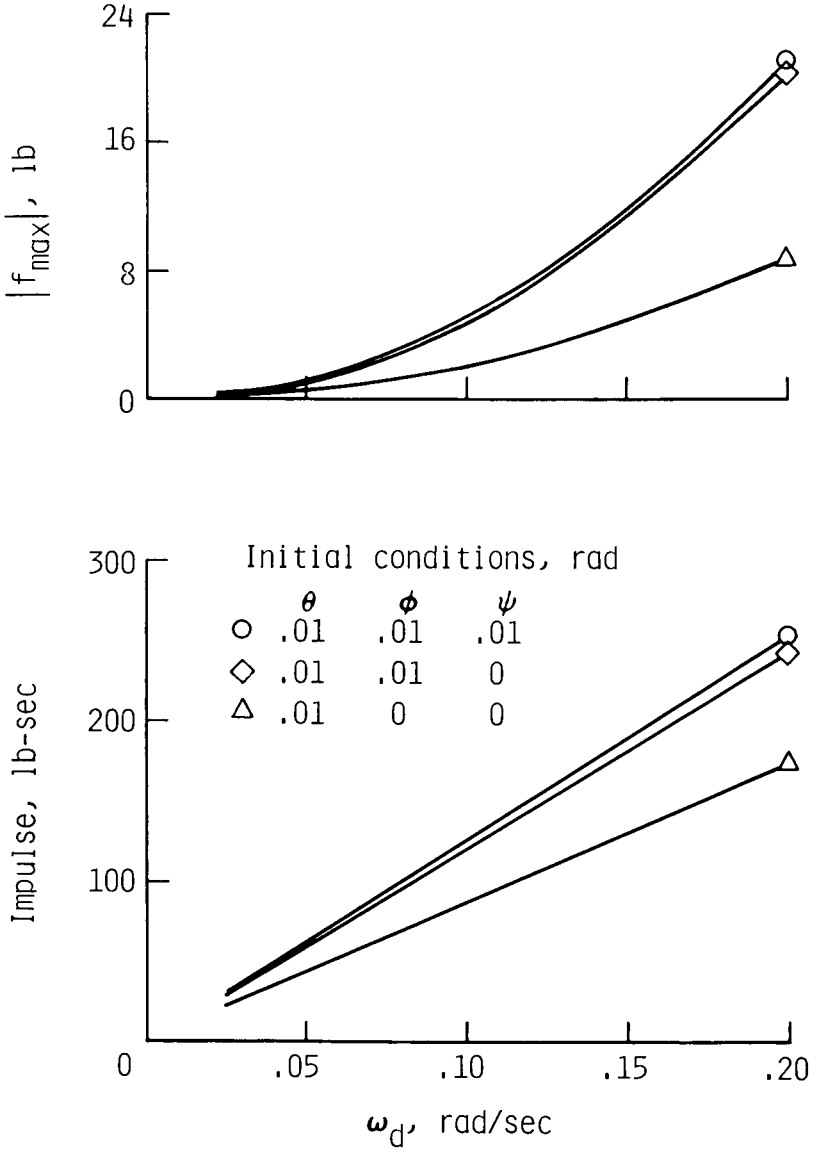

(b) RCS controllers.

Figure 9.- Concluded.

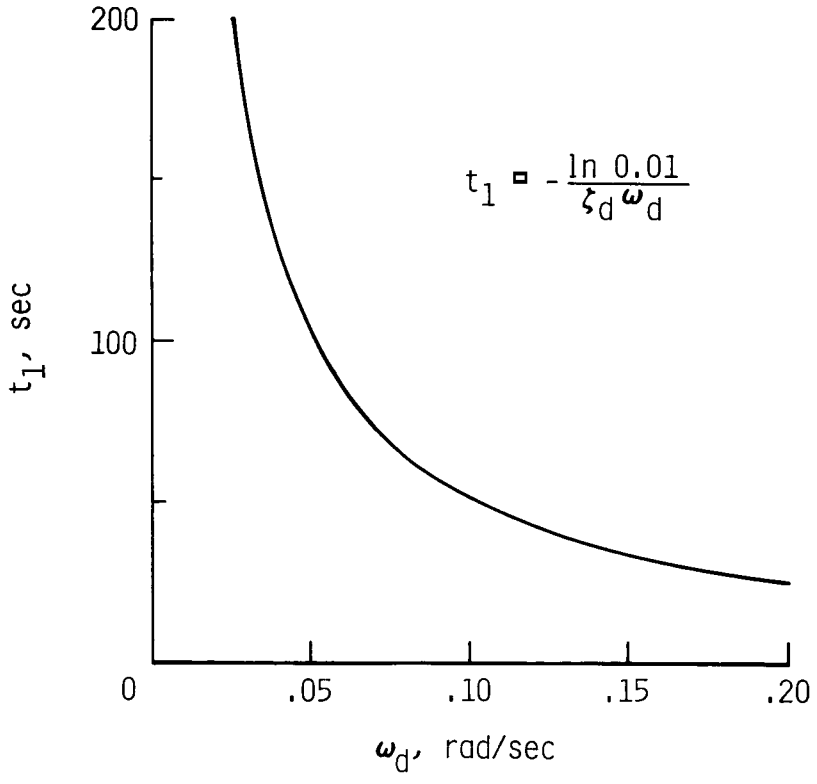

Figure 10.- Variation of time to damp to 1 percent of initial disturbance with rigid-body frequency. $\zeta_d = 0.9$.

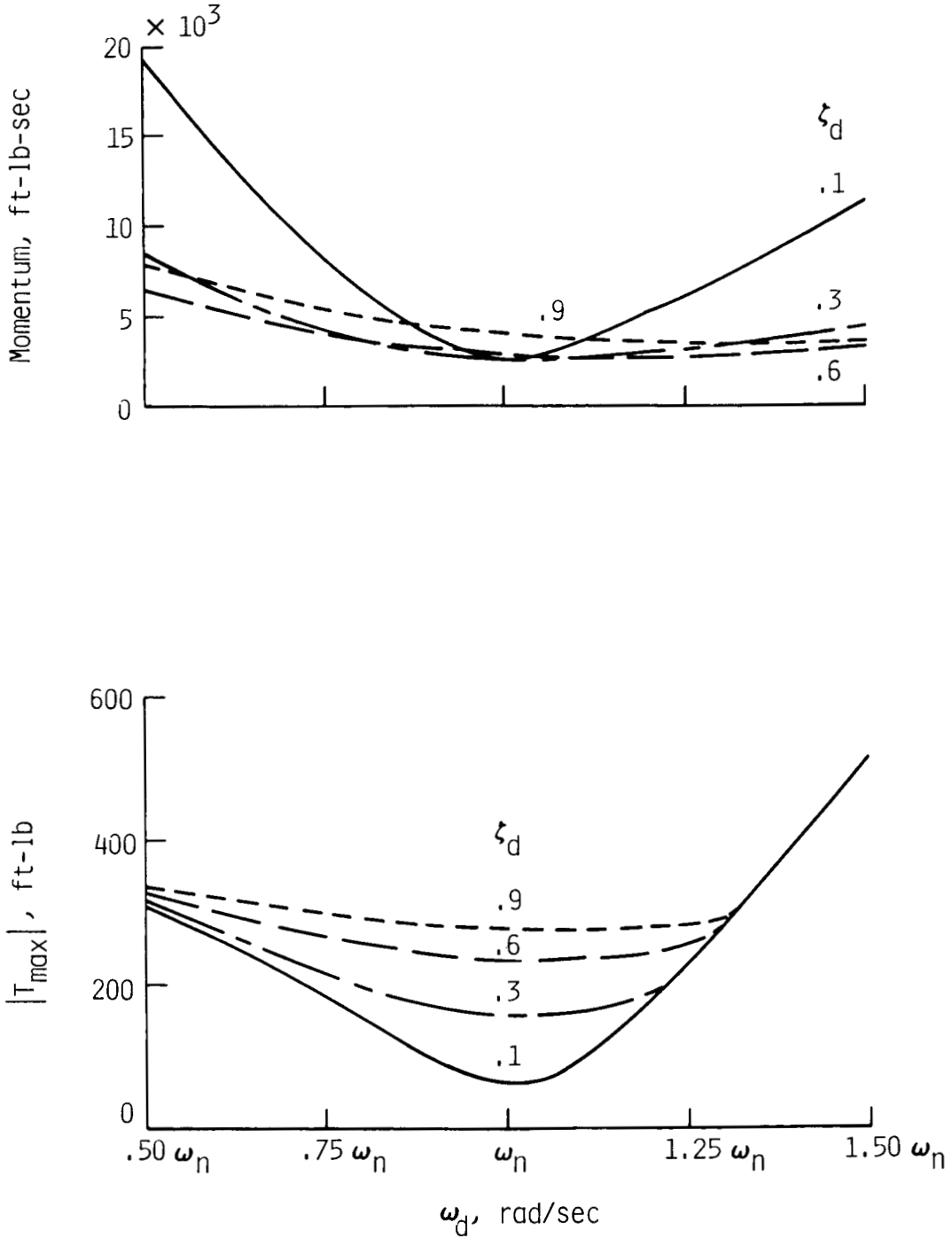

(a) CMG controllers.

Figure 11.- Effect of flexible-mode closed-loop frequency on control requirements. Table III control arrangements; Initial flexible-mode disturbances = 1 in.

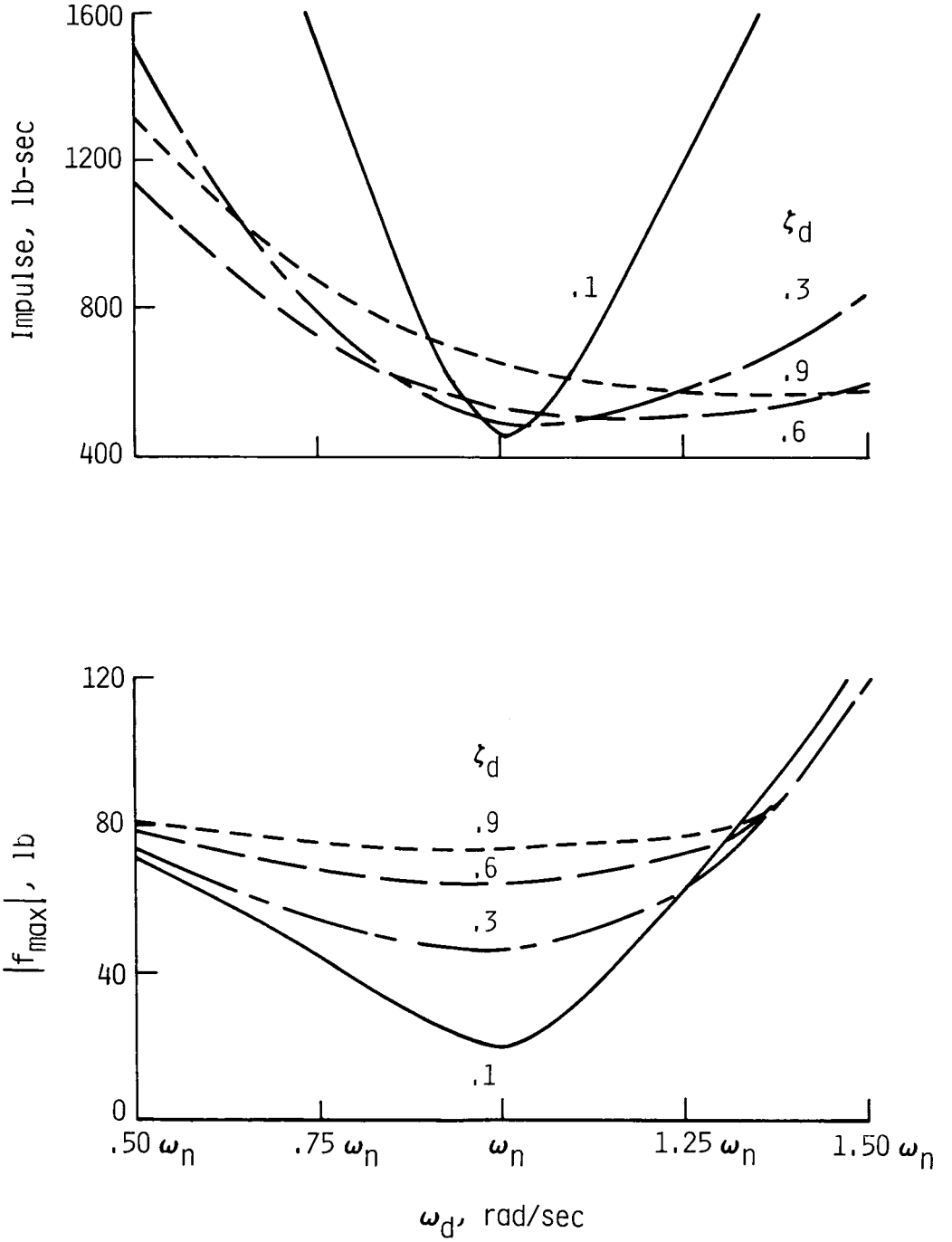

(b) RCS controllers.

Figure 11.- Concluded.

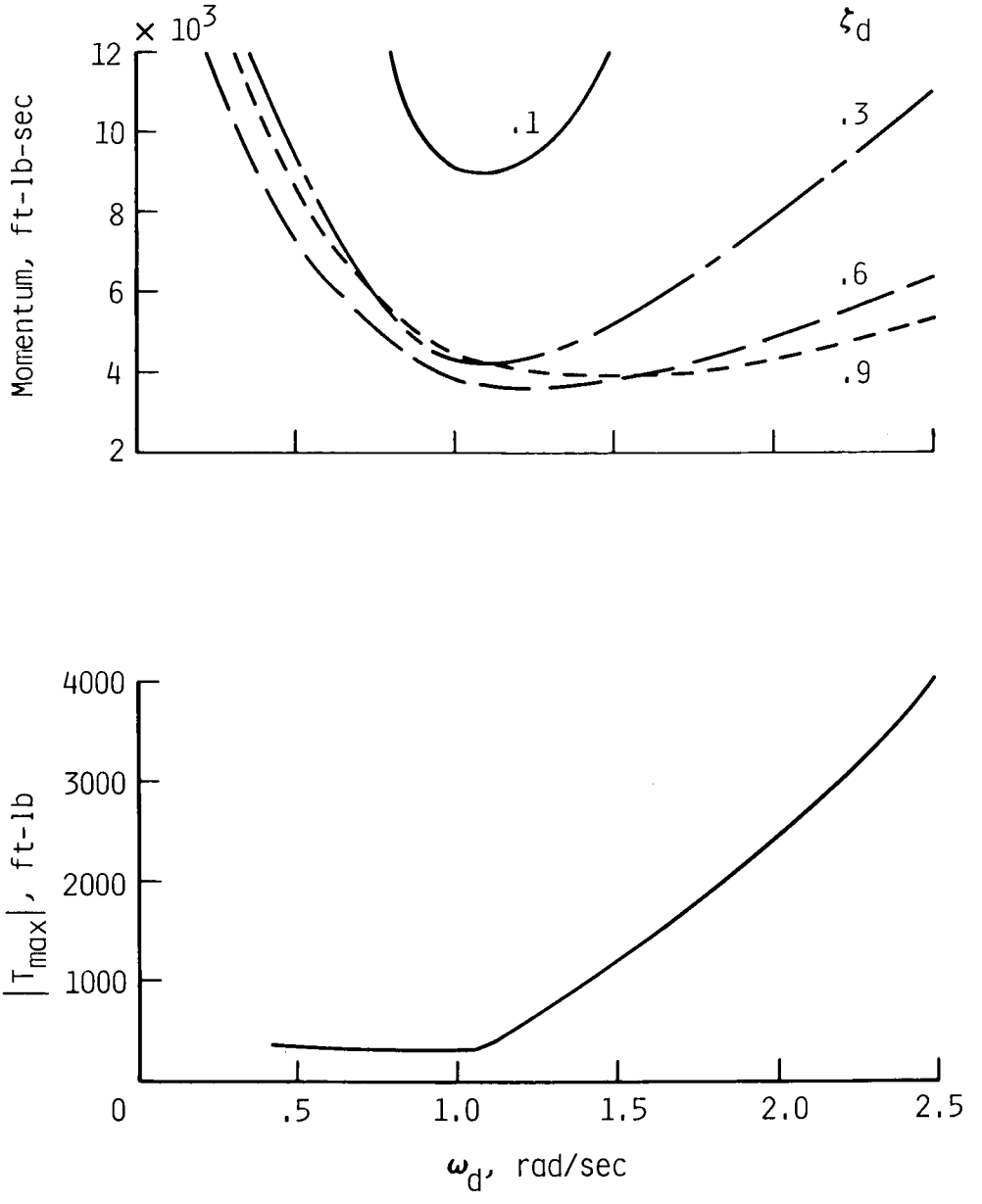

(a) CMG controllers.

Figure 12.- Effect on control requirements of using the same closed-loop frequency for all flexible modes. Table III actuator arrangements; Initial disturbances = 1 in.

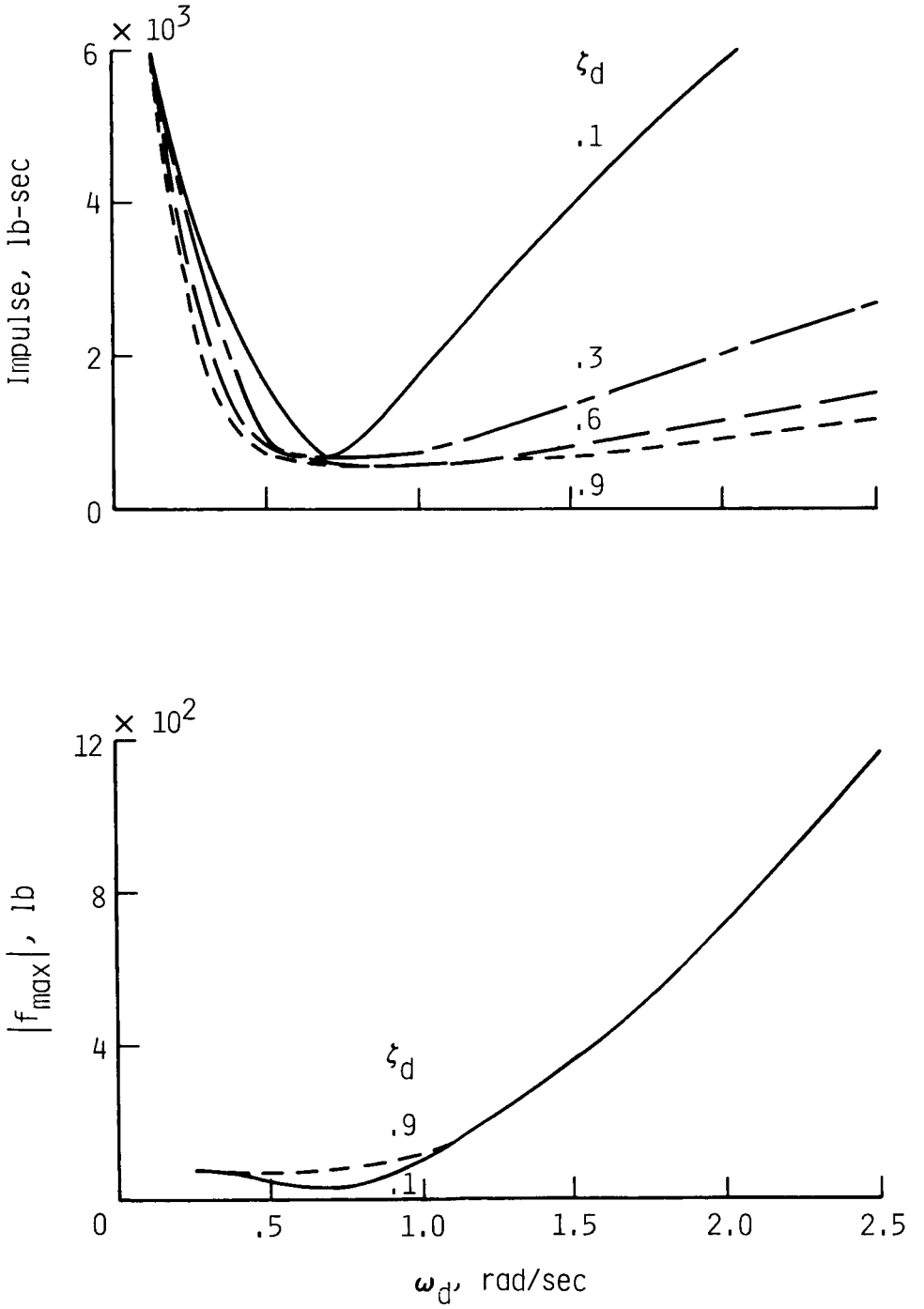

(b) RCS controllers.

Figure 12.- Concluded.

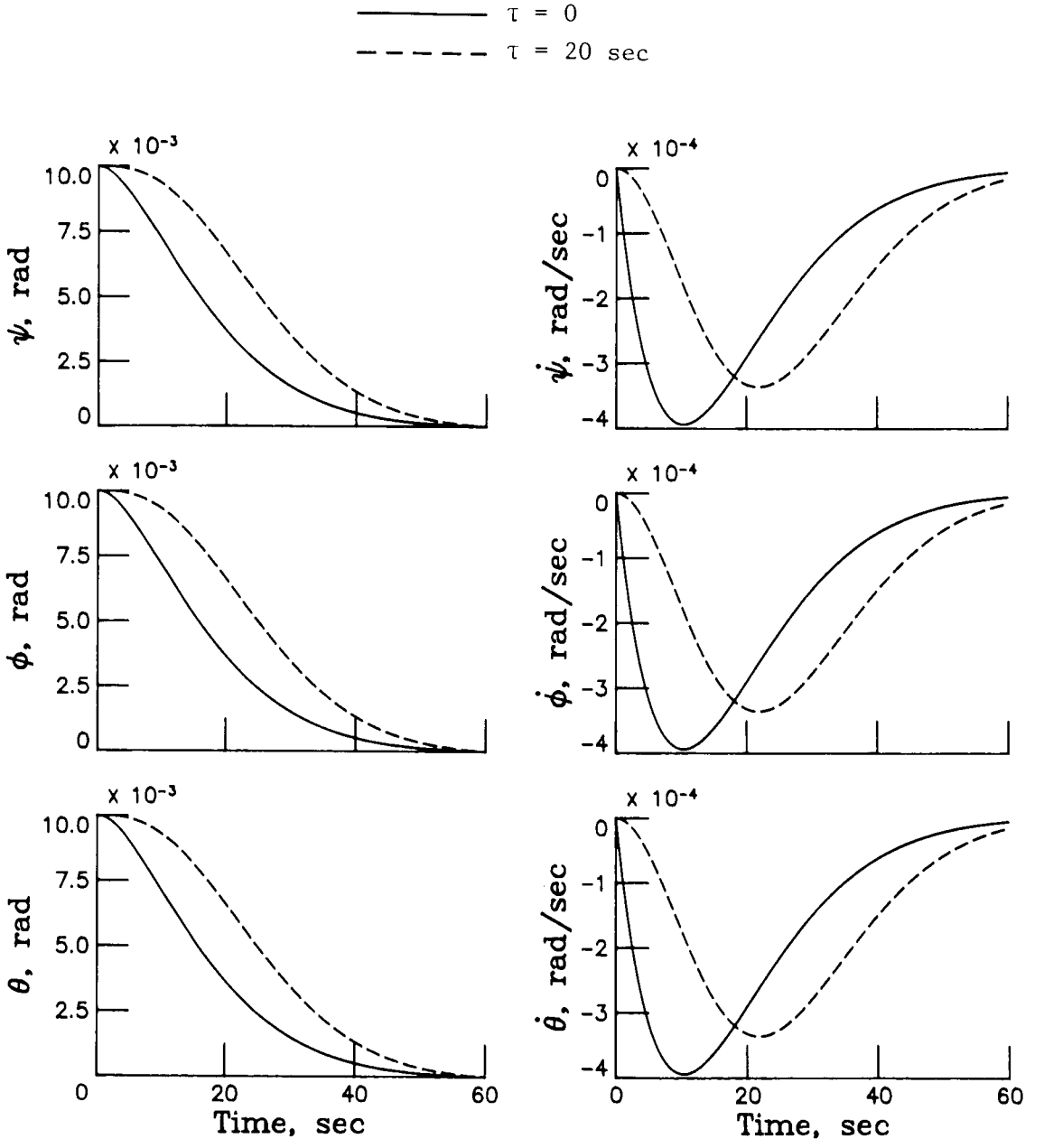

(a) Rigid-body disturbances.

Figure 13.- Typical responses with and without time delay for CMG case of table III.

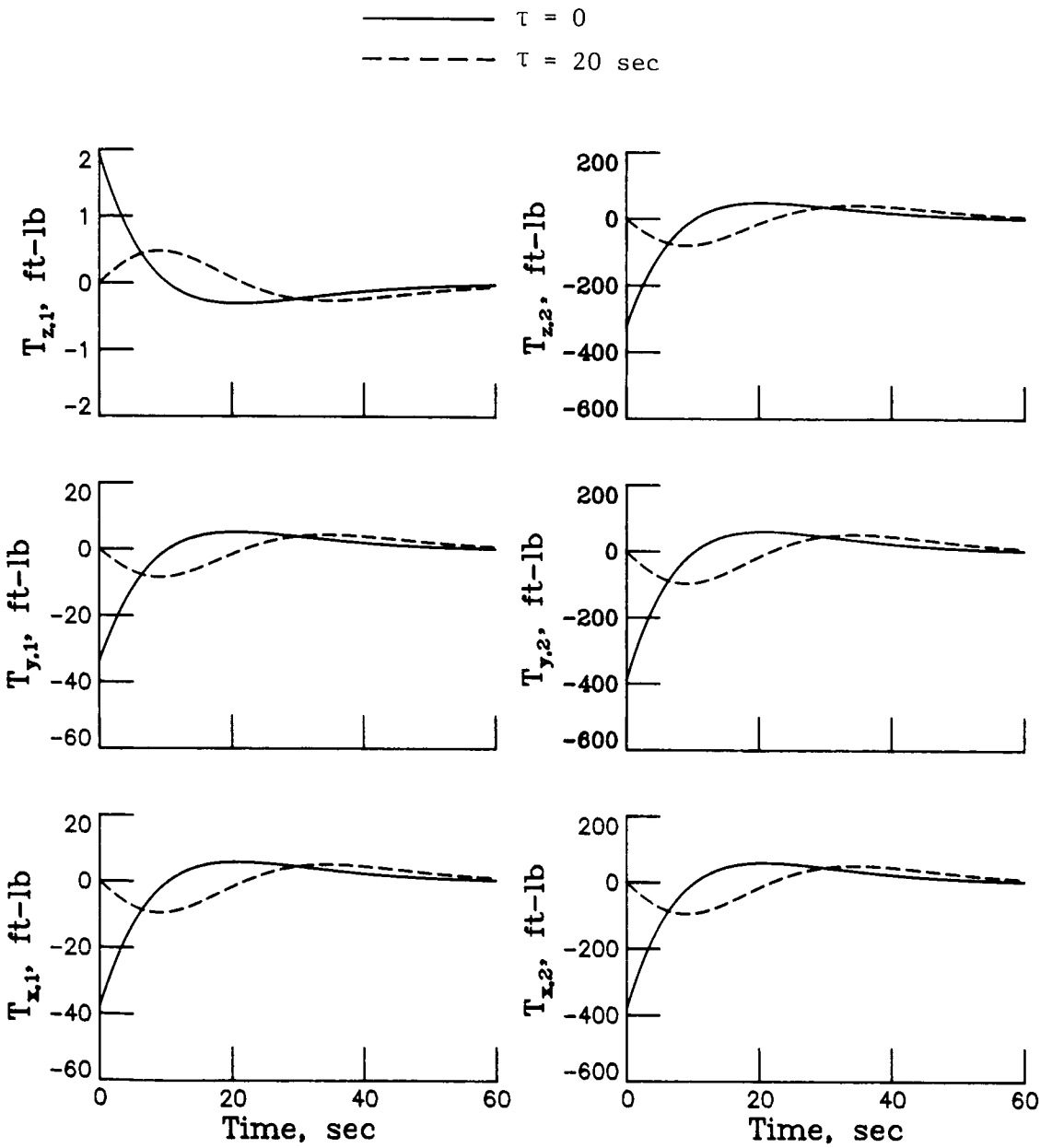

(a) Continued.

Figure 13.- Continued.

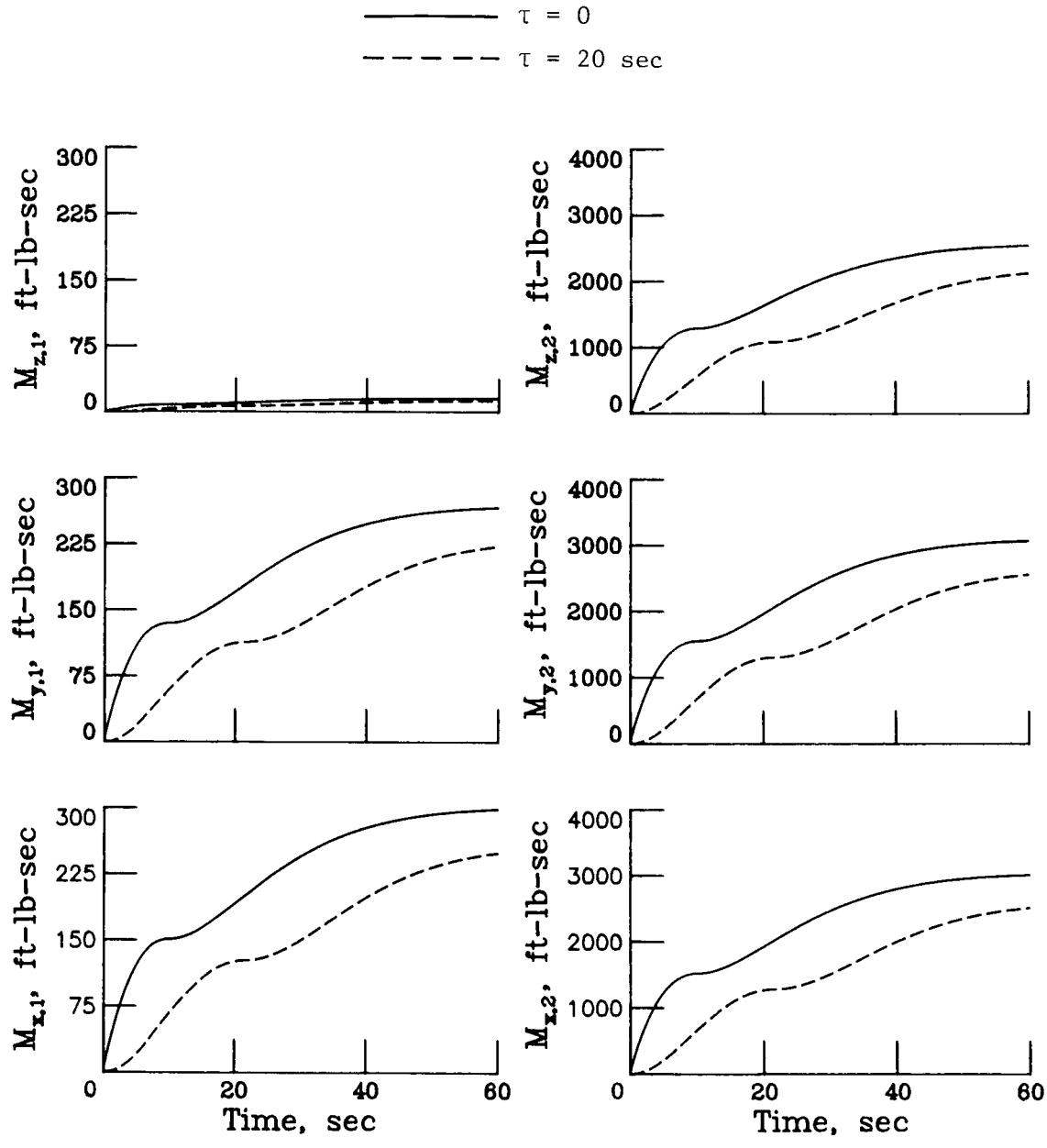

(a) Concluded.

Figure 13.- Continued.

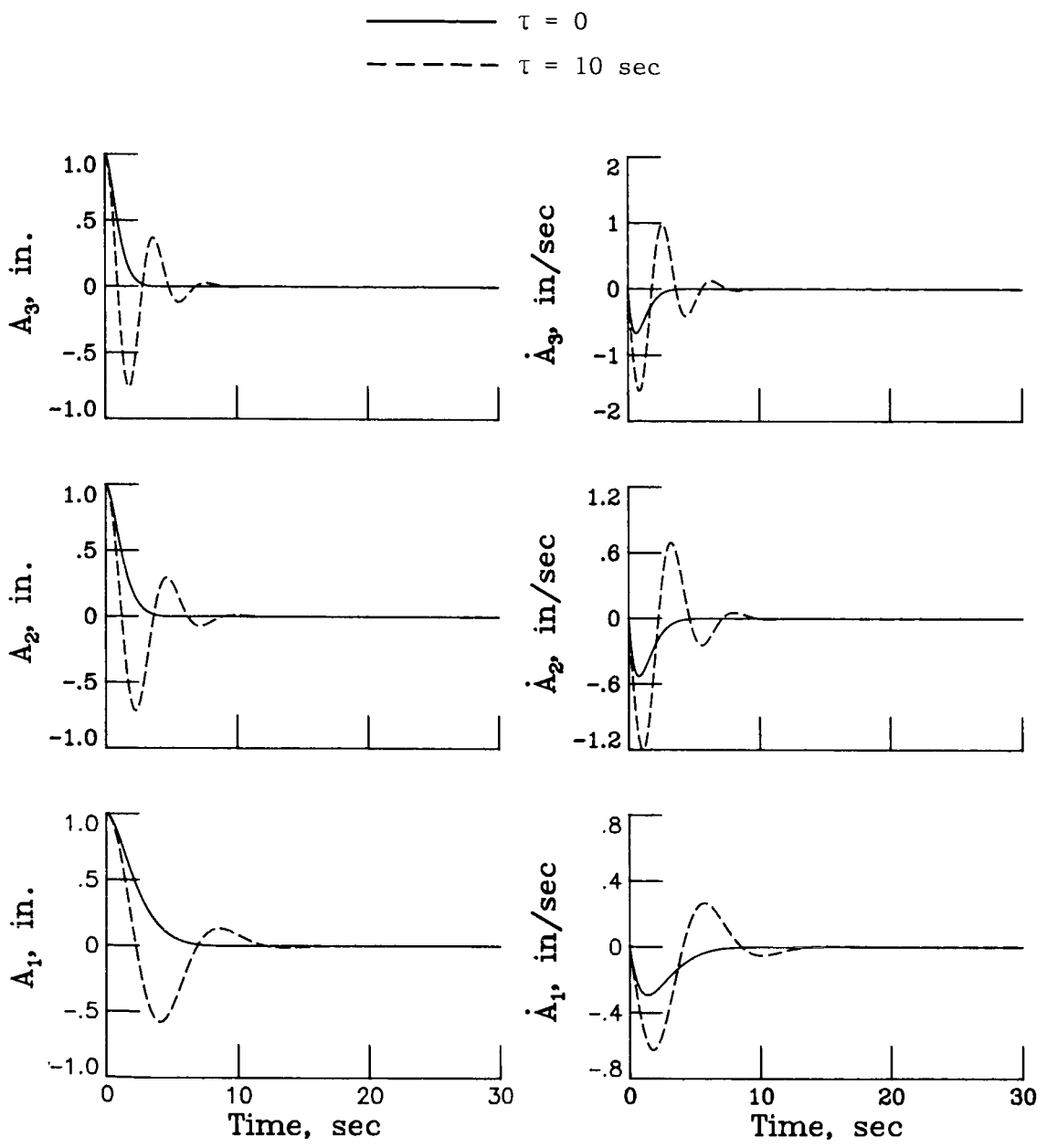

(b) Flexible-mode disturbances.

Figure 13.- Continued.

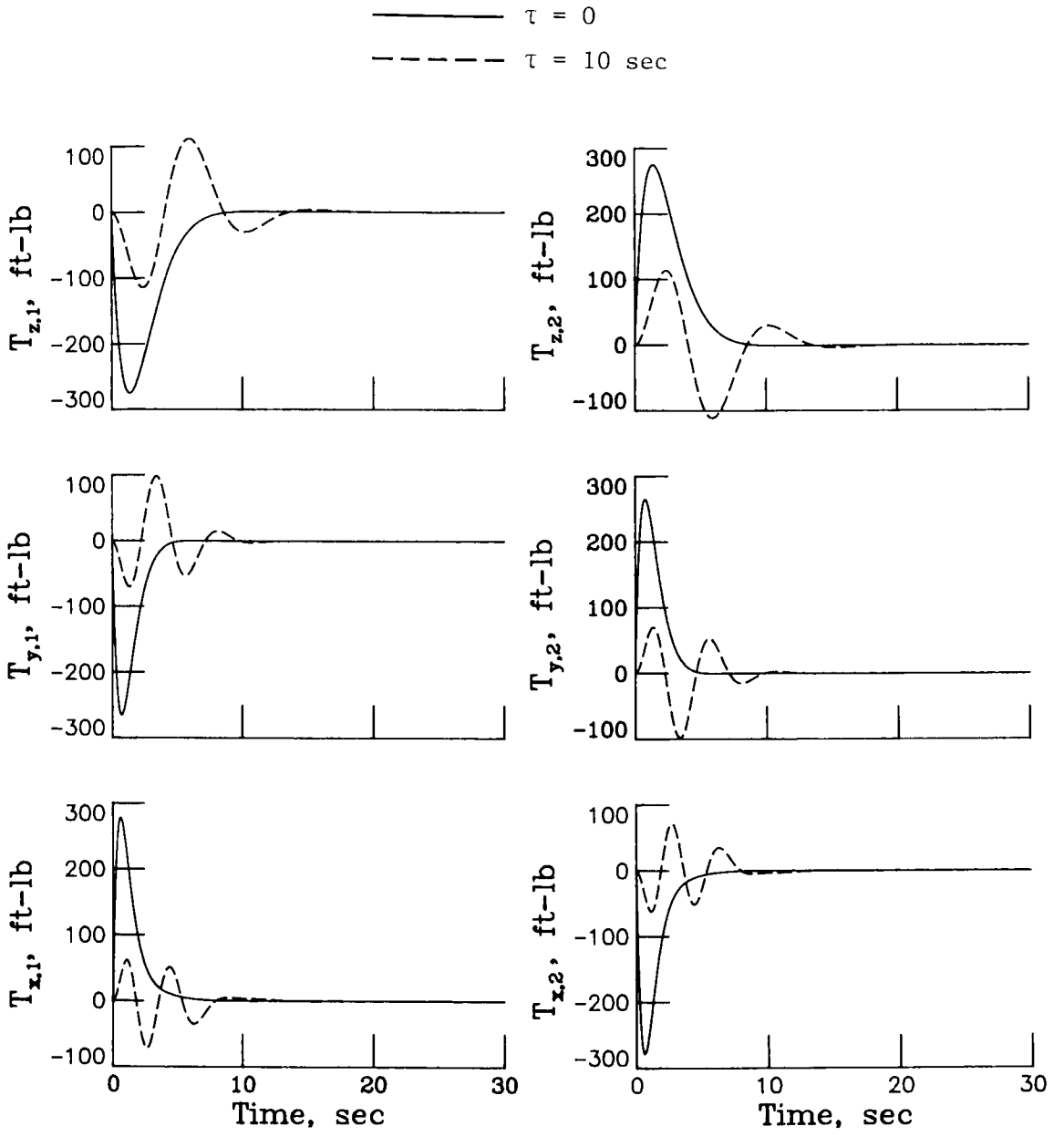

(b) Continued.

Figure 13.- Continued.

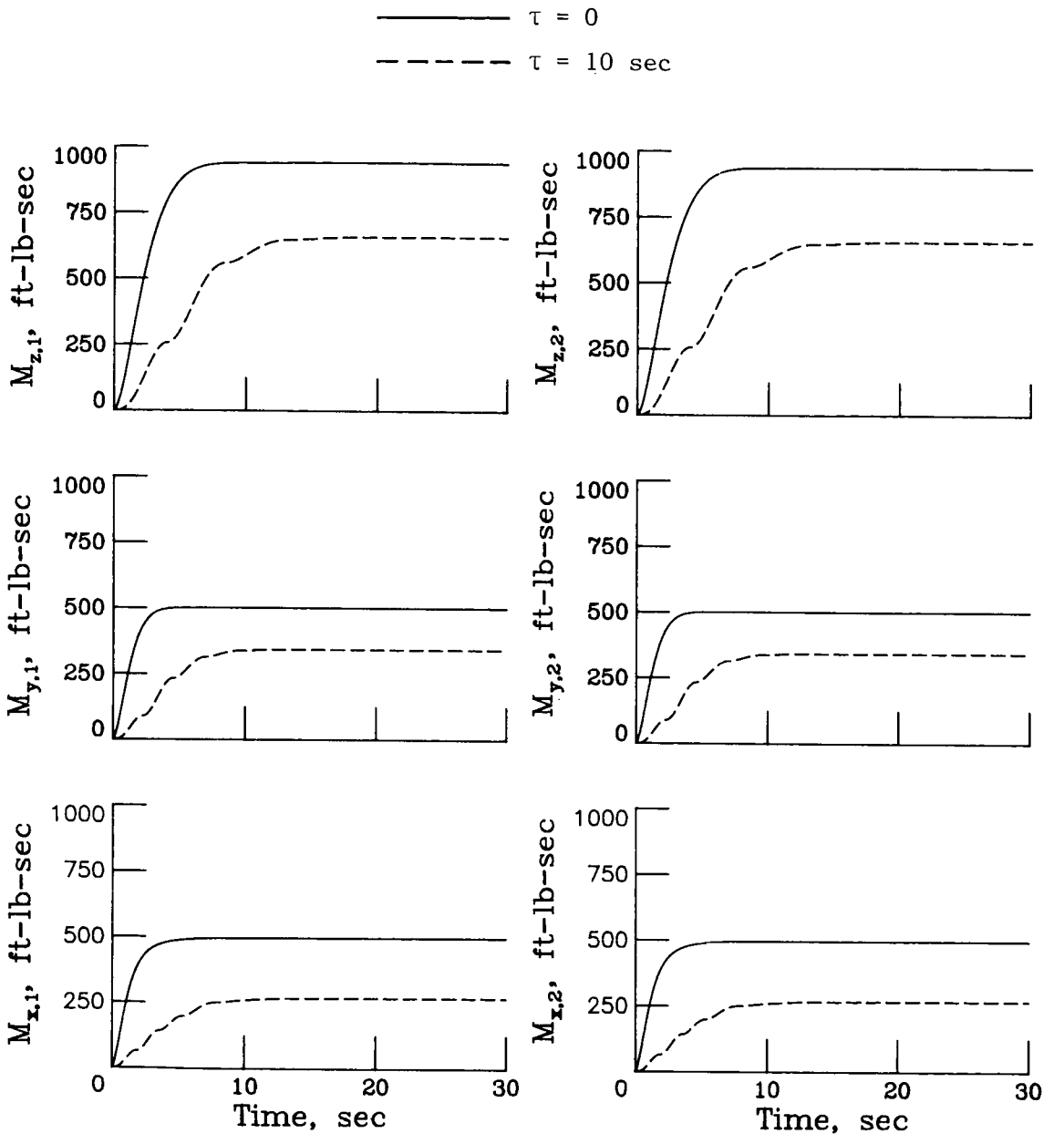

(b) Concluded.

Figure 13.- Concluded.

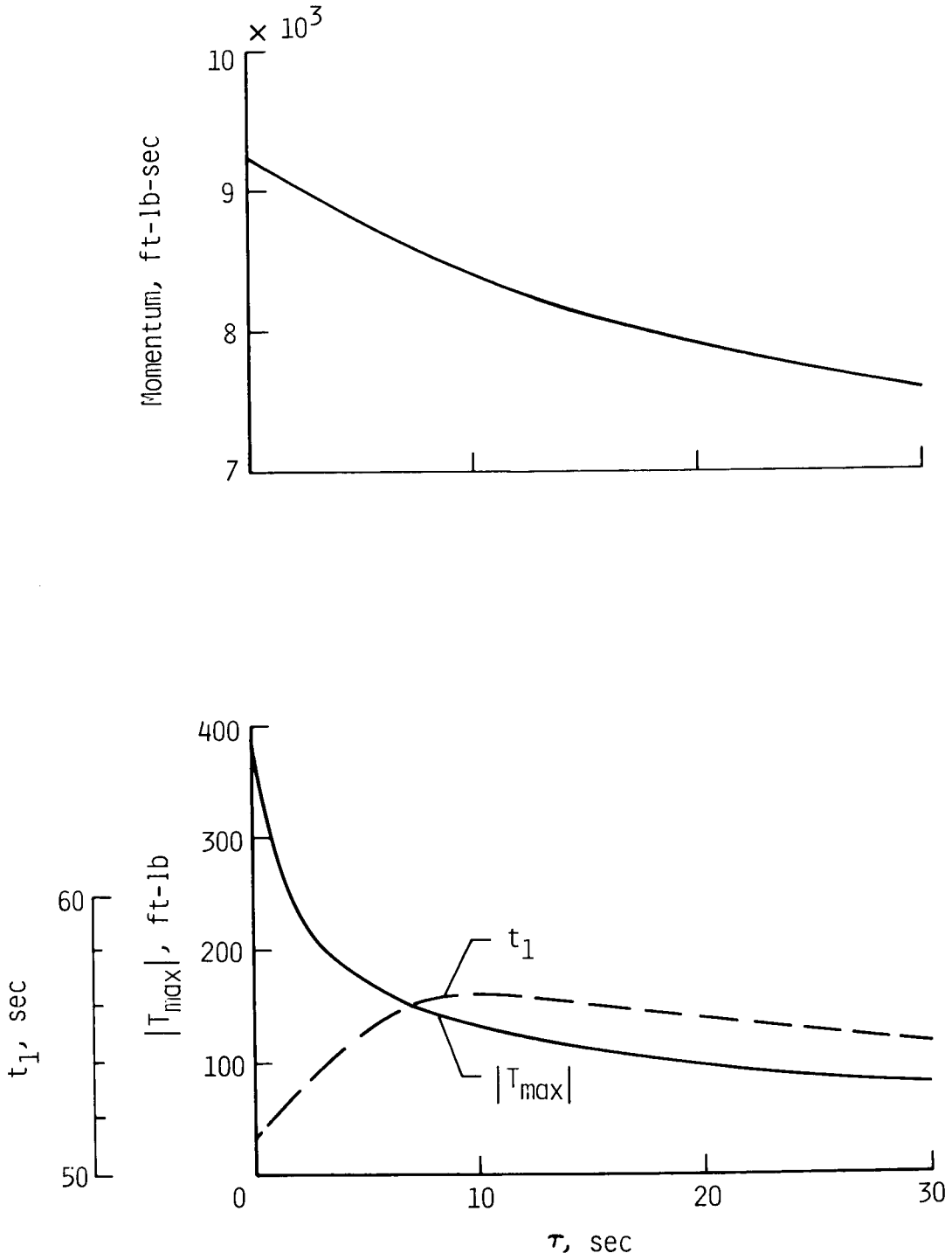

(a) Rigid-body disturbances.

Figure 14.- Effect of lag on control requirements for CMG case of table III.

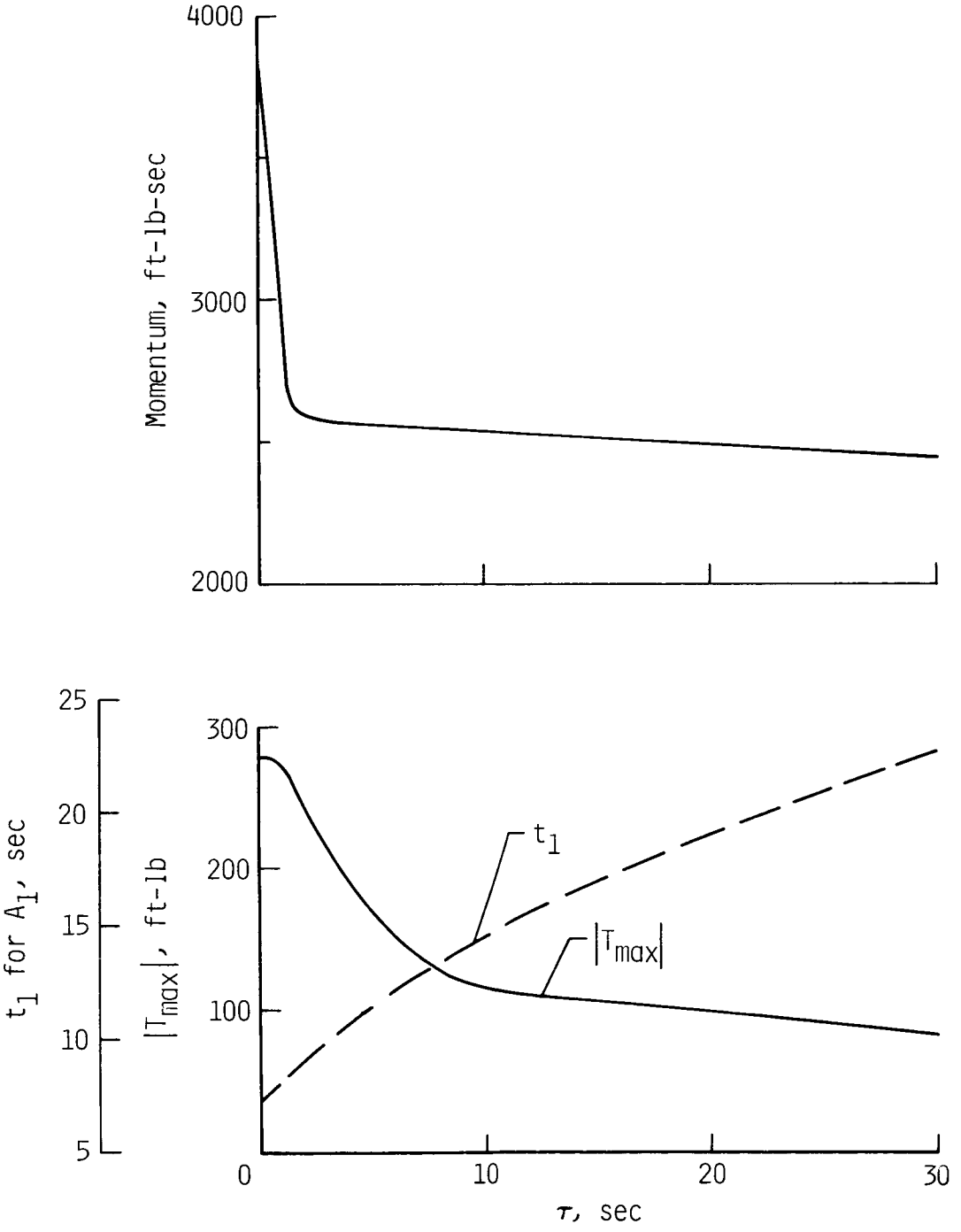

(b) Flexible-mode disturbances.

Figure 14.- Concluded.

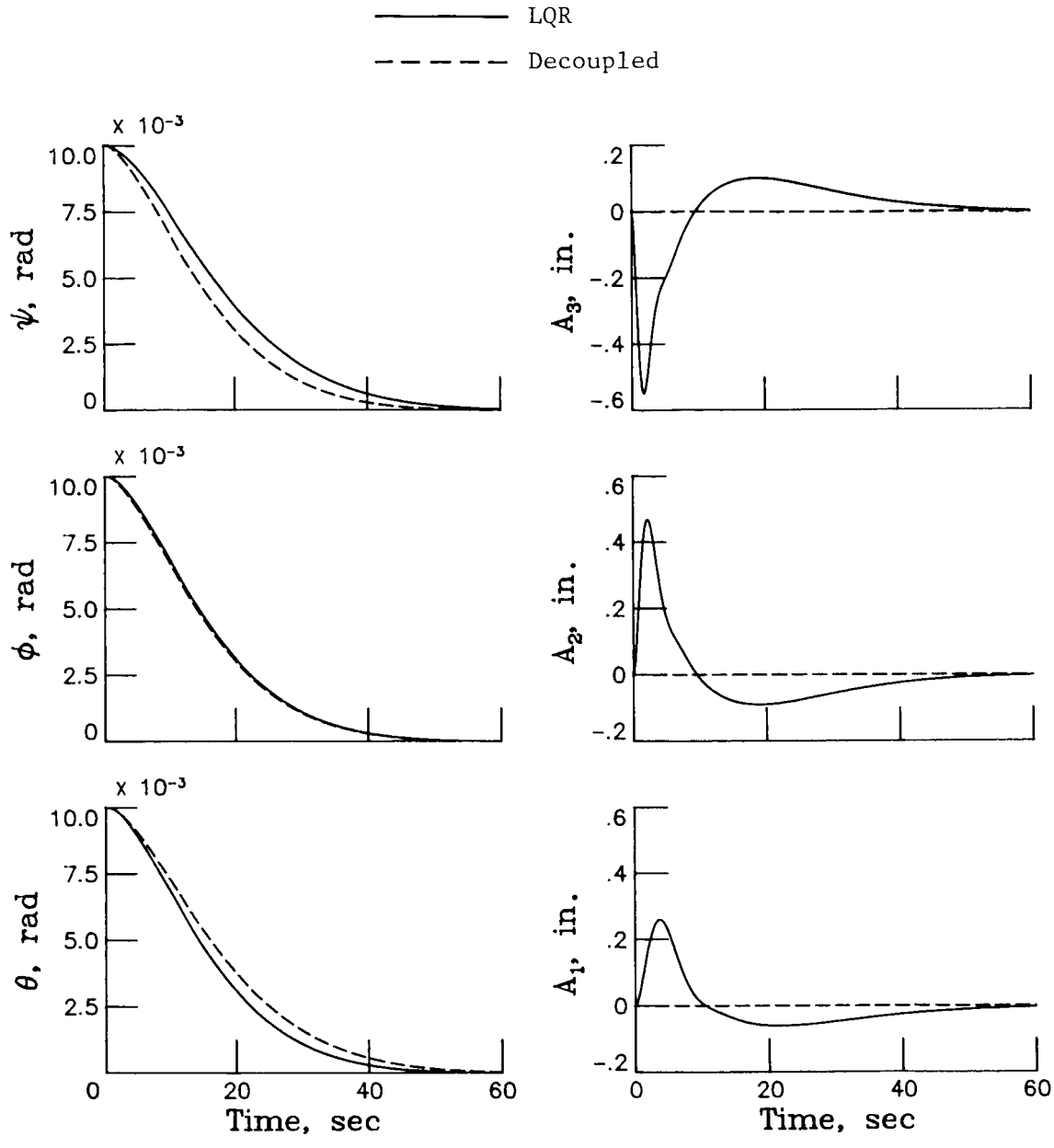

(a) Rigid-body disturbances.

Figure 15.- Comparison of LQR and decoupled responses for case 2 of table XI.

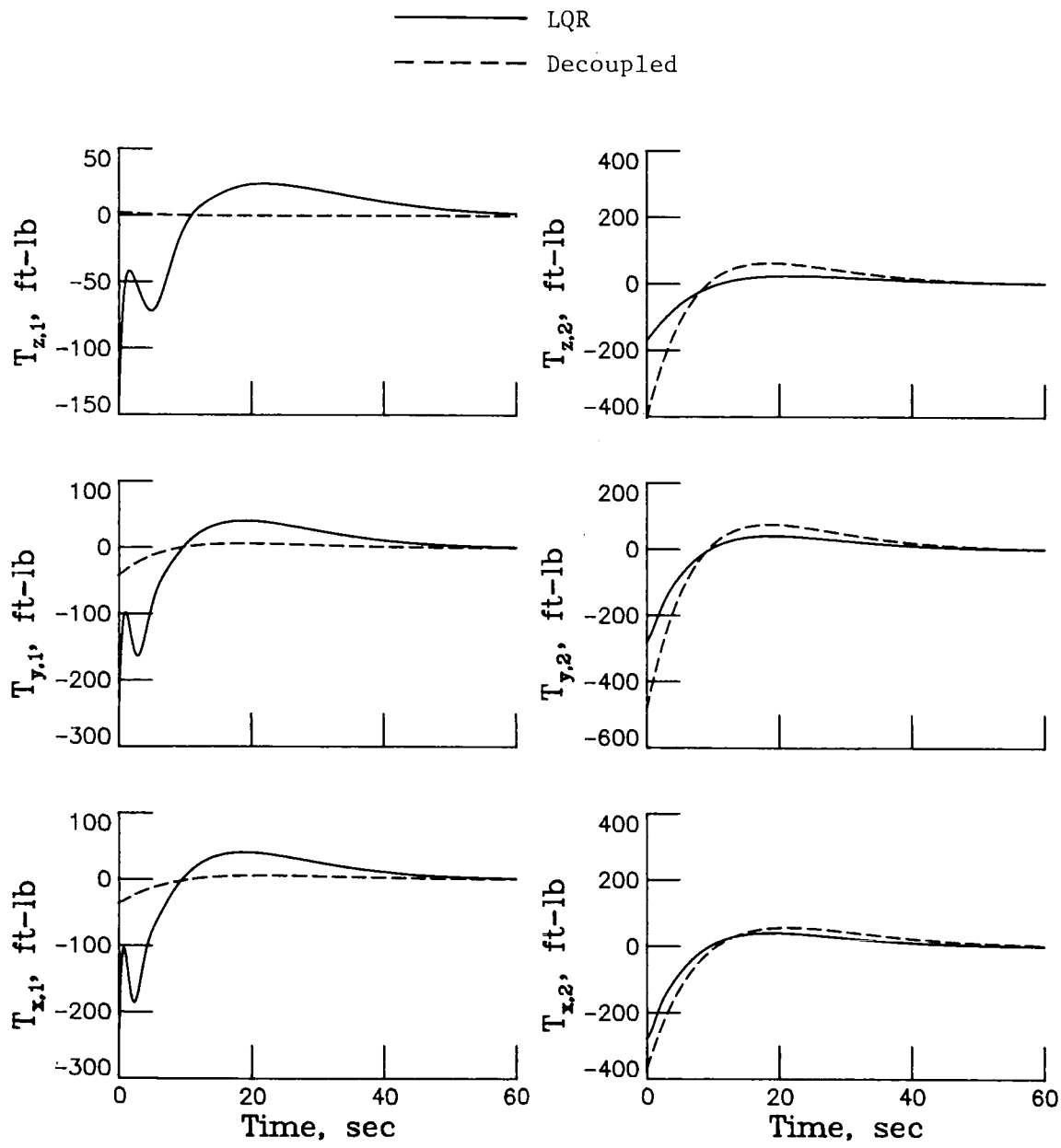

(a) Continued.

Figure 15.- Continued.

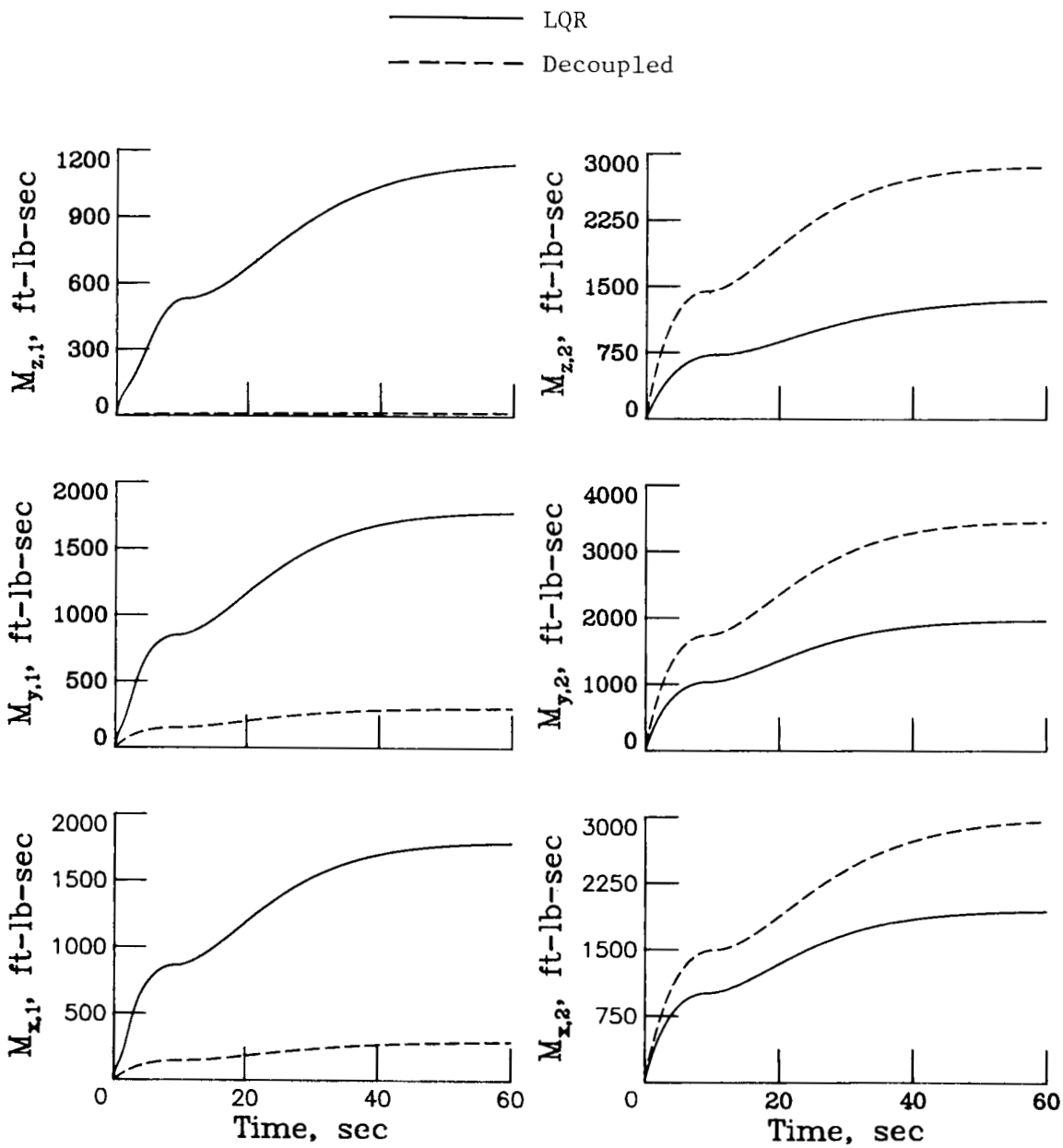

(a) Concluded.

Figure 15.- Continued.

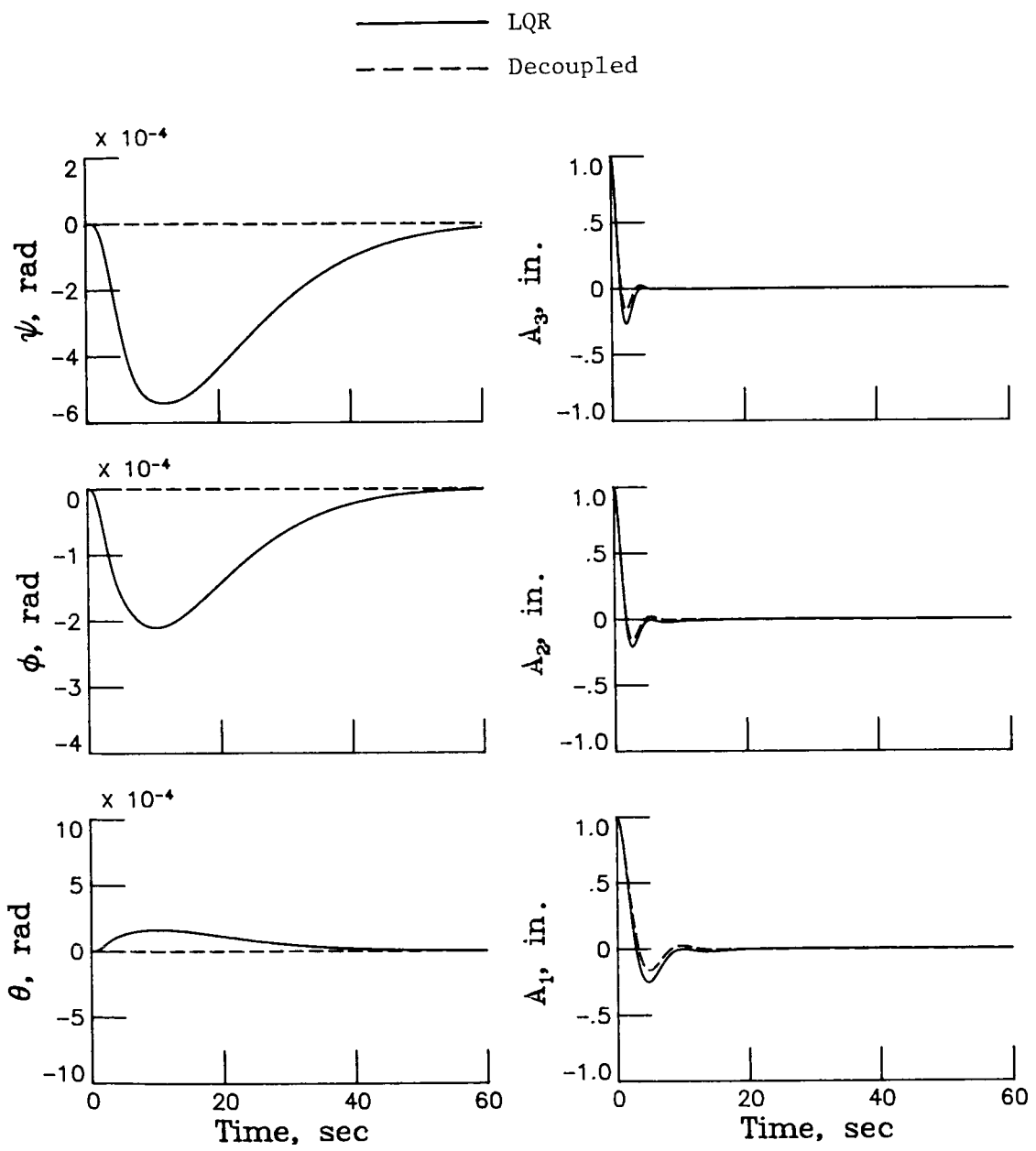

(b) Flexible-mode disturbances.

Figure 15.- Continued.

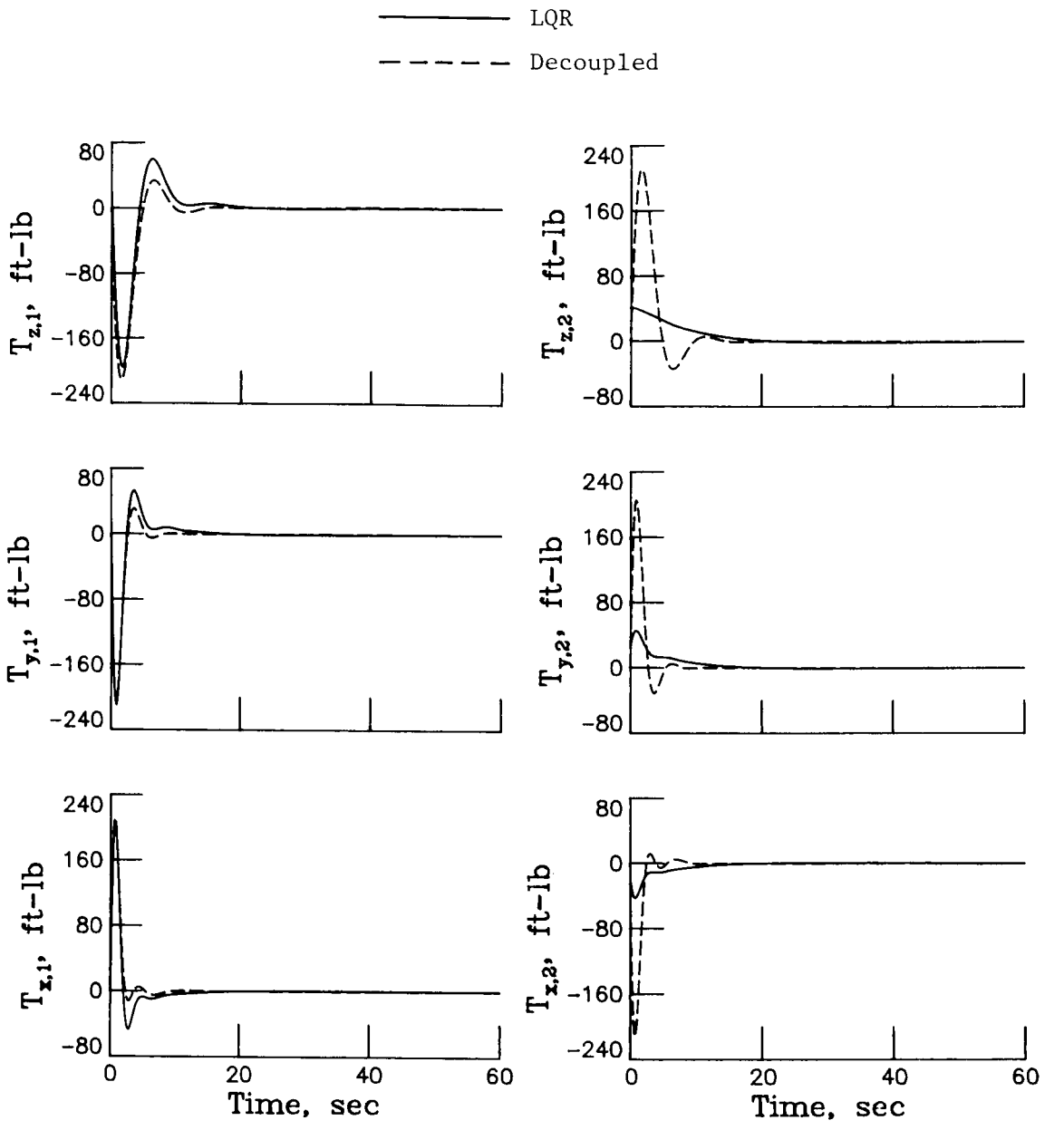

(b) Continued.

Figure 15.- Continued.

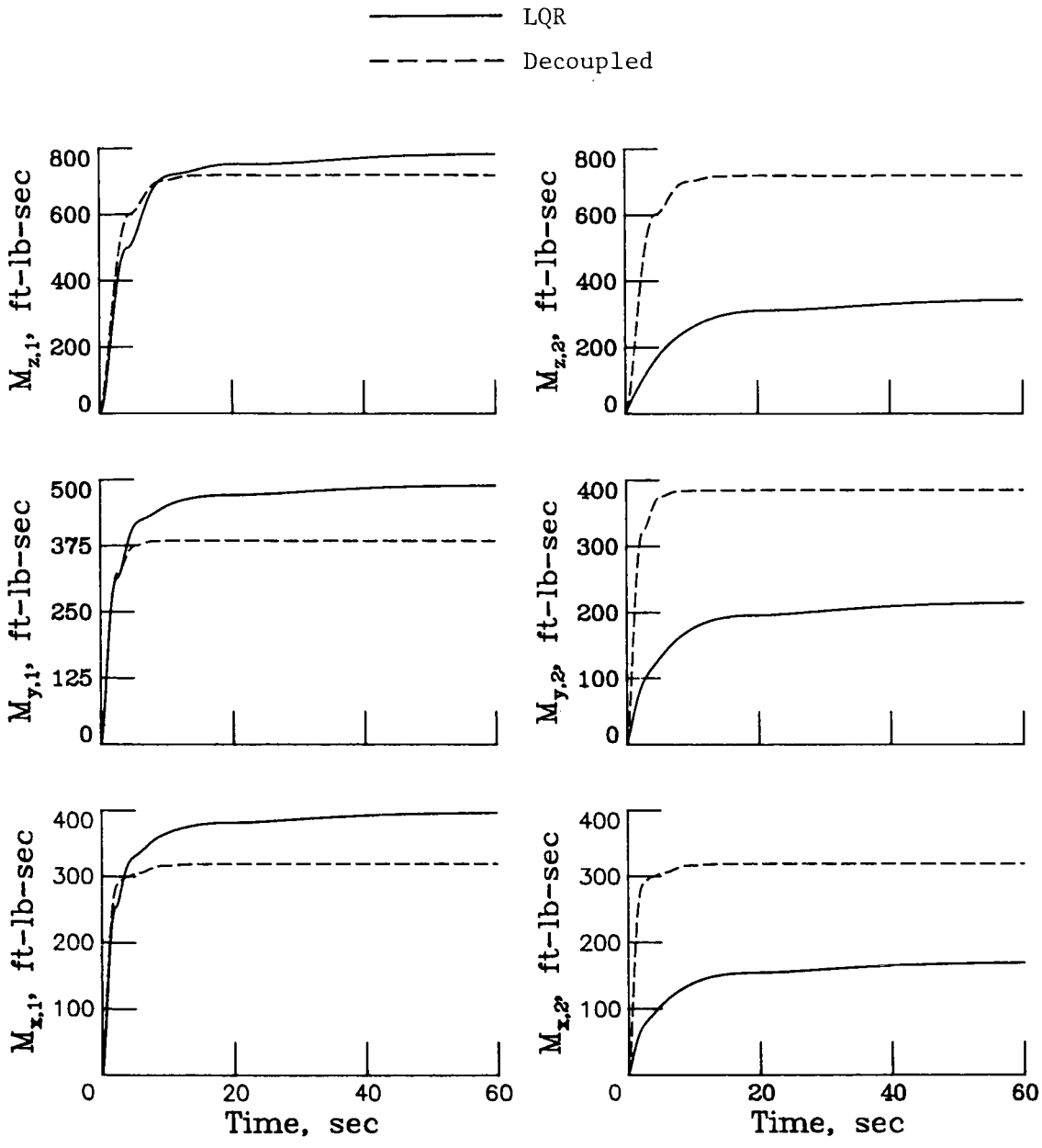

(b) Concluded.

Figure 15.- Concluded.

1. Report No.	2. Government Accession No.	3. Recipient's Catalog No.
NASA TP-2293		

4. Title and Subtitle	5. Report Date
DECOUPLED-CONTROL ANALYSIS OF A LARGE FLEXIBLE SPACE ANTENNA WITH LINEAR QUADRATIC REGULATOR COMPARISONS	May 1984
	6. Performing Organization Code 506-57-13-01

7. Author(s)	8. Performing Organization Report No.
John W. Young, Harold A. Hamer, and Katherine G. Johnson	L-15696
	10. Work Unit No.

9. Performing Organization Name and Address	11. Contract or Grant No.
NASA Langley Research Center Hampton, VA 23665	
	13. Type of Report and Period Covered Technical Paper

12. Sponsoring Agency Name and Address	14. Sponsoring Agency Code
National Aeronautics and Space Administration Washington, DC 20546	

15. Supplementary Notes

16. Abstract

A decoupled-control analysis was performed for a large flexible space antenna. Control involved commanding changes in the rigid-body modes or nulling disturbances in the flexible modes. The study provides parametric-type data which could be useful in the final design of a large space antenna control system. Results are presented to illustrate the effect on control requirements of (1) the number of modes controlled, (2) the number, type, and location of control actuators, and (3) variations in the closed-loop dynamics of the control system. Comparisons are given between the decoupled-control results and those obtained by using a linear quadratic regulator approach. Time history responses are presented to illustrate the effects of the control procedures.

17. Key Words (Suggested by Author(s))	18. Distribution Statement
Decoupling Large space structures Linear quadratic regulator Modal control	Unclassified - Unlimited Subject Category 18

19. Security Classif. (of this report)	20. Security Classif. (of this page)	21. No. of Pages	22. Price
Unclassified	Unclassified	80	A05

For sale by the National Technical Information Service, Springfield, Virginia 22161

NASA-Langley, 198

1 2 1U,B, 840511 S00161DS
DEPT OF THE AIR FORCE
ARNOLD ENG DEVELOPMENT CENTER(AFSC)
ATTN: LIBRARY/DOCUMENTS
ARNOLD AF STA TN 37389